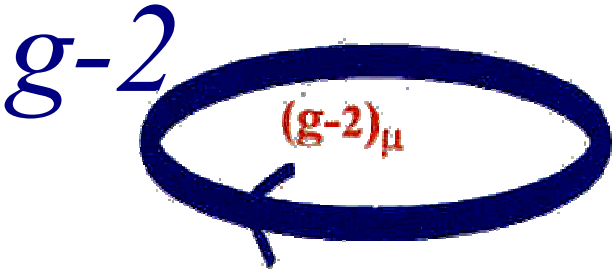

Brookhaven National Laboratory

Brookhaven Science Associates

Upton, New York 11973

Muon g-2 Note No. 447

Title: **Ratio Method Based ω_a Analysis of the 2001 G2Too Data**

Author: **Petr M. Shagin**

Affiliation: **University of Minnesota**

Date: **December 10, 2003**

Ratio Method Based ω_a Analysis of the 2001 G2Too Data

Petr M. Shagin
University of Minnesota

December 10, 2003

Abstract

This note is the updated version of my ω_a analysis report, full runlist was used. Data selection and fitting procedure is described. Detectors phase alignment and the choice of earliest fit start times are briefly mensioned. Monte Carlo study of the CBO related uncertainties are presented. Combining of two data sets for different CBO frequencies are discussed. I expect reader is familiar with the ratio method formalism (see brilliant Long's thesis [1]), so omit these part from my report. The recommended value for R (at 27.5 μs) is 107.95 ± 0.686 (stat.) ± 0.23 (syst.) (108.14 ± 0.709 (stat.) ± 0.21 (syst) at 31.7 μs). The combined uncertainty is ± 0.724 ppm (± 0.74 ppm).

Contents

1 Introduction **3**

2 Data processing and run selection **3**
2.1 Data selection: runlist . . . 3
2.2 Endpoint calibration . . . 4
2.3 Phase alignment/fill randomization . . . 4
2.4 Pileup construction . . . 5
2.5 Gain Correction . . . 6

3 Results **7**
3.1 Fit functions . . . 7
3.2 Fitting . . . 12
3.3 Start time stability . . . 13
3.4 Results versus detector . . . 52
3.5 Results for 7-parameter fit function. CBO sidebands included in fit. . . . 56
3.6 Short summary . . . 89

4 Systematic Studies **90**
4.1 Ratio Method/Fitting Procedure . . . 90
4.2 Fill randomization . . . 91
4.3 Pileup subtraction . . . 91

4.4 Energy threshold variation. 101
4.5 Gain Correction 101
4.6 $G2Too$ and $g2off$ comparison 106
4.7 Muon losses/AGS flashlets 109
4.8 Coherent Betatron Oscillations (CBO) 110
4.9 Summary of systematic uncertainties 129

5 Conclusions **134**

1 Introduction

In 2001 g-2 experiment recorded data for the muons. Totally more than 4 billions of electrons were collected during the run period. It almost doubled the statistical power of the combined ω_a measurement.

It seems interesting to compare the 2001 results with the data for positive muons to test the CPT invariance.

The running conditions were optimized to take unbiased reliable data. Two different quad settings (n values) were selected for running far beyond the region were the coherent betatron beam oscillations (CBO) resonate with double ω_a frequency.

Ben shown for 2000 data that using run-by-run endpoints calibration is essencial for extacting unbiased R value. I used run-by-run endpoints calibration produced by Tao Qian [10] for *G2Too* data set.

The fitting function used to obtain the presented R value is 3-parameter *ratio* function. This function does not contain any terms to account for coherent betatron oscillations (CBO), or effects such as muon losses, gain changes, or other slow effects. It is shown that including CBO terms in the fitting function (7-parameter) does not change the results a lot. The systematic uncertainty associated with neglecting the CBO terms is shown to be small. As shown by Long the slow effects (gain changes, muon losses etc.) contribute small uncertainties to the R value obtained by ratio method of analysis.

Fill randomization and pileup subtraction (1999 Mediterranean form) were applied to the data prior to fitting.

2 Data processing and run selection

2.1 Data selection: runlist

The present analysis used the *G2Too* data produced at Illinois. Data runs were selected by Chris Polly [6] and later revised to produce the full runlist by the alliance of Chris, Mario and Xiaobo (see their reports for details). Some runs were excluded by Ernst Sichterman as problematic for magnetic field measurements. Criteria for the run selection include (see details[6]):

- no problems indicated in the g-2 logbook
- passed calorimeter HVs and thresholds stability test
- existence of analyzable field data
- presence of Heidelberg clock (so that one can synchronize ω_p and ω_a)
- presence of T0 info
- minimum $\sim$ 5 min duration of the run (relates to field)
- minimum number of electrons detected in all calorimeters
- minimum number of AGS cycles (112)
- at least some quad traces, no excessive sparking

In total, this full runlist contains 1048 runs from 9423 to 11384. I have specified 10 problematic runs for certain detectors (13, 17, 18 or all), those runs data were omitted. See run list on my web page (webusers.physics.umn.edu/ shagin/g-2/).

All results presented in this report were made for my subset of full runlist, which contains 1038 runs (. My data subset differs from the main set very little. No laser runs or data for detector 20 have been included. The total number of electrons detected later 27.5 μs for low energy threshold 1.8 GeV for this data set is 4.11 billion. Table 1 lists the total number of events (after cuts and before pileup subtraction) for two run data sets.

Table 1: Number of electrons before pileup subtraction ($E > 1.8$ GeV, $27.5 < t < 586$ μs).

Data Set	Runs	B e^-
low n	9423-9754, 10032-10272, 10713-10960, 11026-11328	2.51
Nigh N	9756-9989, 10274-10707, 10968-11009, 11357-11384	1.60
Total	9423-11384	4.11

2.2 Endpoint calibration

My energy calibration is based on the run-by-run endpoint values produced by Tao Qian [10] for 2001 *G2Too* data. The endpoint calibration procedure was done for every run. Two-dimensional area vs. time histogram constructed for each detector (and for each run) are projected out to provide the area distribution. A 200 μs time cut was applied to minimize contribution from pileup and gain changes. The resultant area distribution was fitted to a straight line between 60% and 20% of the maximum number of counts and then extrapolated to the area axis. This extrapolated value is assigned to the endpoint energy of 3.1 GeV. Over a few iterations, this procedure assignes detector energy endpoint values for all 23 calorimeters for the particular run. Energy spectra for all runs were reproduced using run-by-run calibration coefficients.

All data runs were added together. The energy spectrum for each detector was fitted to obtain the average endpoint. Average energy endpoints for 23 detectors were shown in Fig. 1.

2.3 Phase alignment/fill randomization

The histograms for the ratio method contained 4500 time bins of width 148.185 ns. This binwidth was chosen to be close to the fast rotation period. The systematic fitting error due to the choice of binwidth is discussed later in Sec. 4.1.

The technique of *fill randomization* is used to eliminate the effects of the fast rotation. Six random seeds were used for each detector.

Detectors phase alignment was done in a few iterations. At the first step all runs were added to produce the summary data set. Than ratio histograms were produced using 2000 phase values. Data were fitted using 2000 parameters and 3-parameter ratio functional form. The resultant phases for 23 detectors are plotted in Fig. 2 (red points). At the next step phases were corrected (by adding or subtracting the fitted values) to calculate the values of small time offsets added (or subtracted) to (from) the fitted pulse time. New set of ratio histograms were produced using

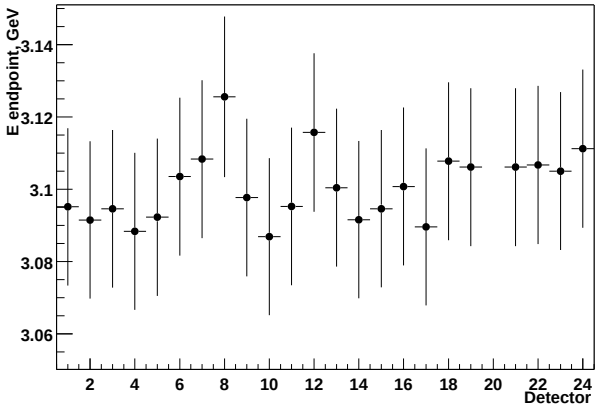

Figure 1: Energy endpoint calibration versus detector. From a linear fit across detectors, the mean value is 3.1 ± 0.007 GeV with a χ^2/Ndf of 3.43/22.

corrected time offsets. The fitting procedure was repeated for the new set of histograms results in the new phase values. Corrected phases for 23 detectors are plotted in Fig. 2 (black points).

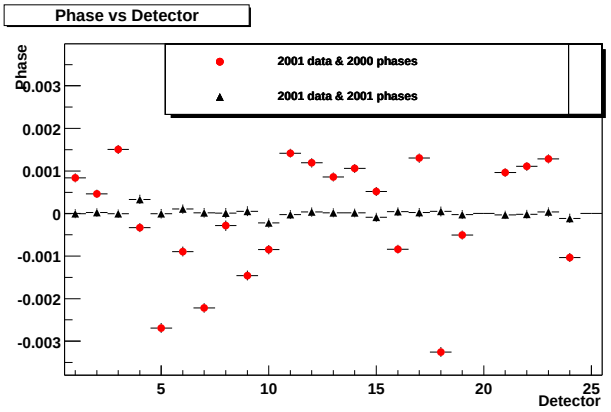

Figure 2: $g-2$ phases versus detector at 31.7 μs. Red points - 3-parameter fit returned phase values if 2000 phases used to produce histograms for 2001 data. Black points - corrected phases used for histograming.

Dectector phases were thus aligned with 0.5 mrad accuracy. Fig. 3 shows a final plot of $g-2$ phase versus detector.

Low energy threshold 1.8 GeV was used when filling all histograms.

2.4 Pileup construction

I used the same method of pileup construction that was used in the 2000 and 1999 ratio method analysises, the so-called *Mediterranean* method [11]. This method exploits the long digitization

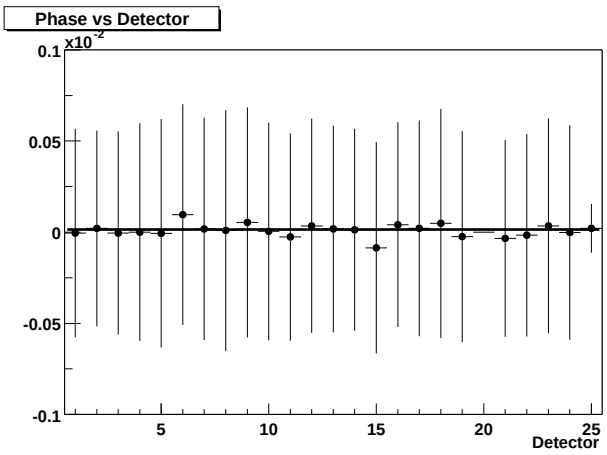

Figure 3: $g-2$ phase versus detector at 31.7 μs.

time of the WFDs in order to construct a spectrum of pileup pulses.

For each pulse S_1 of energy E_1 at time t_1, a second pulse S_2 is searched for within the same digitization island. Specifically, this search is conducted within the time interval: $t_1 + T - \frac{T_r}{2}$,$t_1 + T + \frac{T_r}{2}$ wHere T_r is double pulse resolution time and T is offset time. For the *G2Too* production, resolution time is 5 ns. The offset time shift T is chosen to be 10 ns. Pulse S_2 is then shifted back in time and combined with S_1 to form a double pulse D having a time and energy given by

$$t_D = \frac{t_1 E_1 + (t_2 - T)E_2}{E_1 + E_2}, \quad (1)$$

$$E_D = f(E_1 + E_2). \quad (2)$$

Here, the average coefficient $f = 0.94$ is a characteristic of the *G2Too* pulse reconstruction algorithm. Finally, the pileup spectrum $P = D - S_1 - S_2$ is formed and subtracted from the data. This technique has been shown to effectively remove pileup to the 90% level.

The ratio of constructed double, single and pile-up events to the total number of the detected electrons were measured for time $27.5 < t < 586$ μs. The fraction values across the detectors are shown in Fig. 4.

As shown in Table 2, pileup subtraction removes about 0.4% of the data. The pileup-subtracted data set consists of about 4.093 billion electrons.

2.5 Gain Correction

Gain correction was applied to the data using early-to-late changes of the average energy. Time dependence of the average energy can cause the systematic change in R value. In order to correct that uncertainty the data were corrected using time dependent gain factor f(t).

For each detector average energy versus time was fitted and gain factor was calculated using detector sensitivity multiplier (the same for all detectors). The following functional form was used to correct detector energy:

$$f(t) = (1 + A_1 e^{-t/A_2})(1 + A_3 e^{-(t-A_4)^2/A_5^2}) \quad (3)$$

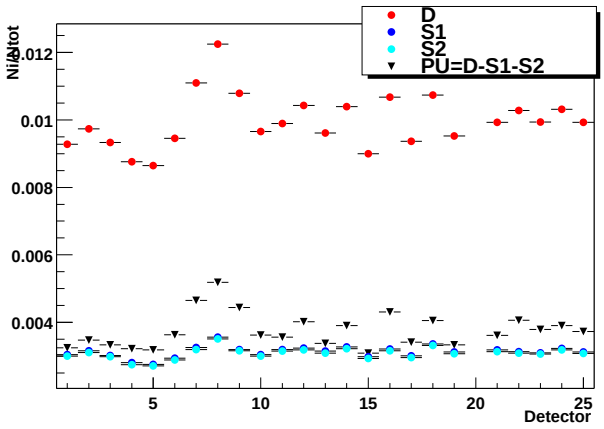

Figure 4: Fractions of the constructed pile-up, double and single events versus detector (integrated by time; started at 27.5 μs).

Table 2: Number of electrons involved in pileup construction (entire data set, $E > 1.8$ GeV, $27.5 < t$ μs).

	M e^-
Before PUS	4109.78
D	42.33
S_1	13.15
S_2	12.75
$P = D - S_1 - S_2$	16.44
After PUS	4093.34

where parameters A_1-A_5 depend on the detector.

Normalized average energies for each detector before and after gain correction were plotted in Figs. 5-8 as a function of time.

The effect of gain correction for R will be discussed later.

3 Results

3.1 Fit functions

The results of the fit using two different functions are described, both are based on the ratio method formulation [1].

The ratio fitting function in its most basic form has 3 parameters:

$$r(t) = A\ \cos(\omega_a t + \phi) + \frac{1}{16}\left(\frac{\tau_a}{\tau_\mu}\right)^2 = A\ \cos(\omega_a t + \phi) + 0.000287. \tag{4}$$

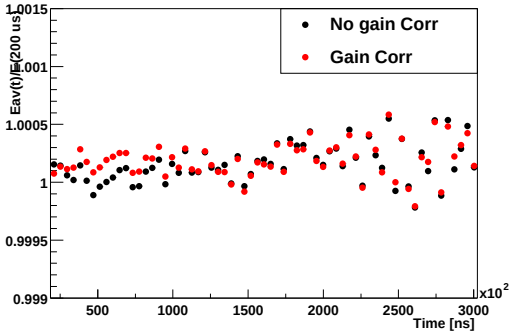

(a) E det 1

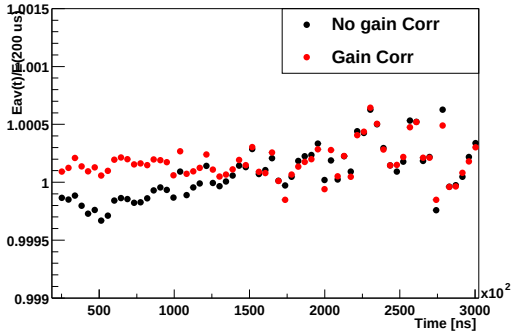

(b) E det 2

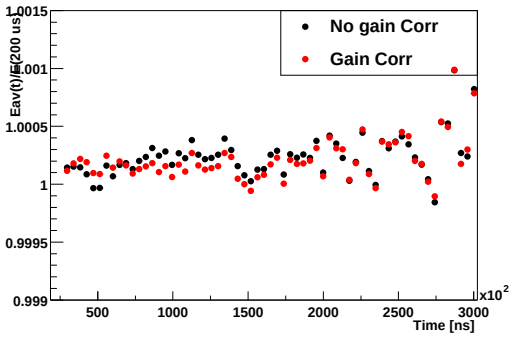

(c) E det 3

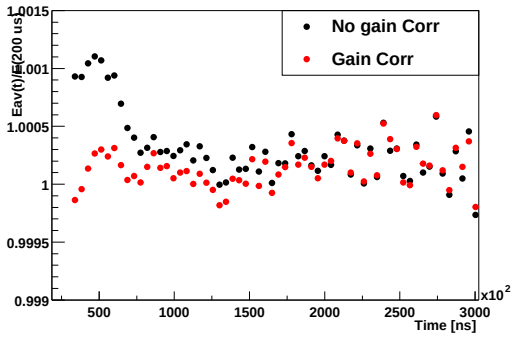

(d) E det 4

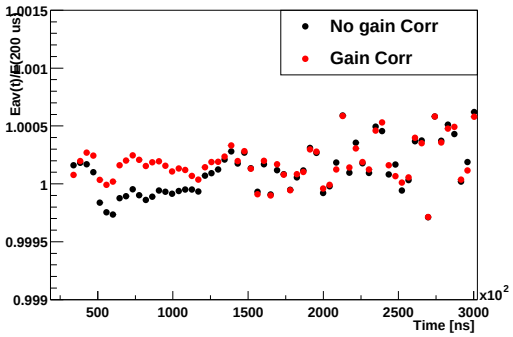

(e) E det 5

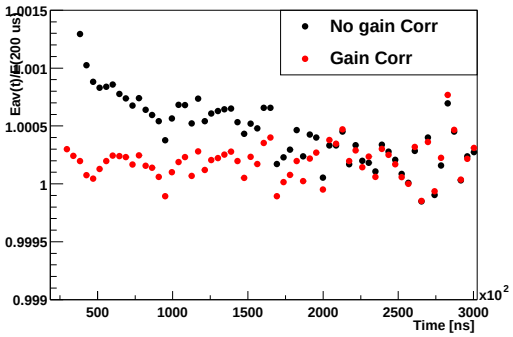

(f) E det 6

Figure 5: Normalized average energy versus time. Detectors 1-6

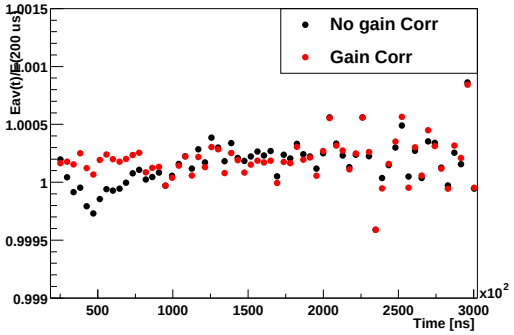

(a) E det 7

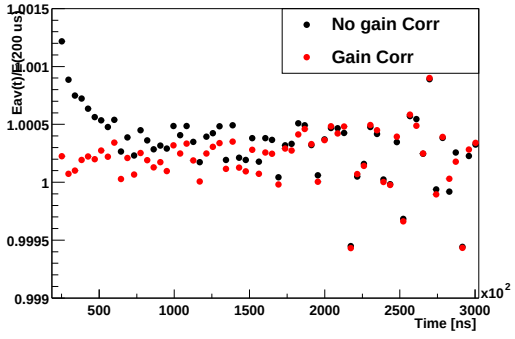

(b) E det 8

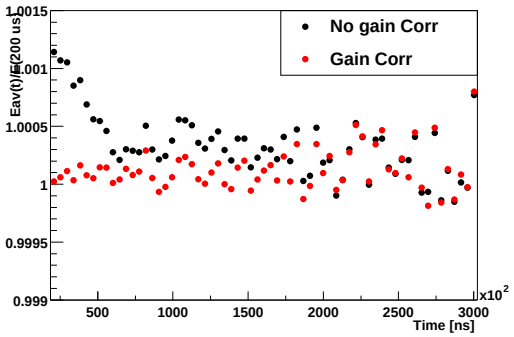

(c) E det 9

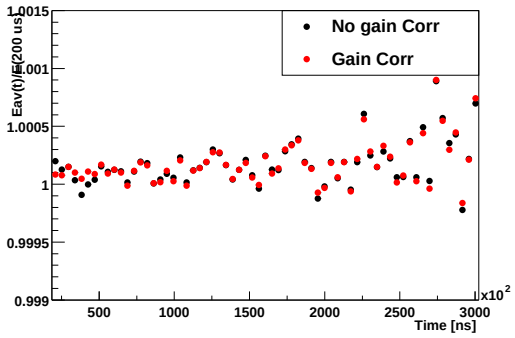

(d) E det 10

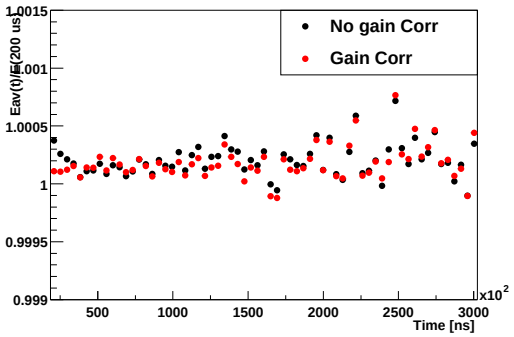

(e) E det 11

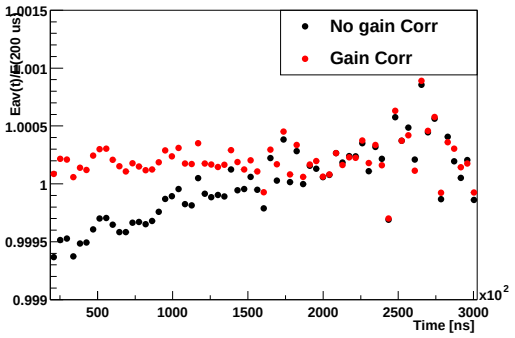

(f) E det 12

Figure 6: Normalized average energy versus time. Detectors 7-12

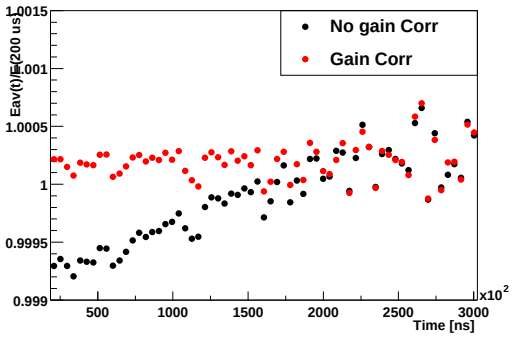

(a) E det 13

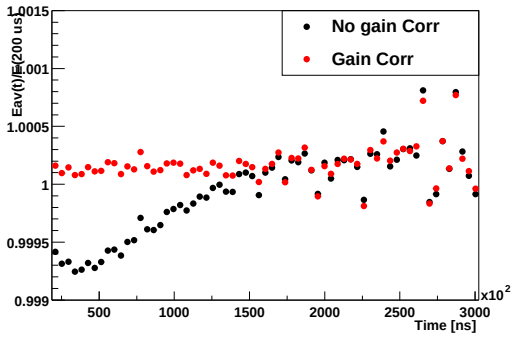

(b) E det 14

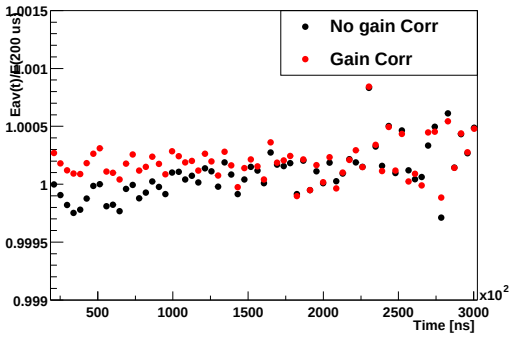

(c) E det 15

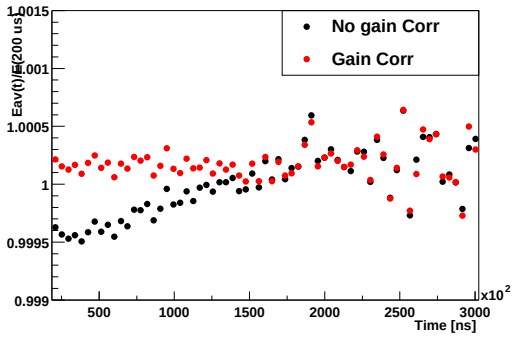

(d) E det 16

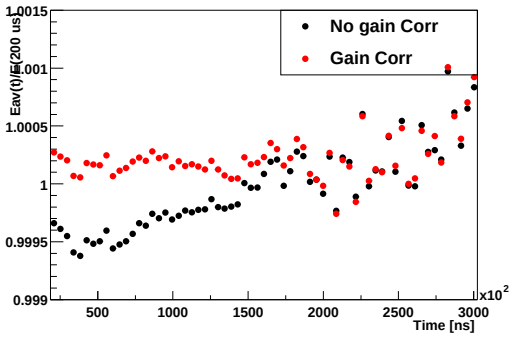

(e) E det 17

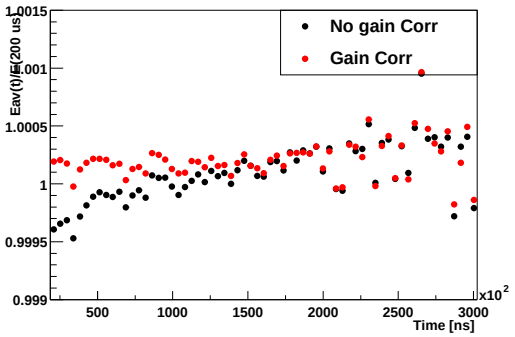

(f) E det 18

Figure 7: Normalized average energy versus time. Detectors 13-18

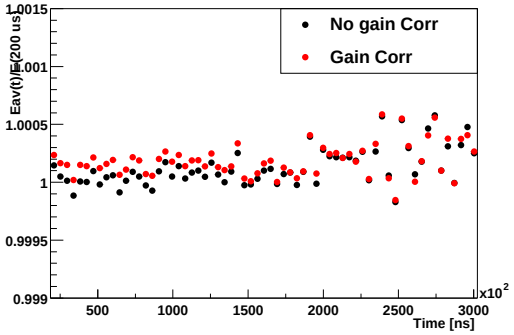

(a) E det 19

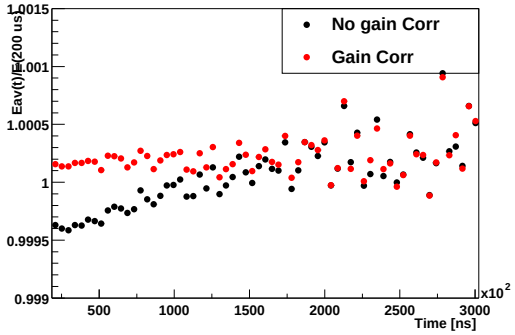

(b) E det 21

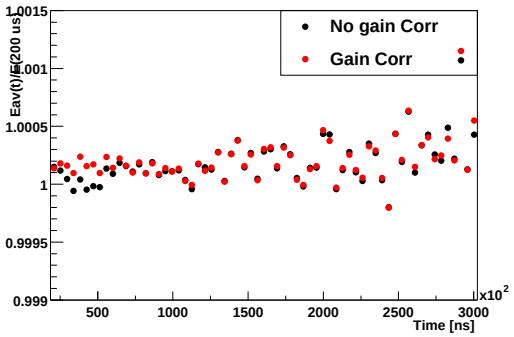

(c) E det 22

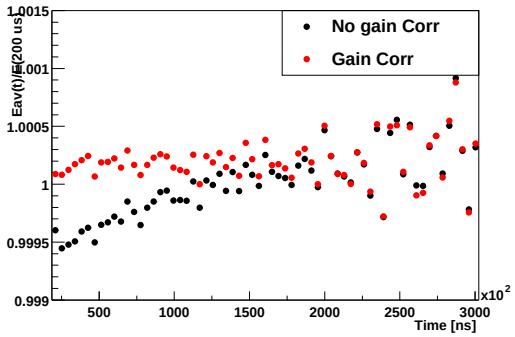

(d) E det 23

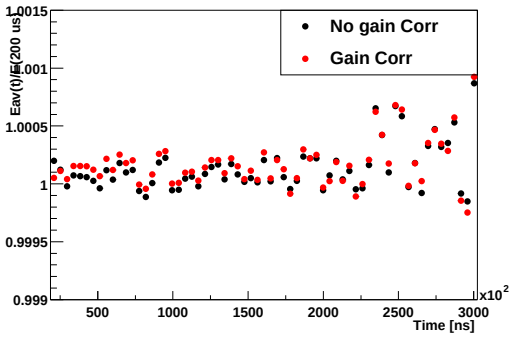

(e) E det 24

Figure 8: Normalized average energy versus time. Detectors 19-24

This so-called 3-parameter or "1999 form" function of the ratio method does not take into account any CBO terms.

The following form of the ratio method has been used to fit for the CBO, so-called 7-parameter fit function [2]:

$$\begin{aligned} r(t) &= A\cos(\omega_a t+\phi)+0.000287 \\ &+ e^{-t/\tau_{cbo}}[A_1\cos(\omega_1 t)+B_1\sin(\omega_1 t)+A_2\cos(\omega_2 t)+B_2\sin(\omega_2 t)]. \end{aligned} \quad (5)$$

Here $\omega_1 = \omega_{cbo} - \omega_a$ and $\omega_2 = \omega_{cbo} + \omega_a$. In my fits, the CBO frequency, $\omega_{cbo} = 2\pi/f_{cbo}$, and exponential lifetime were fixed. The numerical value depends on the quad voltage settings. 2001 data can be divided into two data sets with different CBO frequencies and lifetimes. For low n data set $f_{cbo} = 419.1$ kHz; $\tau_{cbo} = 92.0$ μs, and $f_{cbo} = 490.6$ kHz; $\tau_{cbo} = 130.5$ μs for high n data set respectively (see Chris, Jon, Mario and Xiaobo reports).

It will be shown later that using 7-parameter function for fitting doesn't change the results significantly, so my final values are the result of 3-parameter fitting.

3.2 Fitting

MINUIT was used to perform the χ^2 minimization for fitting. Correlation matrix for fitted parameters is shown in Table 3 for 27.5 μs fit start time.

Table 3: Fitting parameters correlation table at 27.5 μs fit start time.

	R	A	ϕ
R	1.0	-0.005	-0.007
A	-0.005	1.0	0.833
ϕ	-0.007	0.833	1.0

The earliest fit start times were determined based on the results of the gate on study discribed below.

The gate on time for a given detector was determined for each run by plotting the time of the first event in the fill. The typical plot is shown in Fig. 9 for detector 8. Note there are no fill randomization performed for that study.

The time corresponding to the maximum electron counts was selected as gate on time for particular run number to be conservative. The stability of the gate on time versus run number is plotted in Fig. 10 for detector 8.

The latest of those times was used as gate on time for all runs.

The shifting of electron time spectra by the ratio method necessitates adding an additional 2.183 μs to that time. Since most detectors were completely gated on long before 25.212 μs, this 2.183 μs shift was only needed for detectors 3-6.

The data were fitted using 3-parameter fit function. The gate on times mensioned above were used as the ealierst fit start times. The fit χ^2/Ndf versus fit start time for detectors 1, 4, 5 and 8 is shown in Fig. 11.

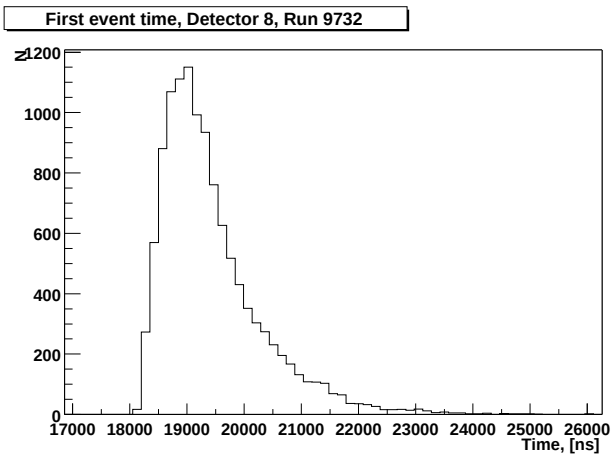

Figure 9: Time distribution of the first event in the fill for detector 8 for Run 9732.

The acceptable value of χ^2/Ndf was required to select final values of fit start times. Table 4 provides the selected fit start times for the ratio method, as determined by the above mensioned procedure, see also Fig. 12. Detectors 4 and 5 are the latest two limiting movement of the fit start time early. The tricky way to overcome this was suggested by Gerco. I can shift detectors 4 and 5 early in time by one g-2 period prior to adding those detector to the others. That shift means that I am adding time spectra for detectors 4 and 5 to the other detectors with relatively smaller weights (or larger errors). This can deteriorates CBO concealation factor and affects CBO related systematic uncertainty (see later).

The number of electron counts at late times determines when fitting has to be stopped, a fit stop time of 550 μs was chosen to contain more than 80 counts in the last time bin. The step size used in fitting was 298.37 ns.

Table 4: Fit start times chosen for the ratio method.

Detector	Time (μs)
1, 2, 7-24	25.21
3,6	27.3
4,5	27.5 (31.7 if not shifted)
Sum of 13-24	25.21
Sums of 1-12, 1-24	27.5 (31.7)

3.3 Start time stability

In this section, the stability of fit parameters versus start time was studied. In Figs. 13-20 the results of 3-parameter fit for each detector are plotted, the 1σ Kawall error bands are also shown. All data runs were added together.

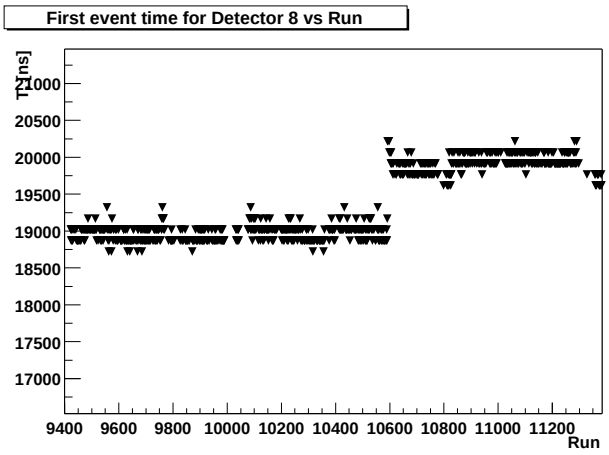

Figure 10: Gate on time for detector 8 versus run number. Note 1.0 μs jump around the run 10600 is the same for all detectors.

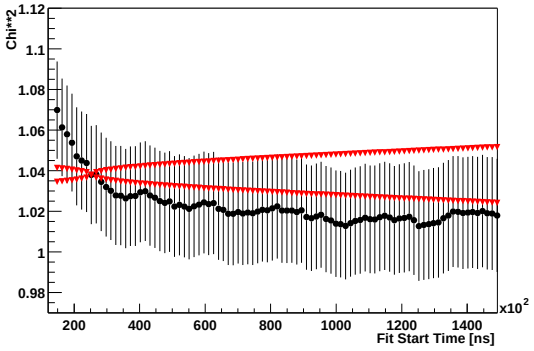

(a) Det 1

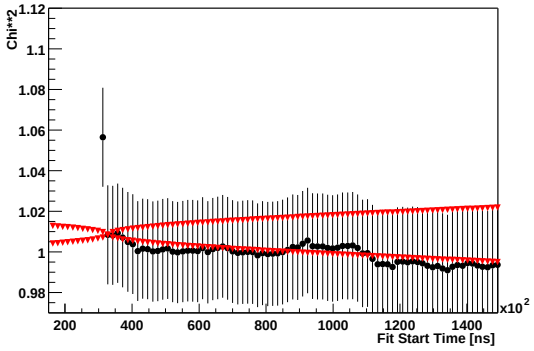

(b) Det 4

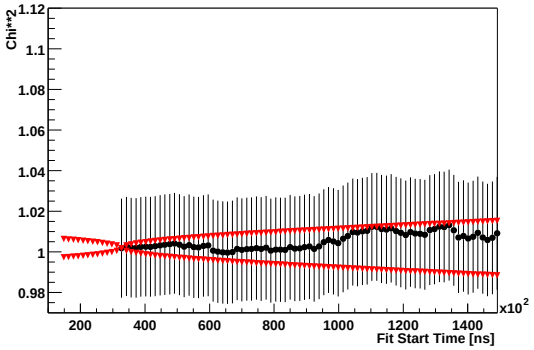

(c) Det 5

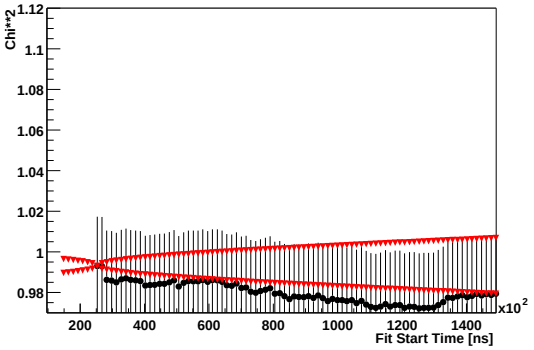

(d) Det 8

Figure 11: The χ^2/Ndf values versus fit start time for detectors 1, 4, 5 and 8.

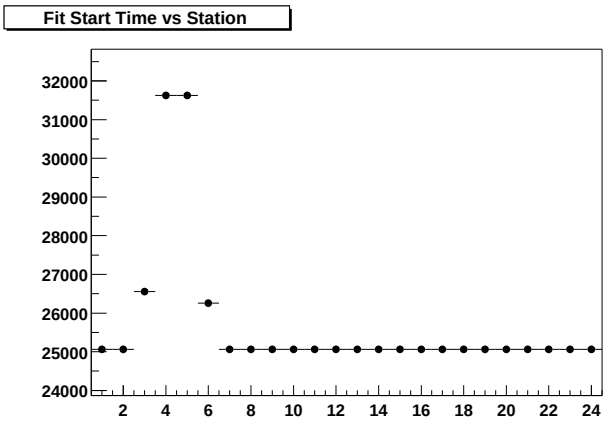

Figure 12: Earliest fit start time values versus detectors.

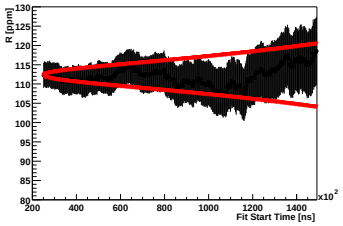

(a) R 1

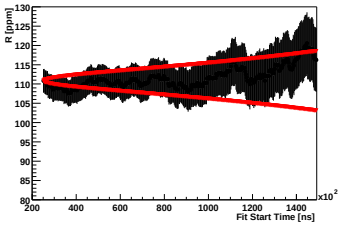

(b) R 2

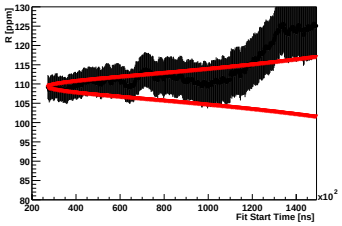

(c) R 3

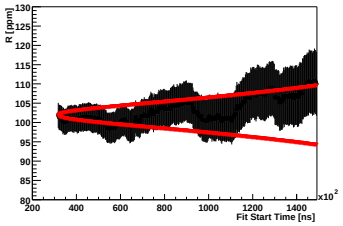

(d) R 4

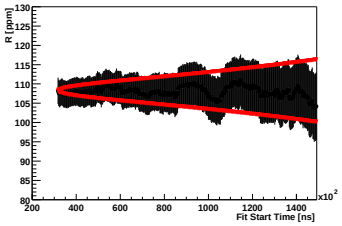

(e) R 5

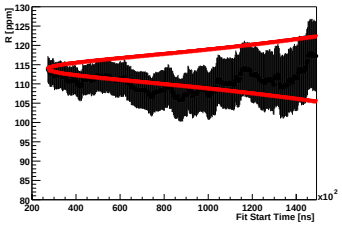

(f) R 6

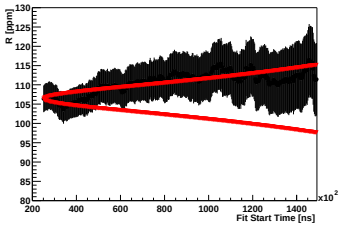

(g) R 7

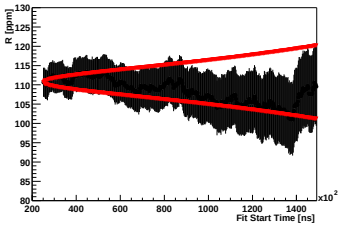

(h) R 8

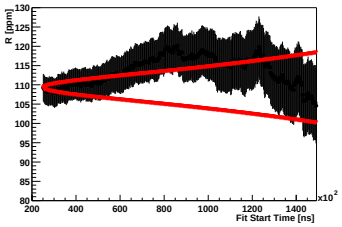

(i) R 9

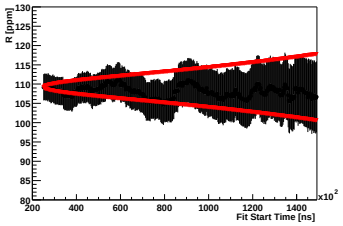

(j) R 10

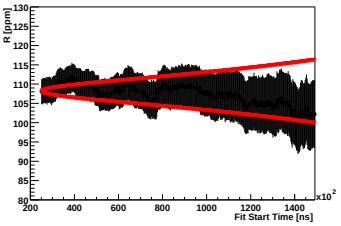

(k) R 11

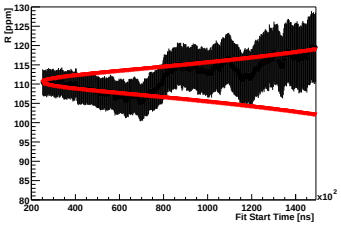

(l) R 12

Figure 13: R (3-parameter) versus fit start time for detectors 1-12. All data sets.

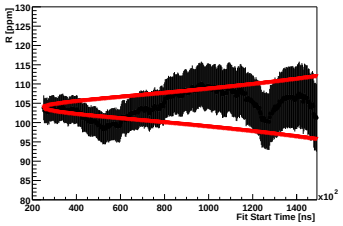

(a) R 13

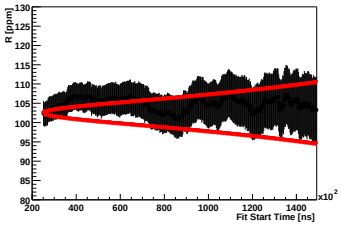

(b) R 14

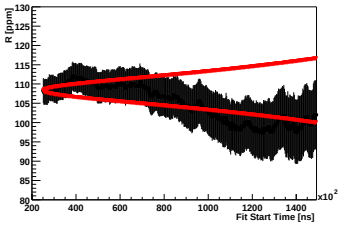

(c) R 15

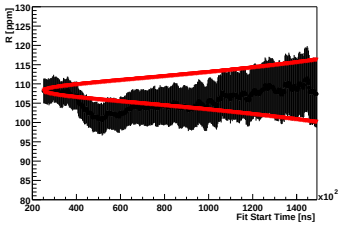

(d) R 16

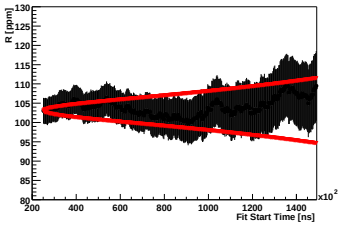

(e) R 17

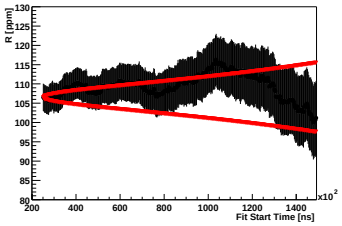

(f) R 18

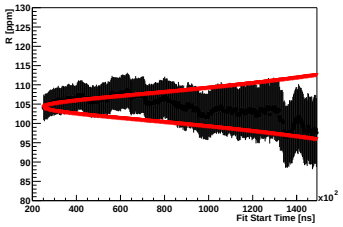

(g) R 19

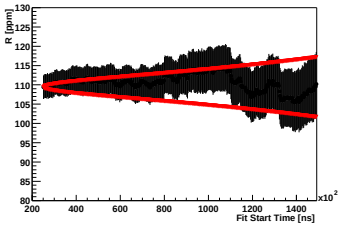

(h) R 21

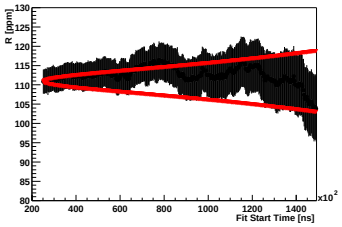

(i) R 22

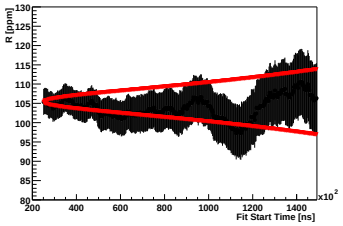

(j) R 23

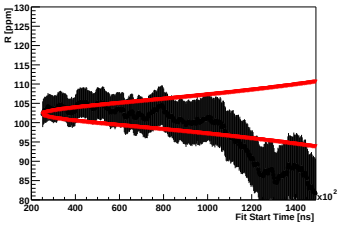

(k) R 24

Figure 14: R (3-parameter) versus fit start time for detectors 13-24. All data sets.

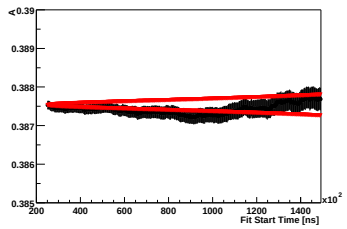

(a) A 1

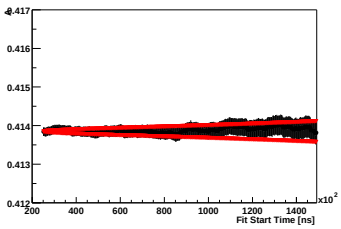

(b) A 2

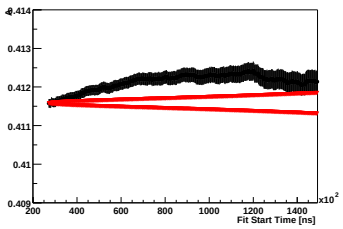

(c) A 3

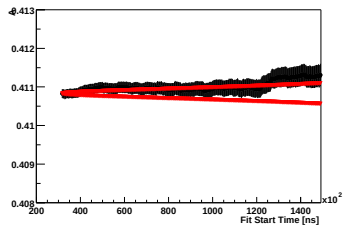

(d) A 4

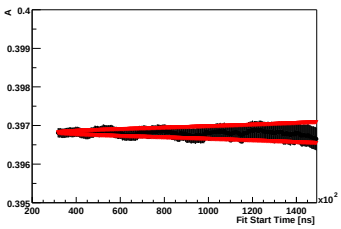

(e) A 5

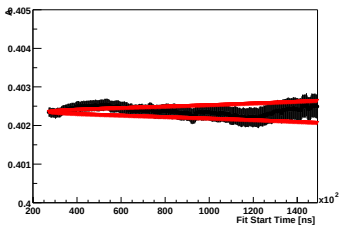

(f) A 6

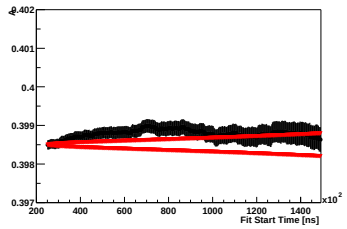

(g) A 7

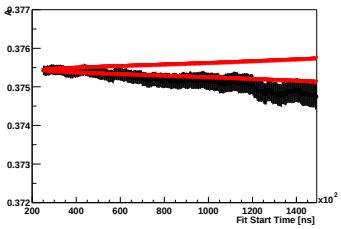

(h) A 8

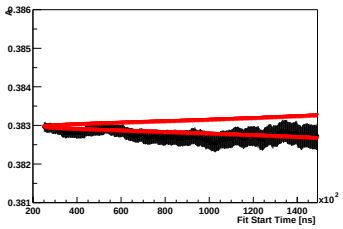

(i) A 9

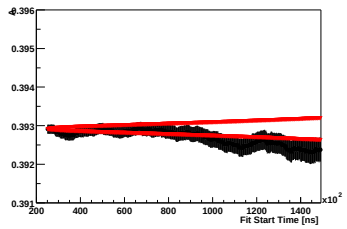

(j) A 10

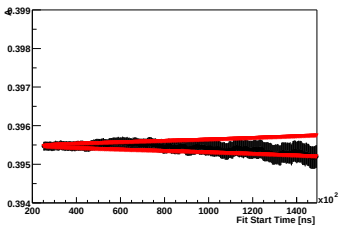

(k) A 11

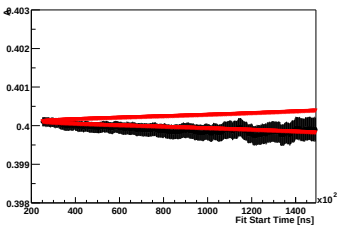

(l) A 12

Figure 15: Asymetry (3-parameter) versus fit start time for detectors 1-12. All data sets.

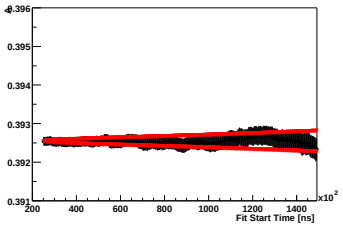

(a) A 13

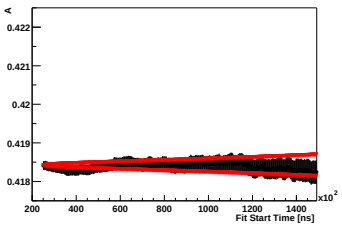

(b) A 14

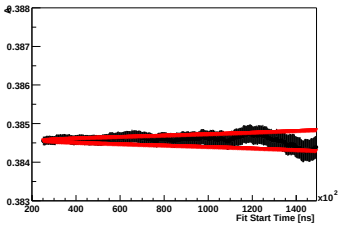

(c) A 15

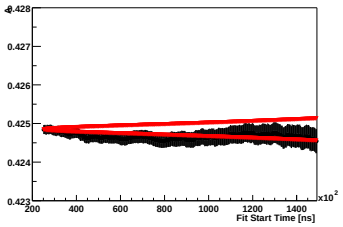

(d) A 16

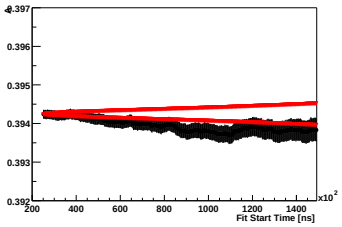

(e) A 17

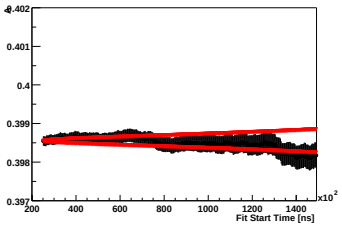

(f) A 18

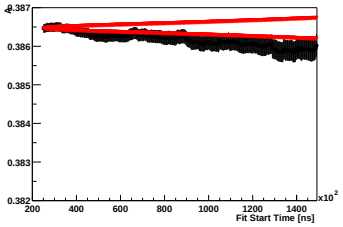

(g) A 19

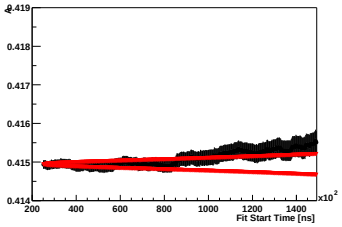

(h) A 21

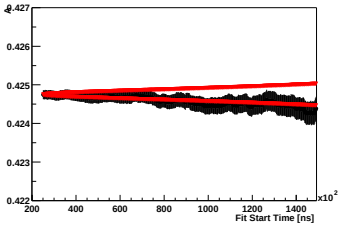

(i) A 22

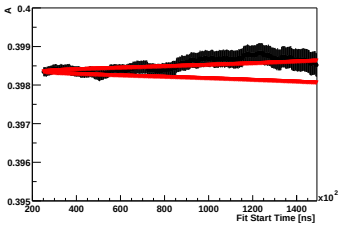

(j) A 23

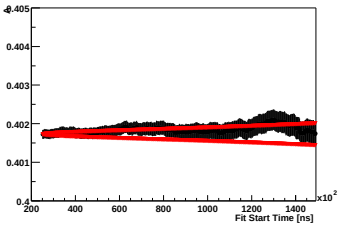

(k) A 24

Figure 16: Asymetry (3-parameter) versus fit start time for detectors 13-24. All data sets.

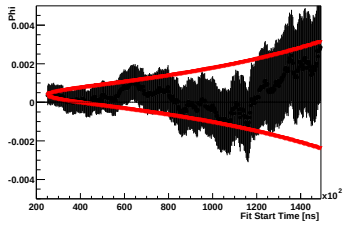

(a) Phase 1

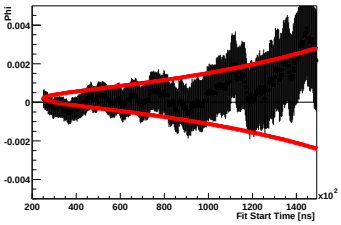

(b) Phase 2

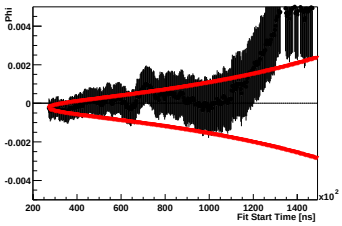

(c) Phase 3

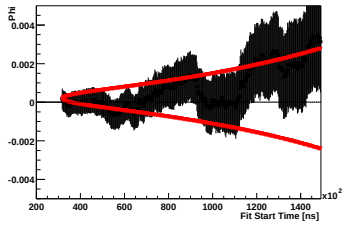

(d) Phase 4

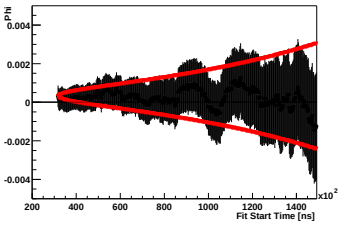

(e) Phase 5

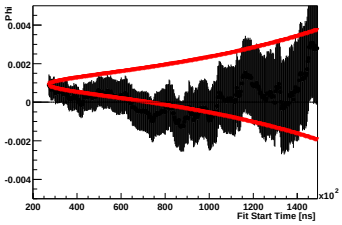

(f) Phase 6

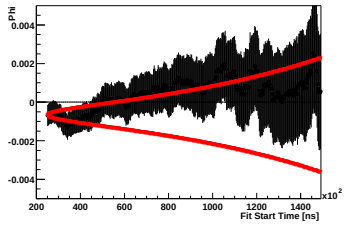

(g) Phase 7

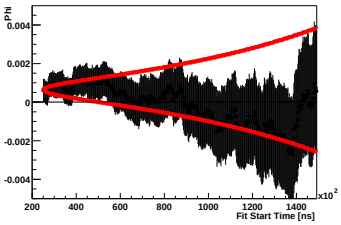

(h) Phase 8

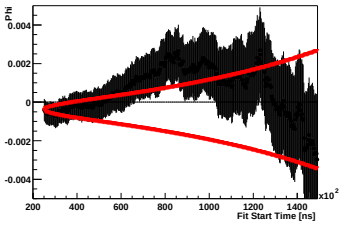

(i) Phase 9

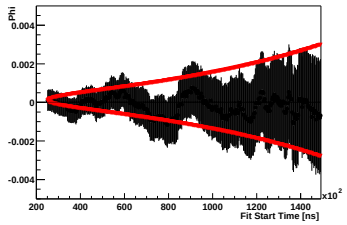

(j) Phase 10

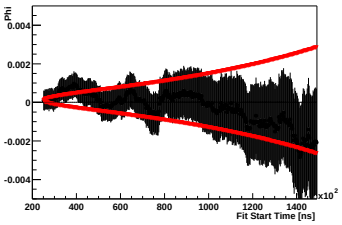

(k) Phase 11

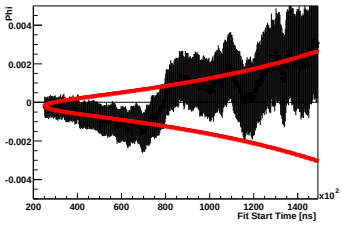

(l) Phase 12

Figure 17: Phase (3-parameter) versus fit start time for detectors 1-12. All data sets.

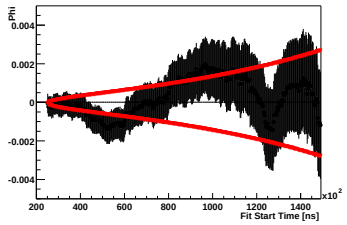

(a) Phase 13

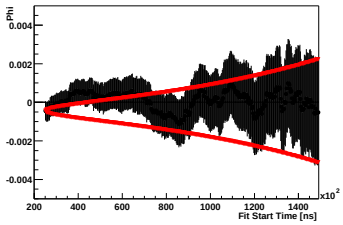

(b) Phase 14

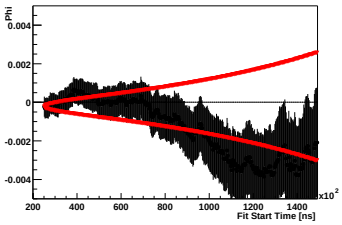

(c) Phase 15

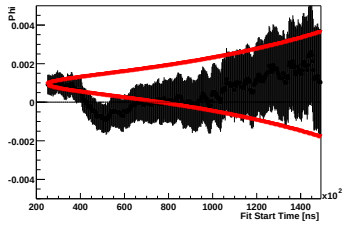

(d) Phase 16

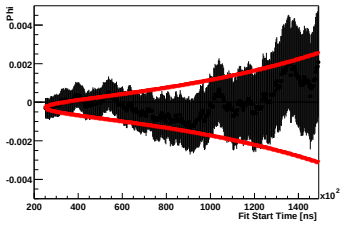

(e) Phase 17

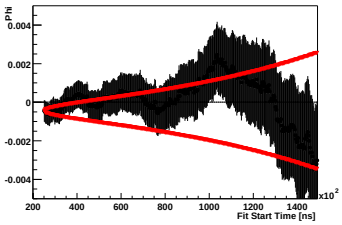

(f) Phase 18

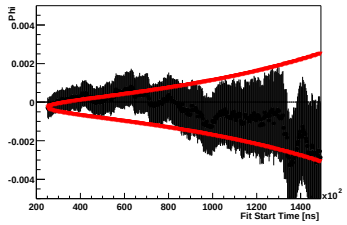

(g) Phase 19

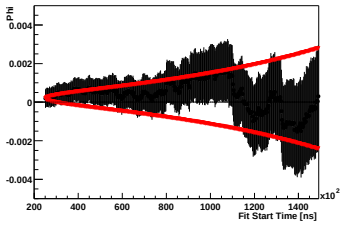

(h) Phase 21

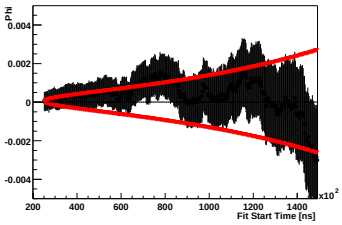

(i) Phase 22

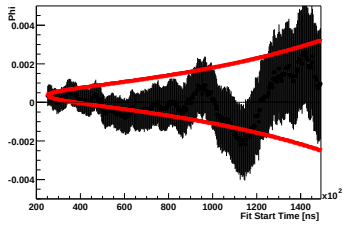

(j) Phase 23

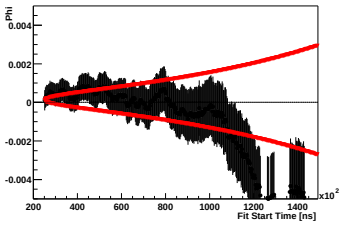

(k) Phase 24

Figure 18: Phase (3-parameter) versus fit start time for detectors 13-24. All data sets.

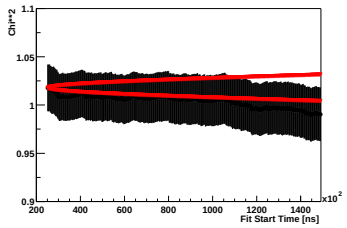

(a) χ^2/Ndf det 1

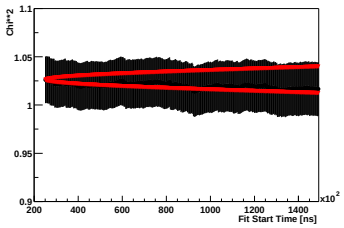

(b) χ^2/Ndf det 2

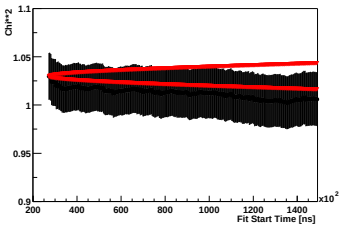

(c) χ^2/Ndf det 3

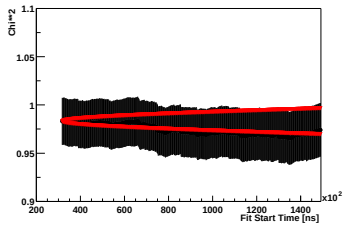

(d) χ^2/Ndf det 4

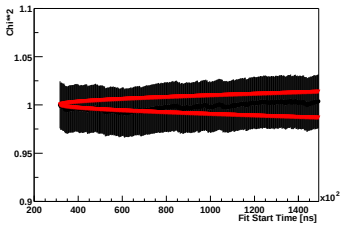

(e) χ^2/Ndf det 5

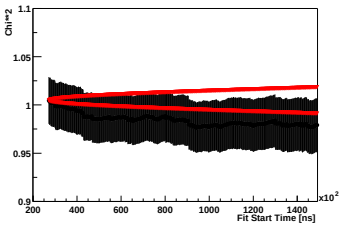

(f) χ^2/Ndf det 6

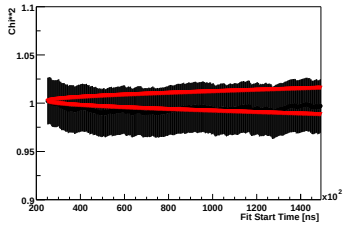

(g) χ^2/Ndf det 7

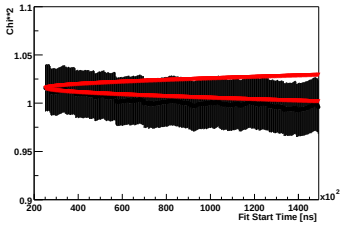

(h) χ^2/Ndf det 8

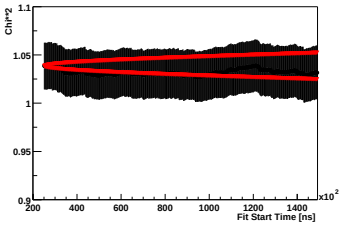

(i) χ^2/Ndf det 9

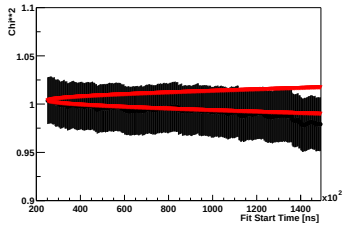

(j) χ^2/Ndf det 10

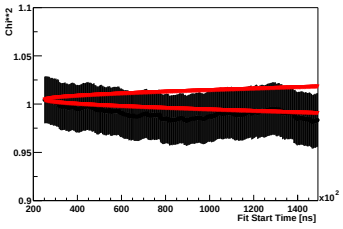

(k) χ^2/Ndf det 11

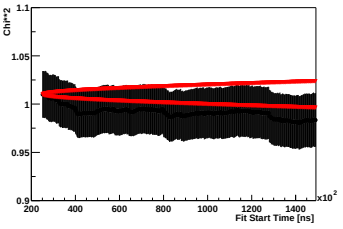

(l) χ^2/Ndf det 12

Figure 19: χ^2/Ndf (3-parameter) versus fit start time for detectors 1-12. All data sets.

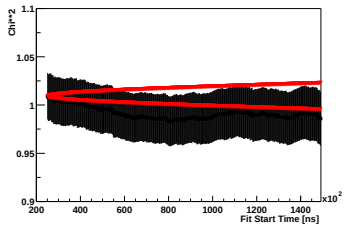

(a) χ^2/Ndf det 13

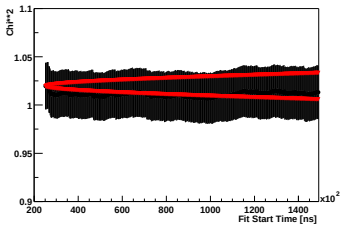

(b) χ^2/Ndf det 14

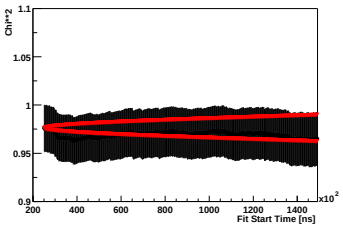

(c) χ^2/Ndf det 15

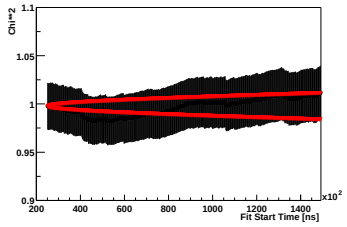

(d) χ^2/Ndf det 16

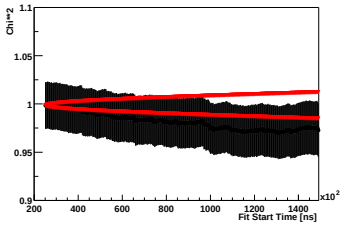

(e) χ^2/Ndf det 17

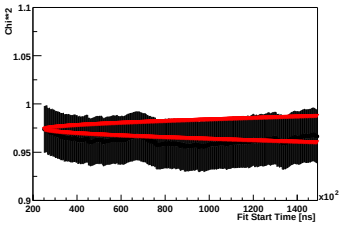

(f) χ^2/Ndf det 18

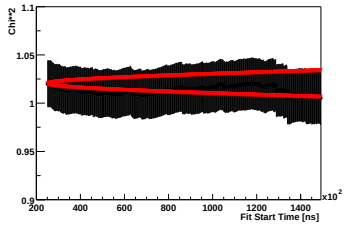

(g) χ^2/Ndf det 19

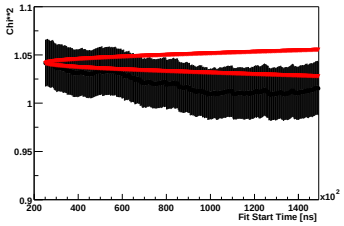

(h) χ^2/Ndf det 21

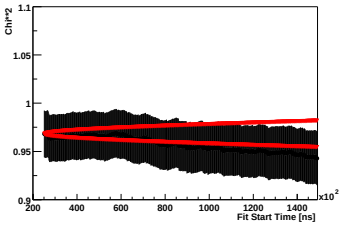

(i) χ^2/Ndf det 22

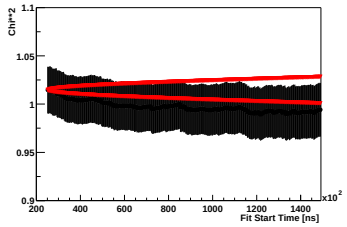

(j) χ^2/Ndf det 23

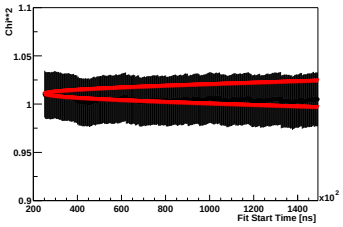

(k) χ^2/Ndf det 24

Figure 20: χ^2/Ndf (3-parameter) versus fit start time for detectors 13-24. All data sets.

The results for sum of 23 detectors is shown in Fig. 21.

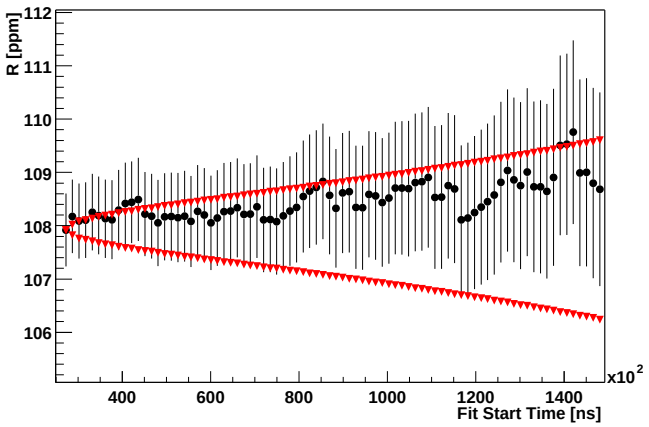

(a) R

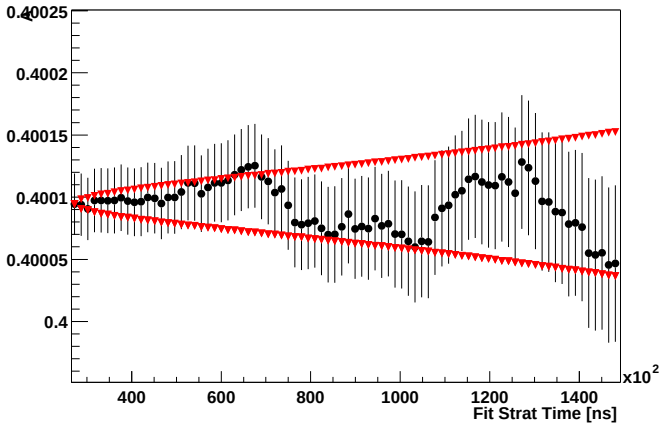

(b) A

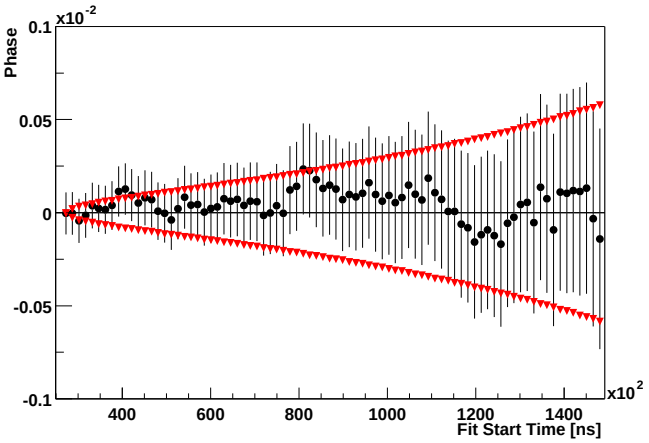

(c) Phase

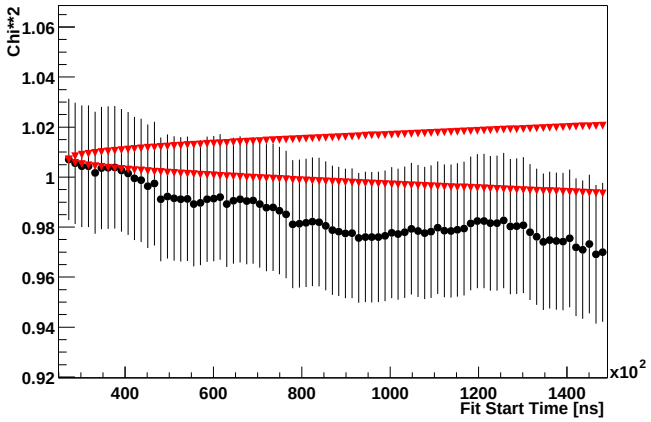

(d) χ^2/Ndf

Figure 21: R (3 par.) (top left), asymetry (top right), phase (bottom left) and χ^2/Ndf (bottom right) versus fit start time for sum of 23 detectors (all data sets).

Results for the sum of 23 detectors (low n data set) is shown in Fig. 22.

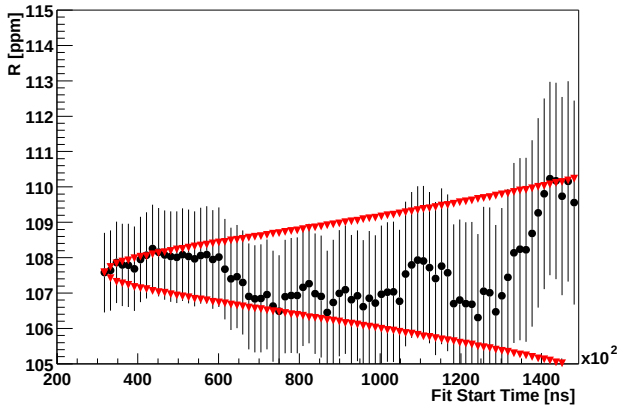

(a) R

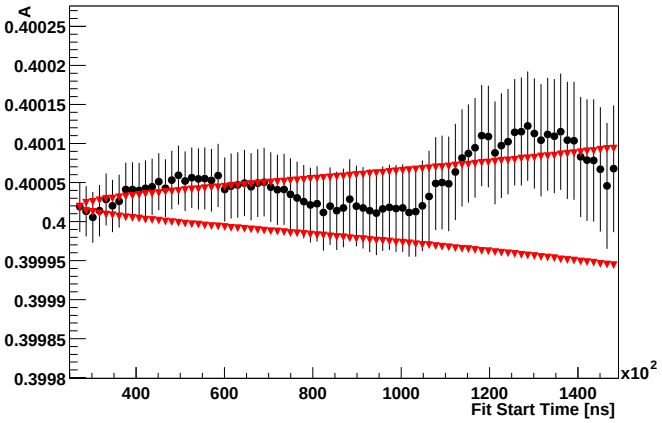

(b) A

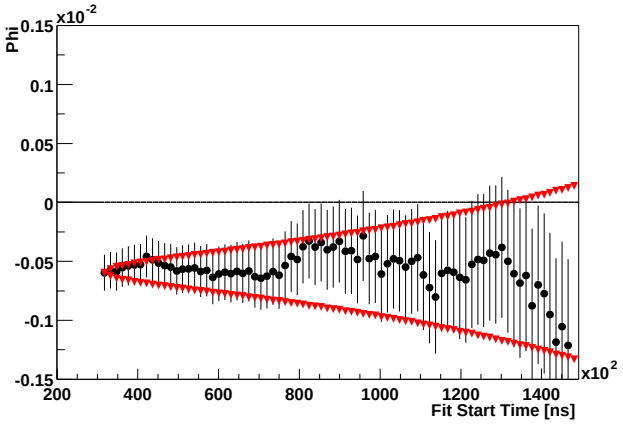

(c) Phase

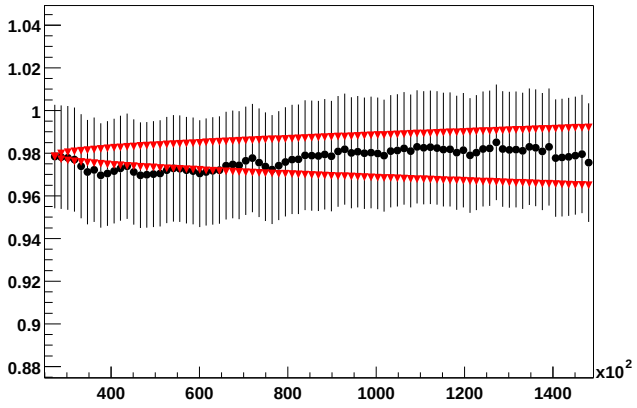

(d) χ^2/Ndf

Figure 22: R (3 par.) (top left), asymetry (top right), phase (bottom left) and χ^2/Ndf (bottom right) versus fit start time for sum of 23 detectors (low n data).

Results for the sum of 23 detectors (high n data set) is shown in Fig. 23.

For comparison purpose R for gain corrected and not corrected data are plotted in Figs. 24-27.

Asymetry for each detector before and after gain correction was plotted in Figs. 28-31 as a function of fit start time.

Phase for each detector before and after gain correction were plotted in Figs. 32-35 as a function of fit start time.

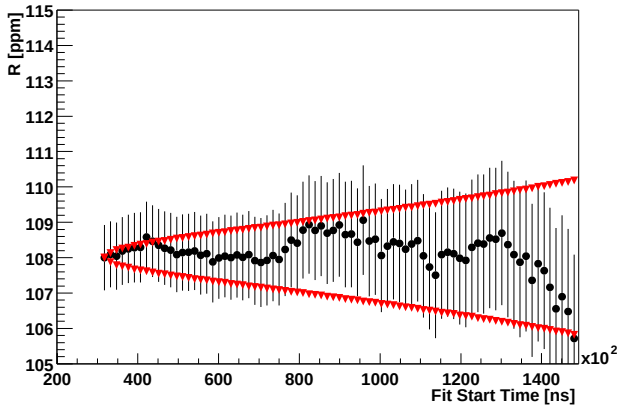

(a) R

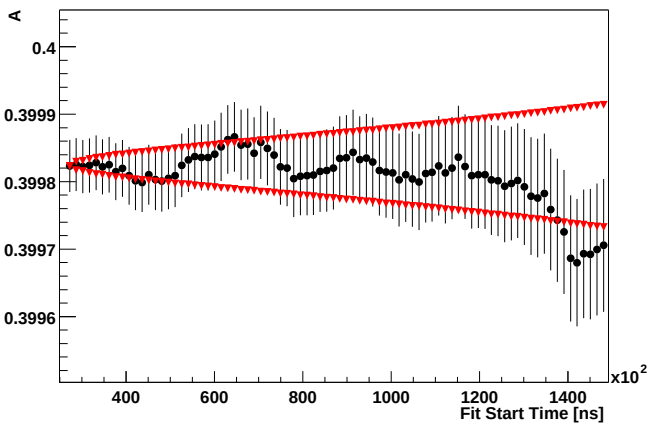

(b) A

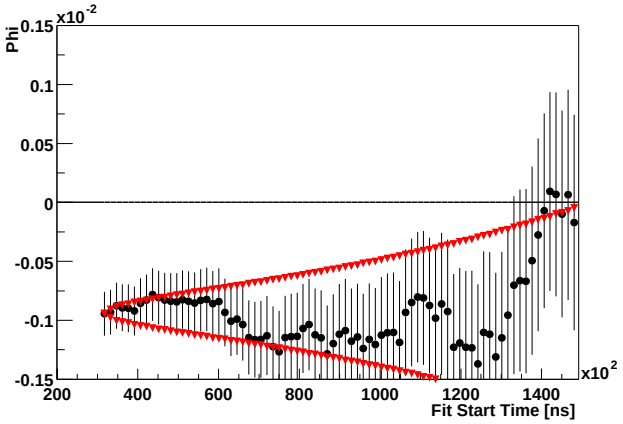

(c) Phase

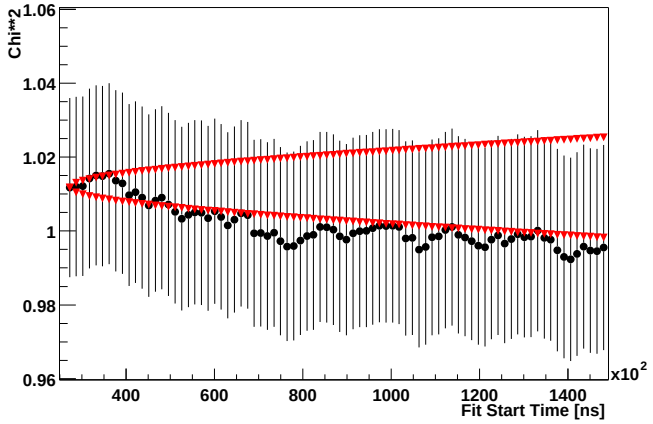

(d) χ^2/Ndf

Figure 23: R (3 par.) (top left), asymetry (top right), phase (bottom left) and χ^2/Ndf (bottom right) versus fit start time for sum of 23 detectors (high n data).

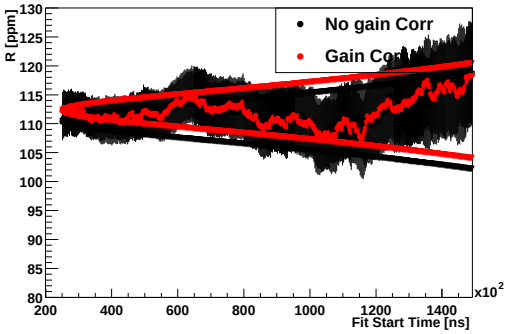

(a) R det 1

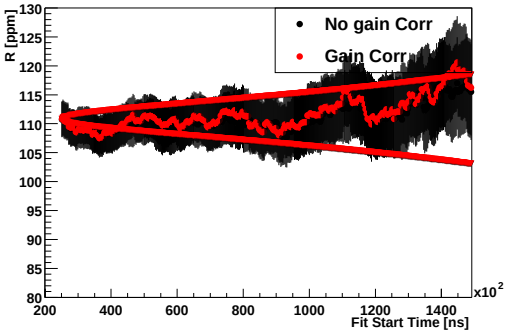

(b) R det 2

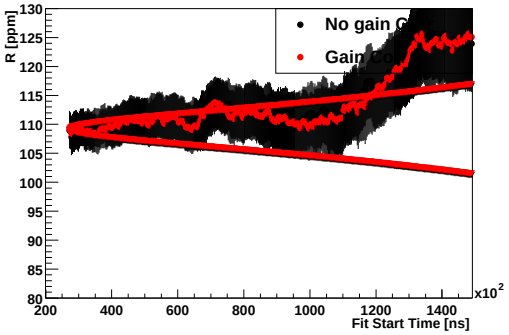

(c) R det 3

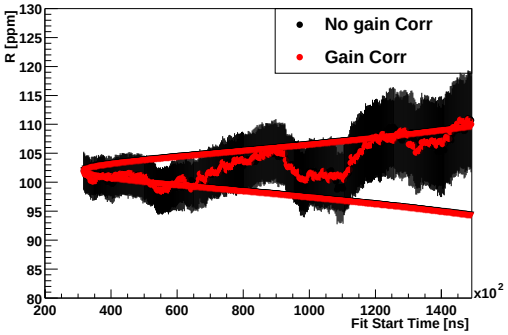

(d) R det 4

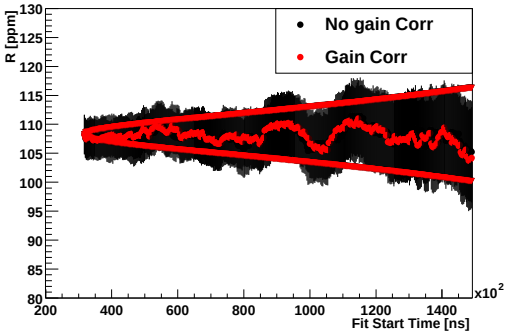

(e) R det 5

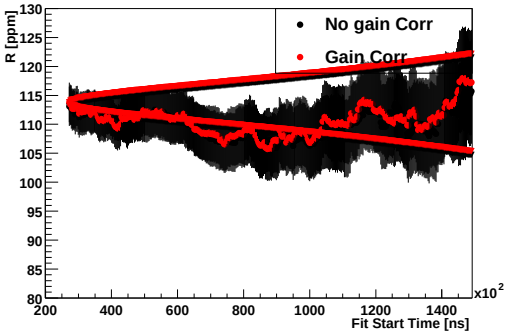

(f) R det 6

Figure 24: R versus Fit Start time. Detectors 1-6

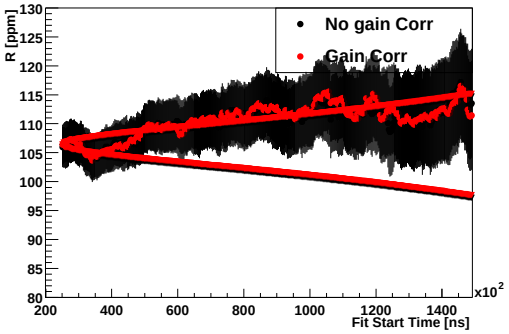

(a) R det 7

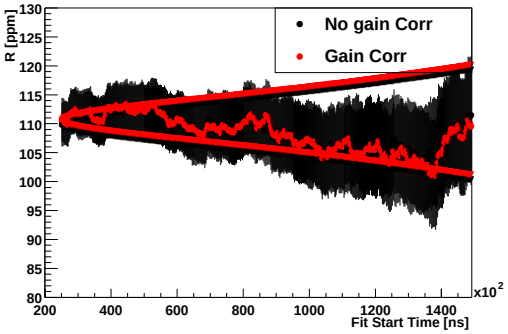

(b) R det 8

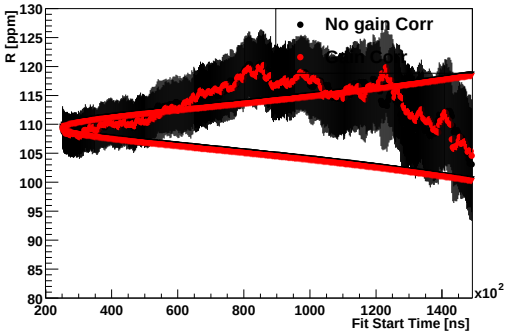

(c) R det 9

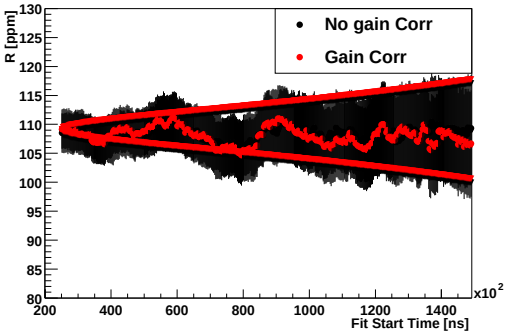

(d) R det 10

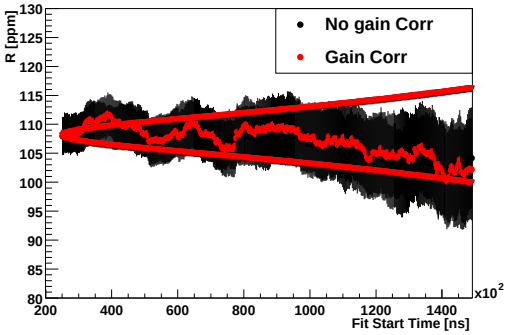

(e) R det 11

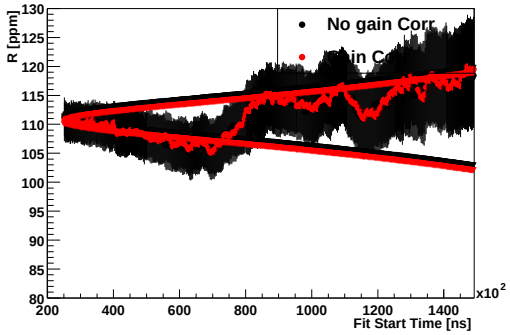

(f) R det 12

Figure 25: R versus Fit Start time. Detectors 7-12

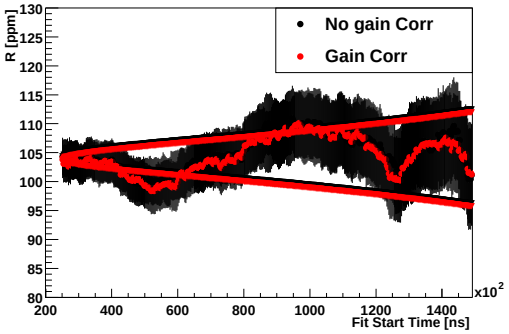

(a) R det 13

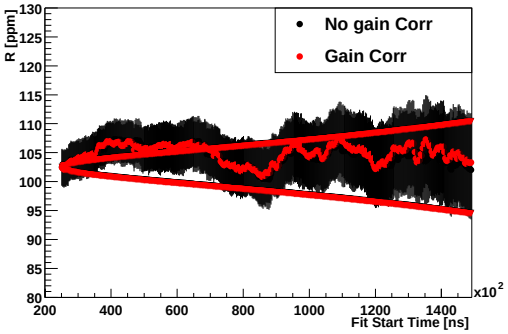

(b) R det 14

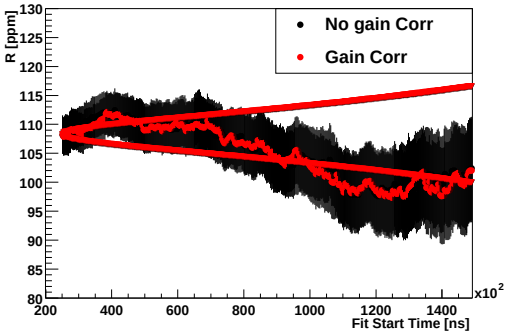

(c) R det 15

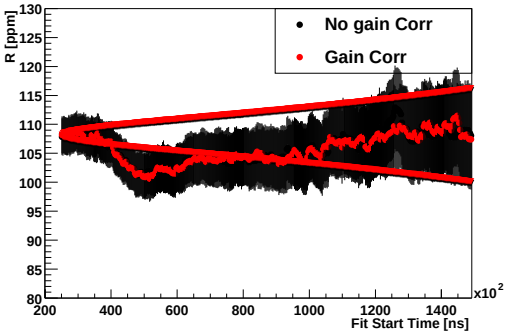

(d) R det 16

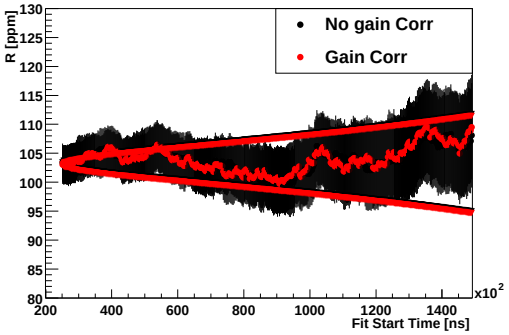

(e) R det 17

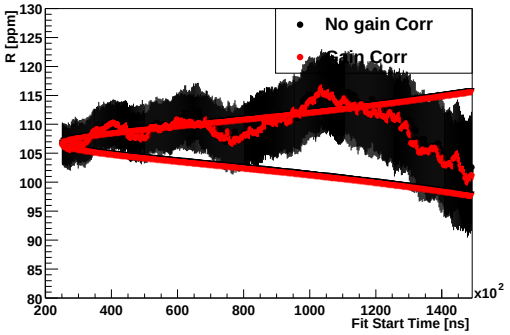

(f) R det 18

Figure 26: R versus Fit Start time. Detectors 13-18

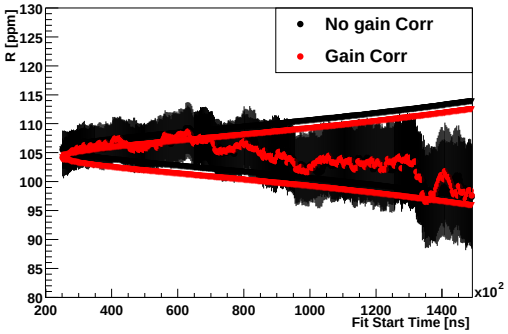

(a) R det 19

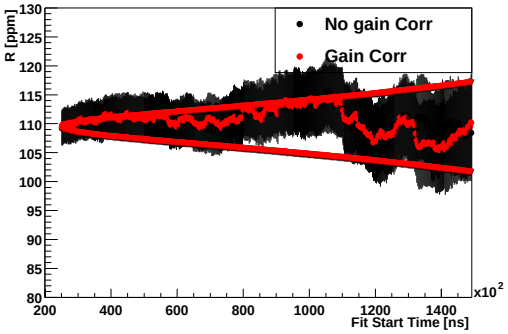

(b) R det 21

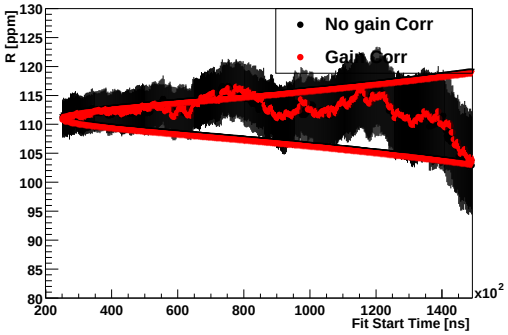

(c) R det 22

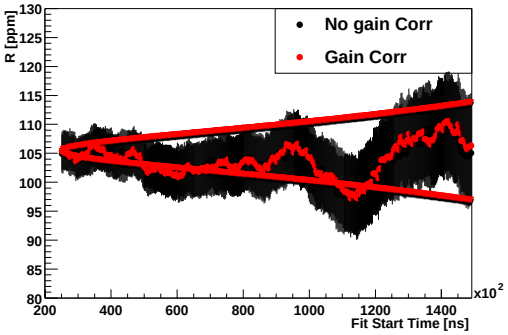

(d) R det 23

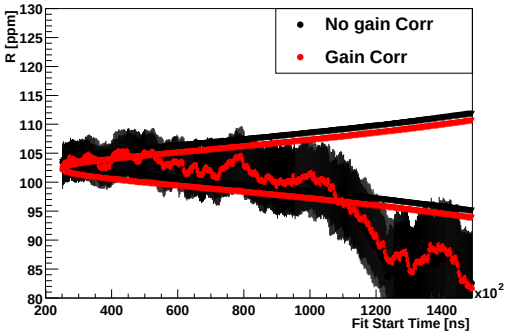

(e) R det 24

Figure 27: R versus Fit Start time. Detectors 19-24

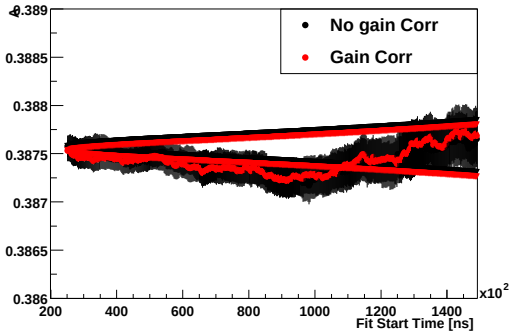

(a) A det 1

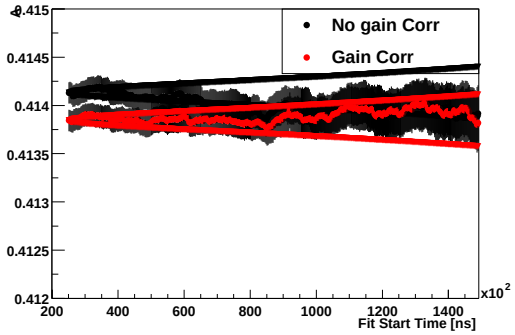

(b) A det 2

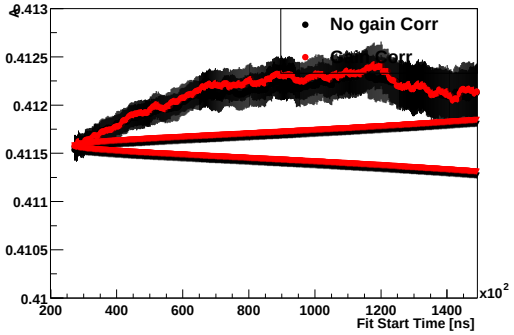

(c) A det 3

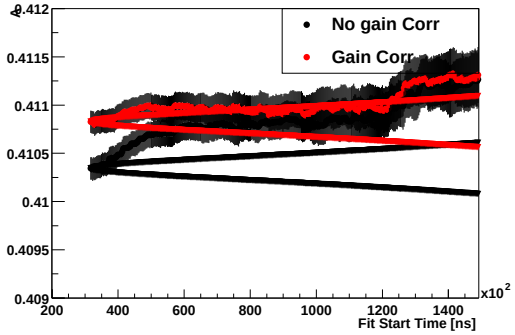

(d) A det 4

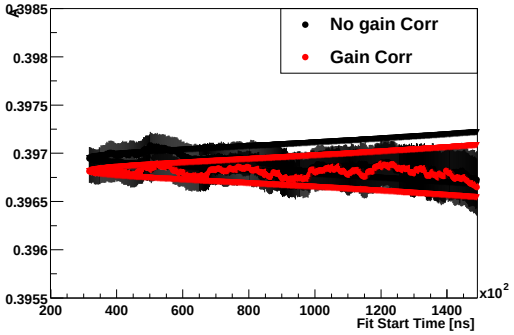

(e) A det 5

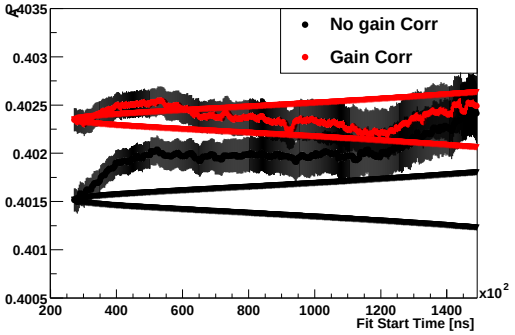

(f) A det 6

Figure 28: A versus Fit Start time. Detectors 1-6

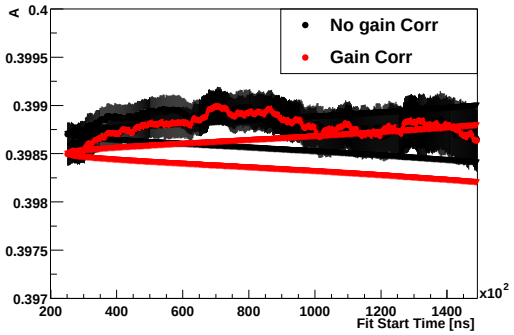

(a) A det 7

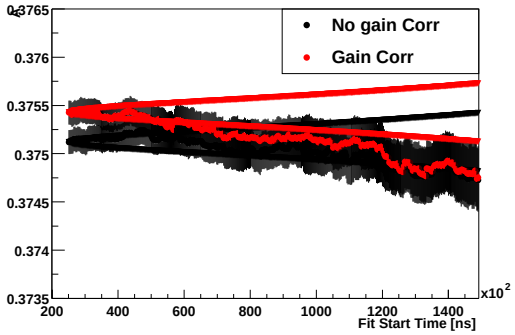

(b) A det 8

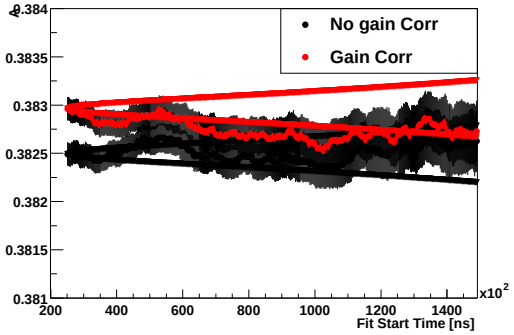

(c) A det 9

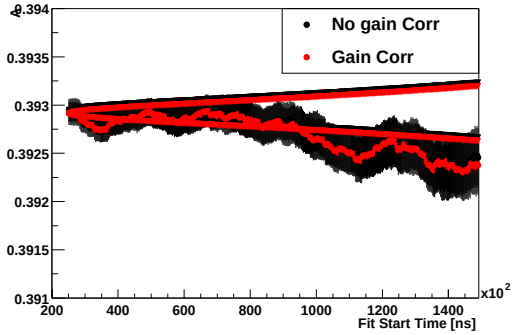

(d) A det 10

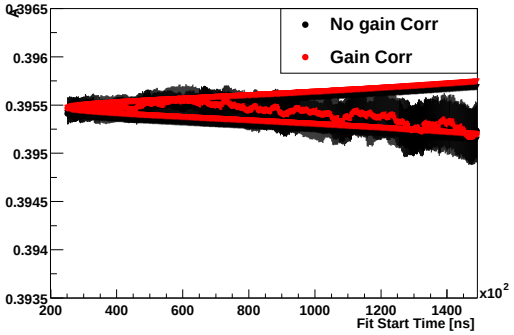

(e) A det 11

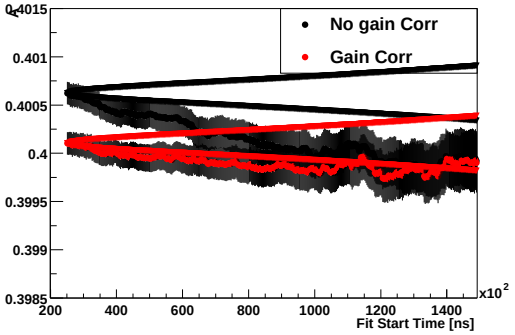

(f) A det 12

Figure 29: A versus Fit Start time. Detectors 7-12

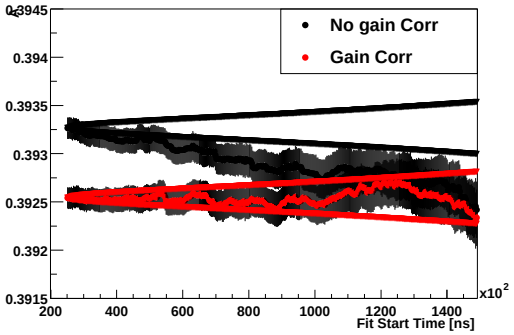

(a) A det 13

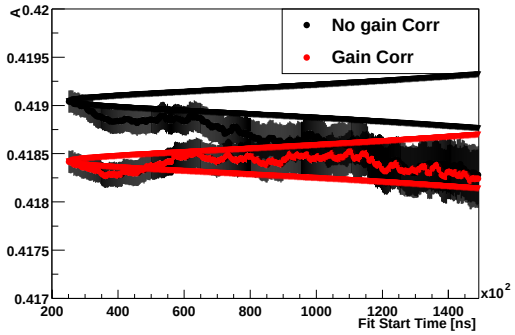

(b) A det 14

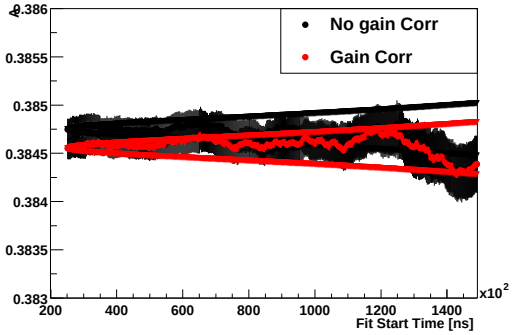

(c) A det 15

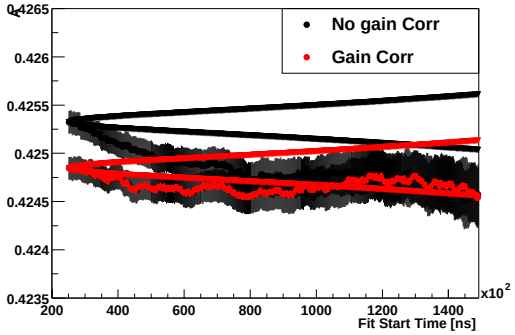

(d) A det 16

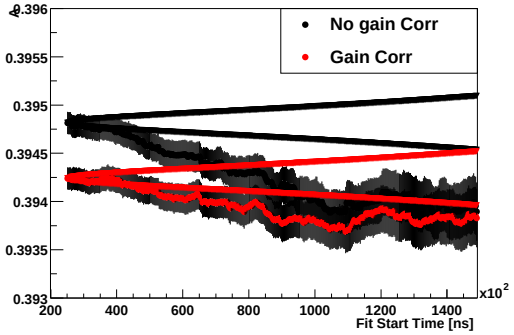

(e) A det 17

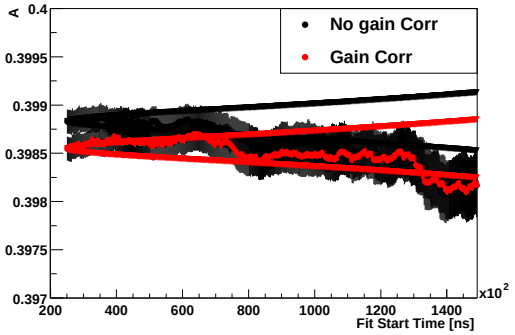

(f) A det 18

Figure 30: A versus Fit Start time. Detectors 13-18

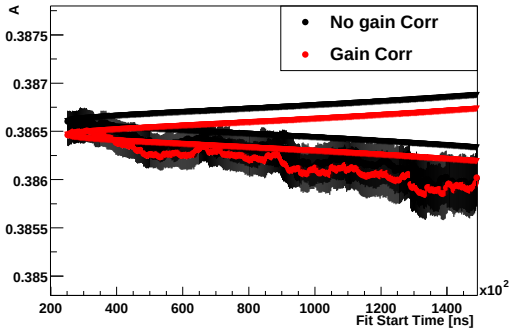

(a) A det 19

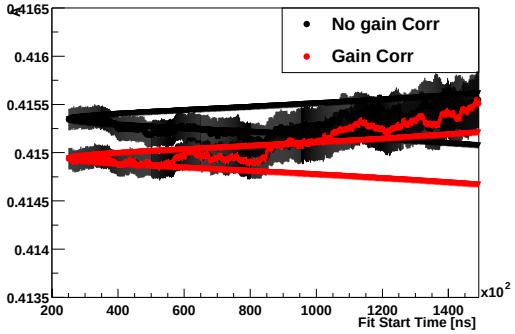

(b) A det 21

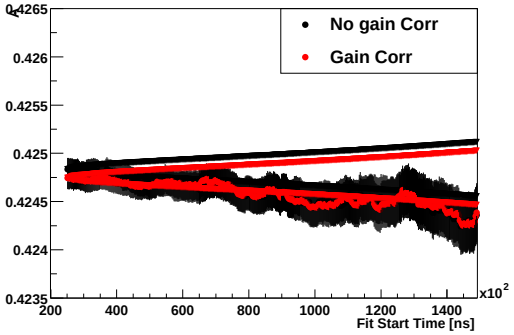

(c) A det 22

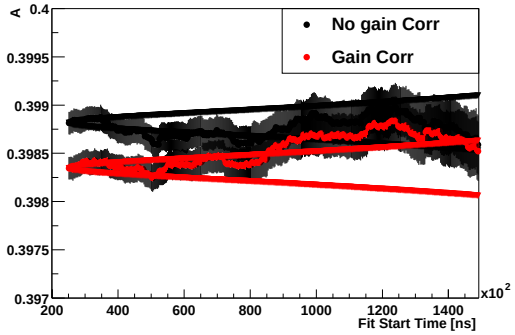

(d) A det 23

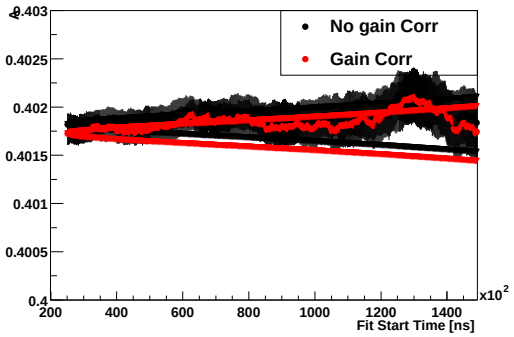

(e) A det 24

Figure 31: A versus Fit Start time. Detectors 19-24

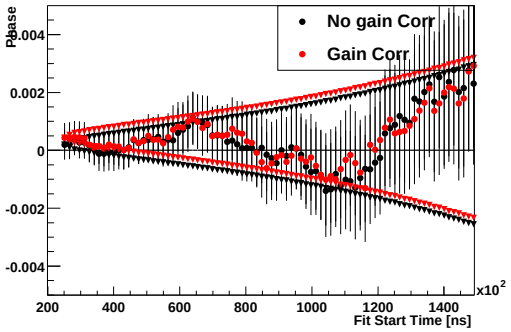

(a) Phi det 1

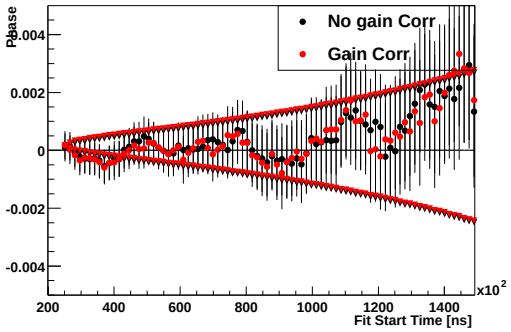

(b) Phi det 2

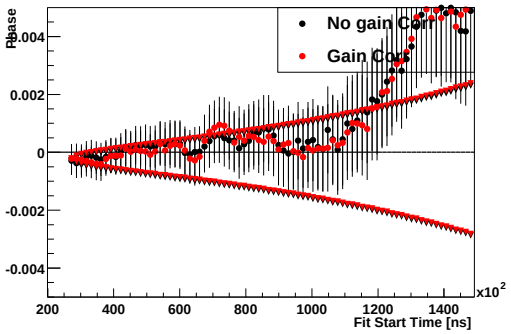

(c) Phi det 3

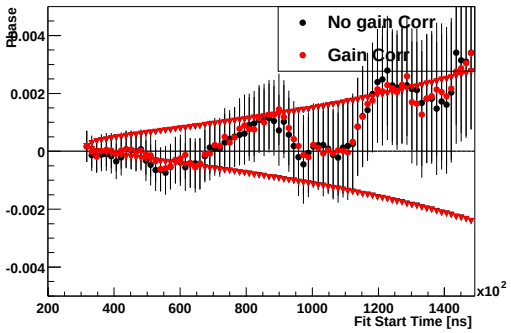

(d) Phi det 4

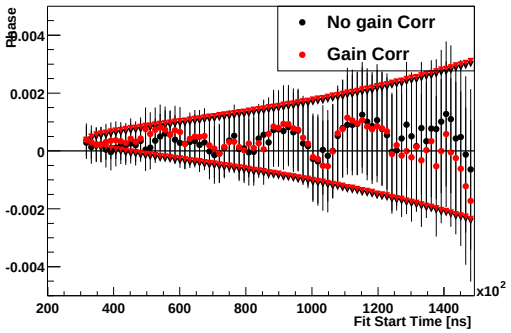

(e) Phi det 5

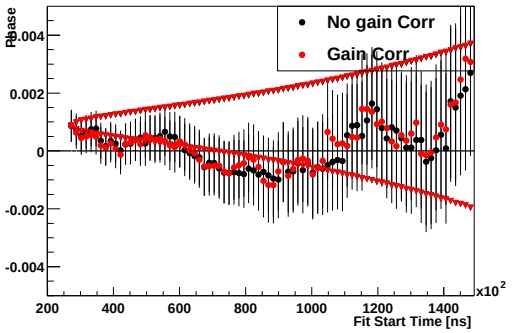

(f) Phi det 6

Figure 32: Phi versus Fit Start time. Detectors 1-6

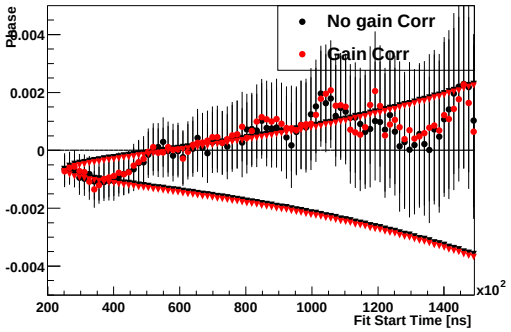

(a) Phi det 7

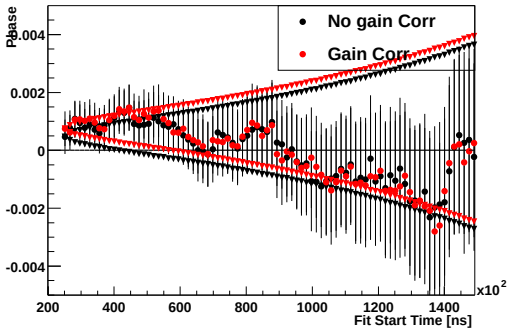

(b) Phi det 8

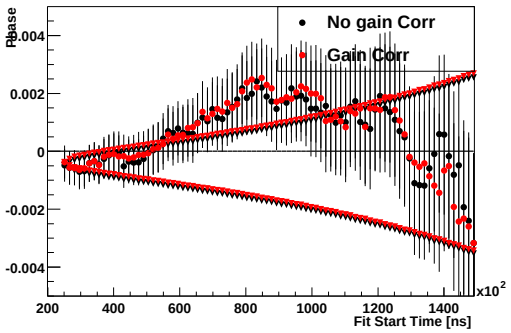

(c) Phi det 9

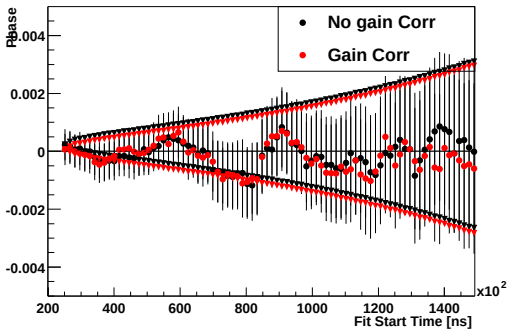

(d) Phi det 10

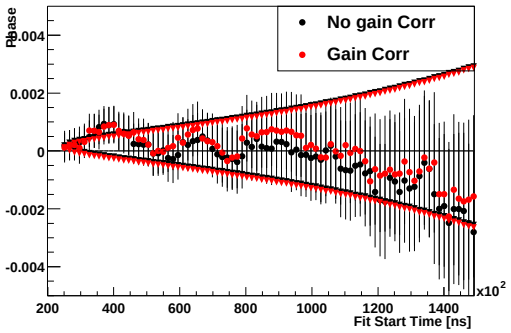

(e) Phi det 11

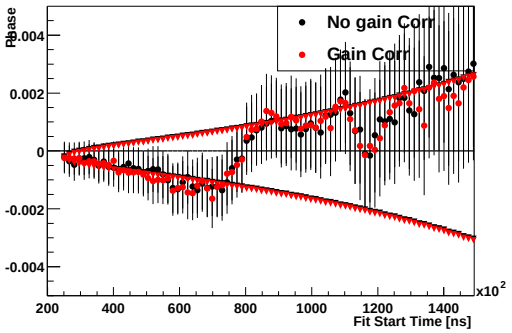

(f) Phi det 12

Figure 33: Phi versus Fit Start time. Detectors 7-12

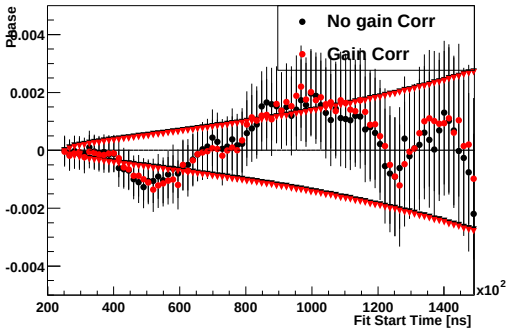

(a) Phi det 13

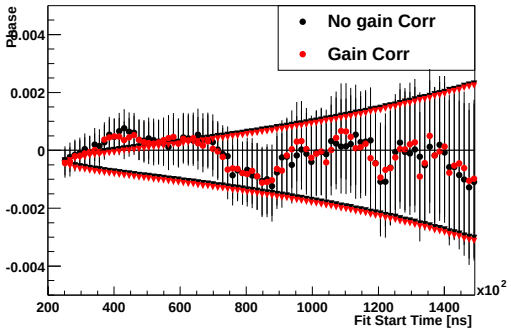

(b) Phi det 14

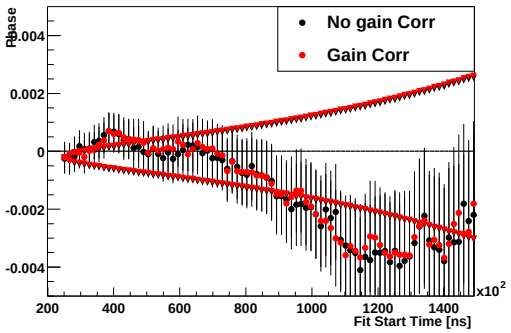

(c) Phi det 15

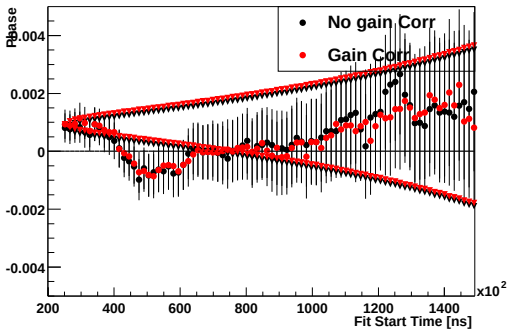

(d) Phi det 16

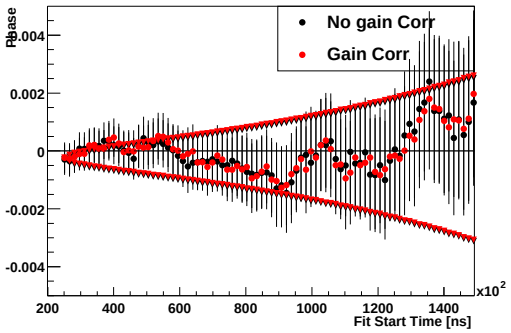

(e) Phi det 17

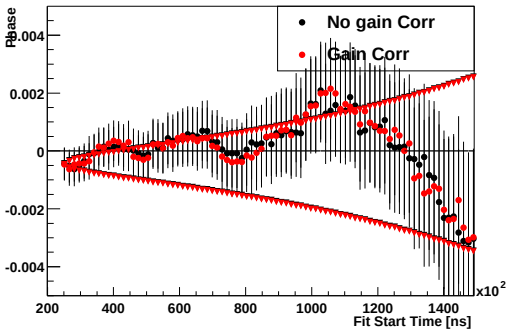

(f) Phi det 18

Figure 34: Phi versus Fit Start time. Detectors 13-18

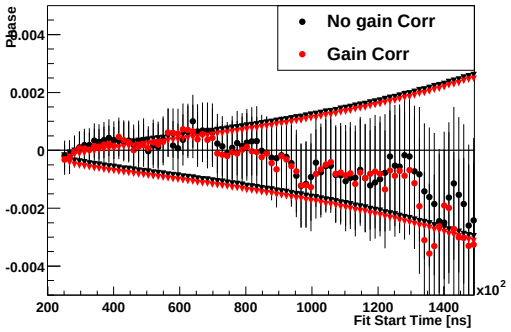

(a) Phi det 19

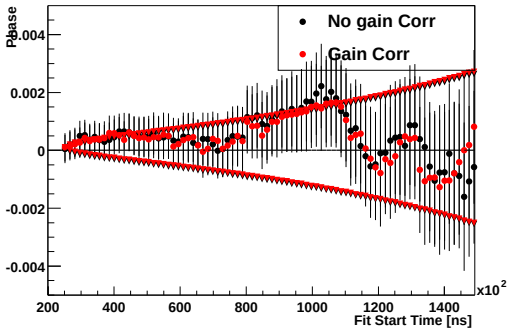

(b) Phi det 21

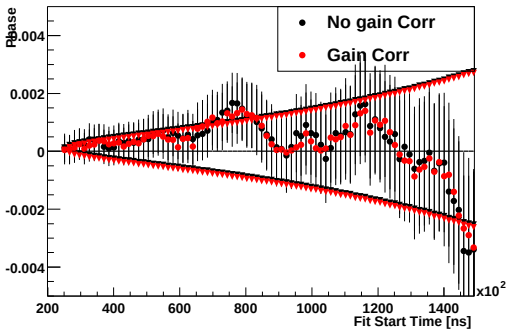

(c) Phi det 22

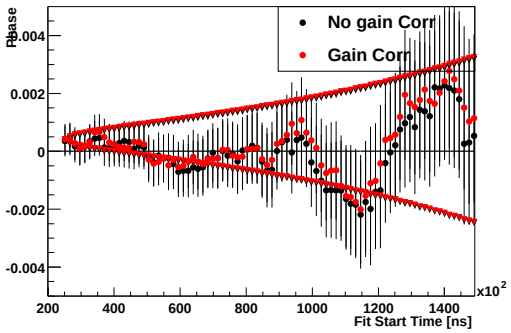

(d) Phi det 23

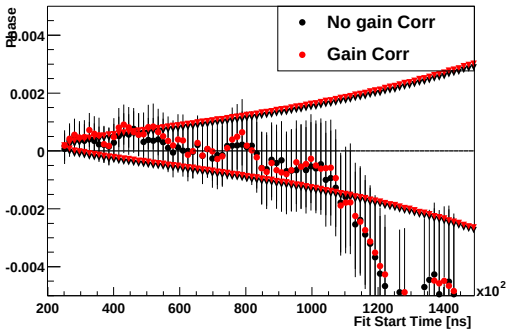

(e) Phi det 24

Figure 35: Phi versus Fit Start time. Detectors 19-24

χ^2/Ndf for each detector before and after gain correction were plotted in Figs. 36-39 as a function of fit start time.

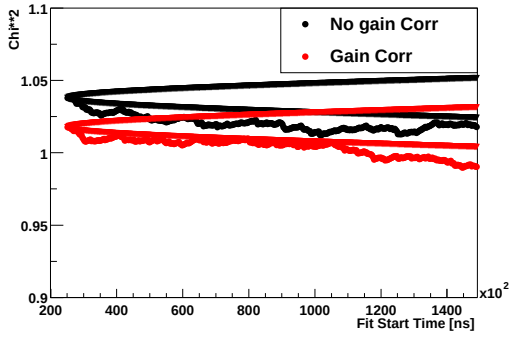

(a) det 1

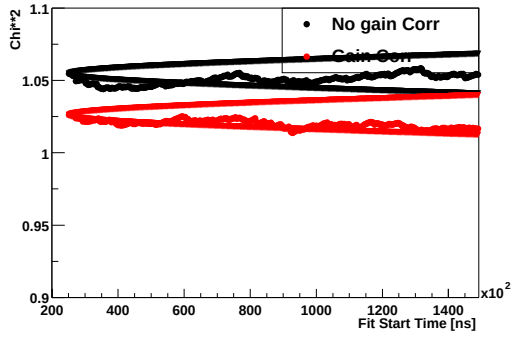

(b) det 2

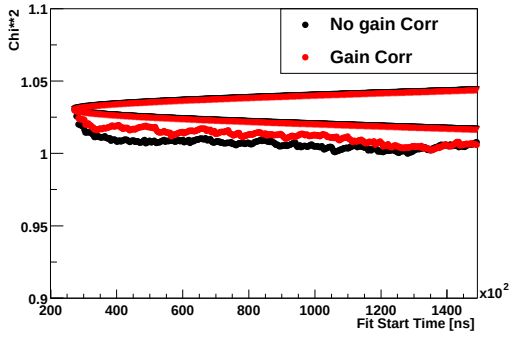

(c) det 3

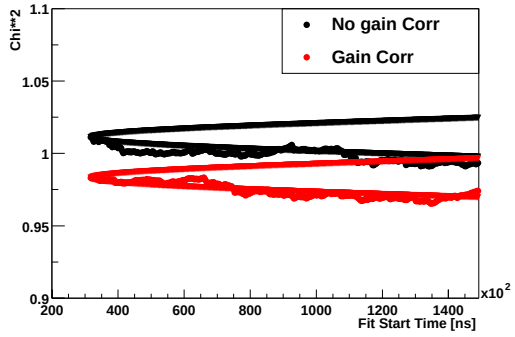

(d) det 4

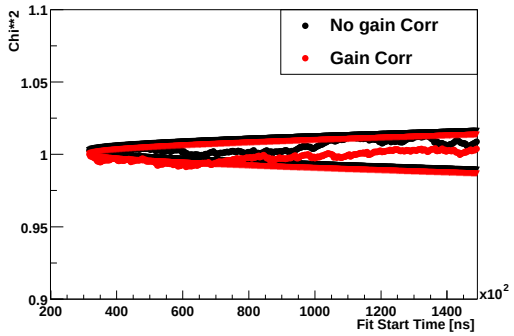

(e) det 5

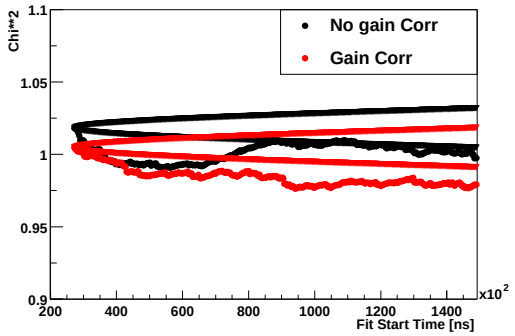

(f) det 6

Figure 36: χ^2/Ndf versus Fit Start time. Detectors 1-6

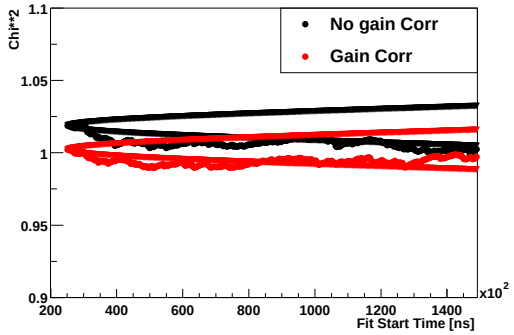

(a) χ^2/Ndf det 7

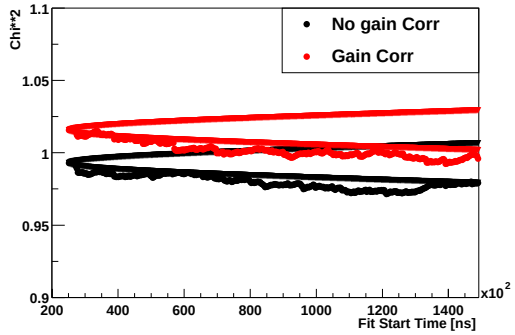

(b) χ^2/Ndf det 8

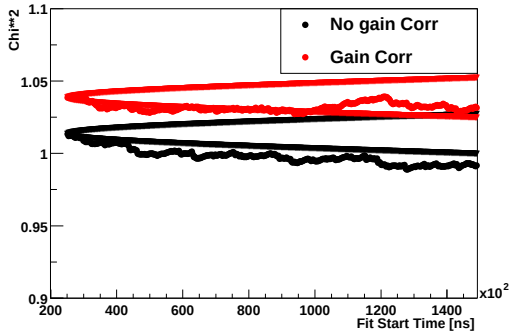

(c) χ^2/Ndf det 9

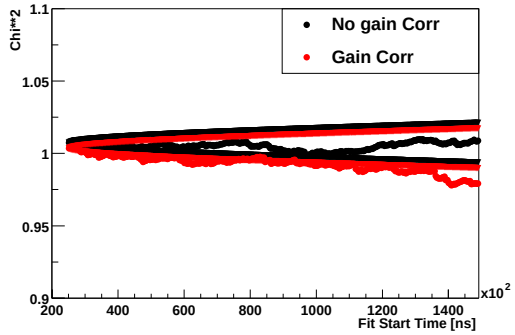

(d) χ^2/Ndf det 10

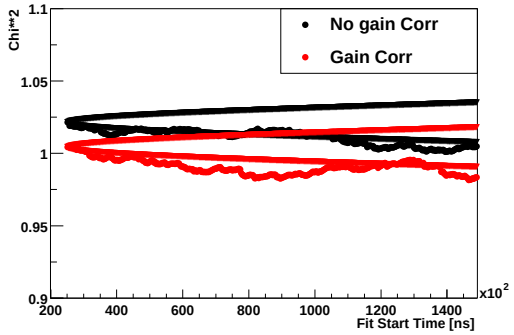

(e) χ^2/Ndf det 11

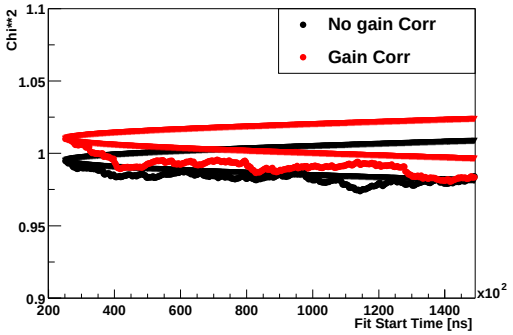

(f) χ^2/Ndf det 12

Figure 37: χ^2/Ndf versus Fit Start time. Detectors 7-12

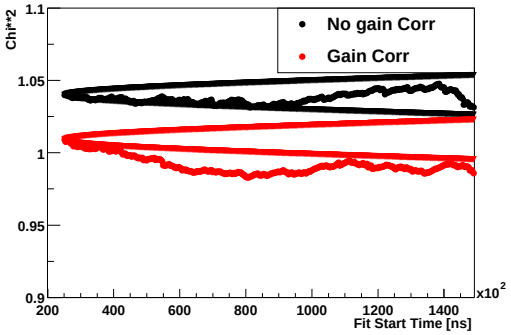

(a) χ^2/Ndf det 13

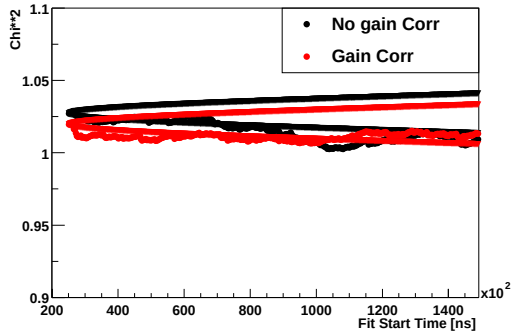

(b) χ^2/Ndf det 14

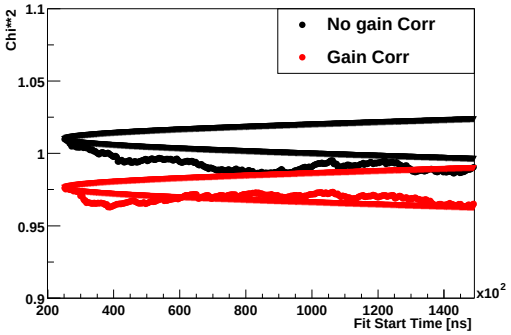

(c) χ^2/Ndf det 15

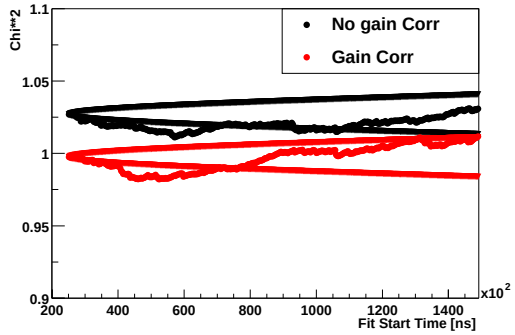

(d) χ^2/Ndf det 16

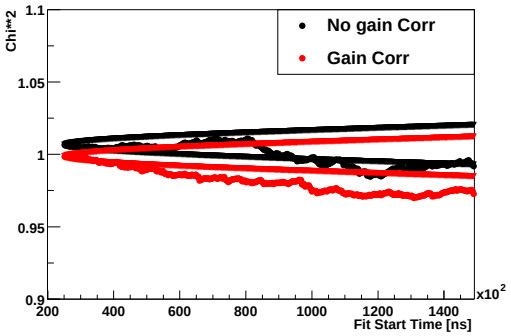

(e) χ^2/Ndf det 17

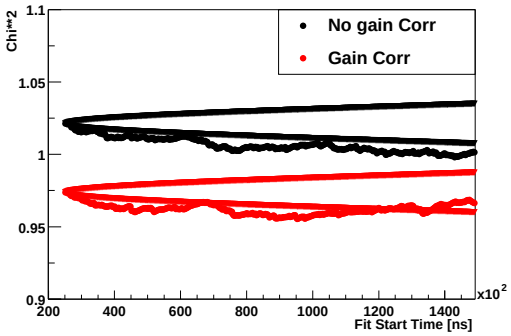

(f) χ^2/Ndf det 18

Figure 38: χ^2/Ndf versus Fit Start time. Detectors 13-18

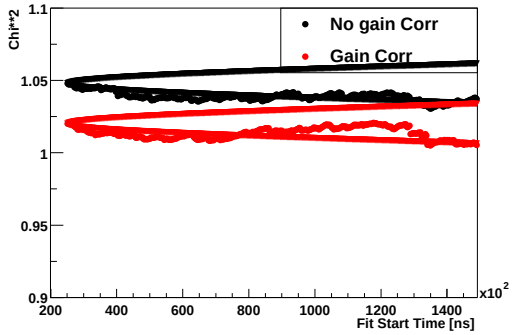

(a) χ^2/Ndf det 19

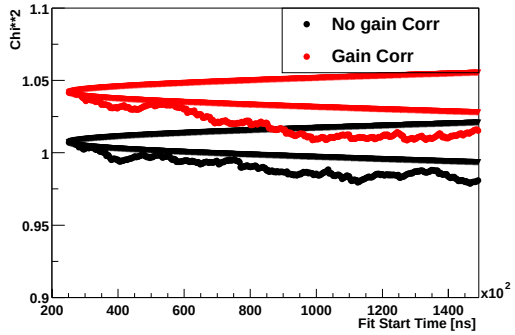

(b) χ^2/Ndf det 21

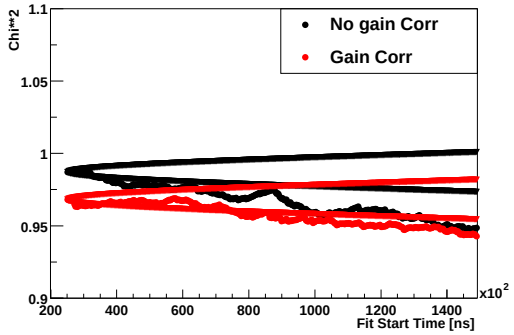

(c) χ^2/Ndf det 22

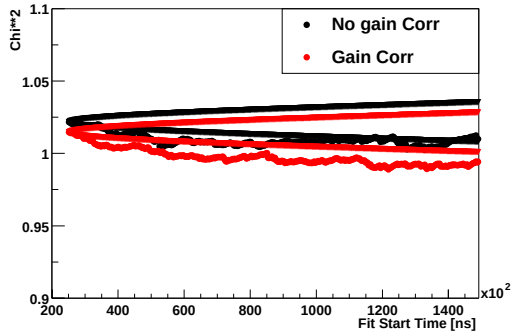

(d) χ^2/Ndf det 23

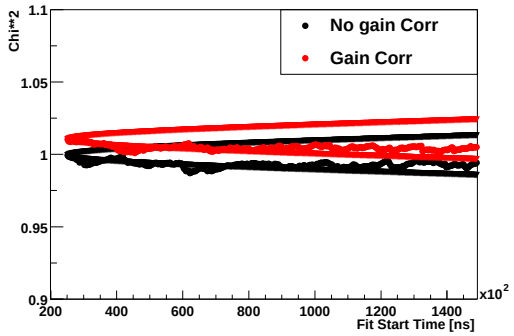

(e) χ^2/Ndf det 24

Figure 39: χ^2/Ndf versus Fit Start time. Detectors 19-24

R, A and χ^2/Ndf (3 parameter ratio fit function) for the sum of 23 detectors are shown in Fig. 40

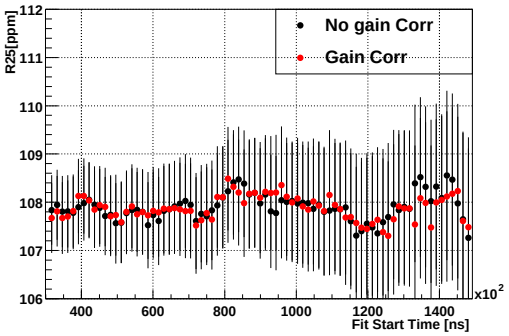

(a) $R25$

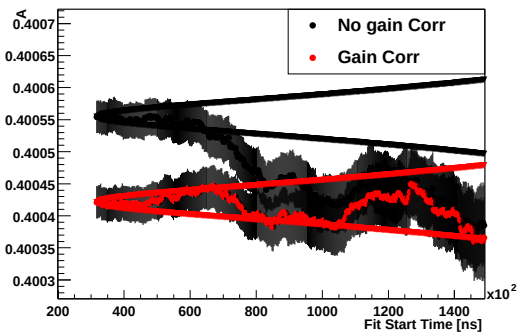

(b) A

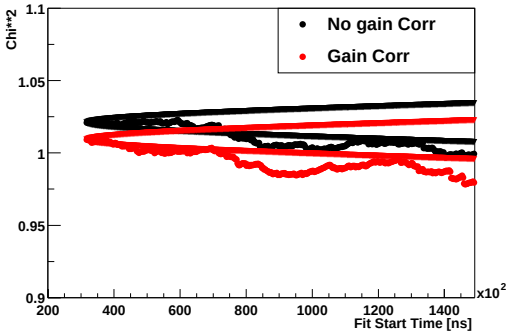

(c) χ^2/Ndf

Figure 40: R, A and χ^2/Ndf (3 par) versus Fit Start Tine. Detector 25.

R values for the sum of 23 detectors, first half (detectors 1-12) and second half (detectors 13-24) of the ring (low n) are shown in Fig. 41. The value of half-ring effect amplitude is close to 1.5 ppm.

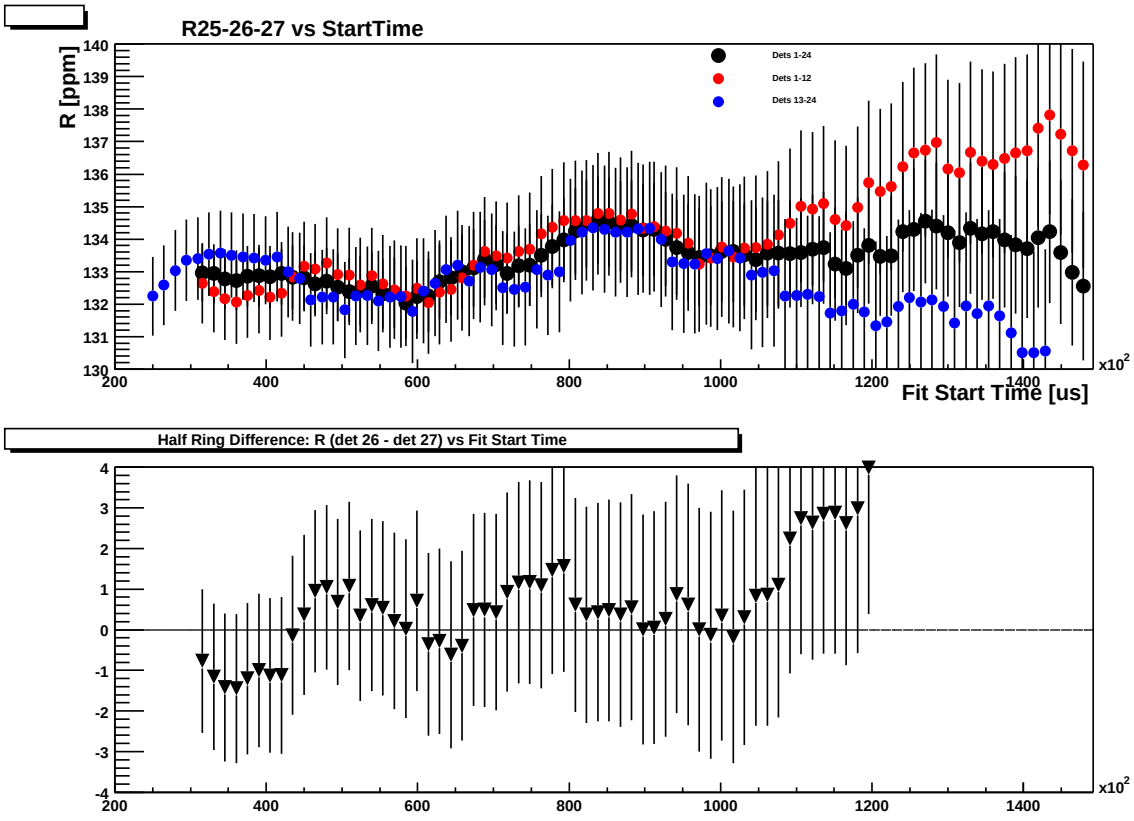

Figure 41: R (3 par.) for the sum of 23 detectors (black points), first (red) and second (blue) halves of the ring versus fit start time (low n).

R values for the sum of 23 detectors, first half (detectors 1-12) and second half (detectors 13-24) of the ring (high n) are shown in Fig. 42. The half-ring effect amplitude is close to 1.8 ppm.

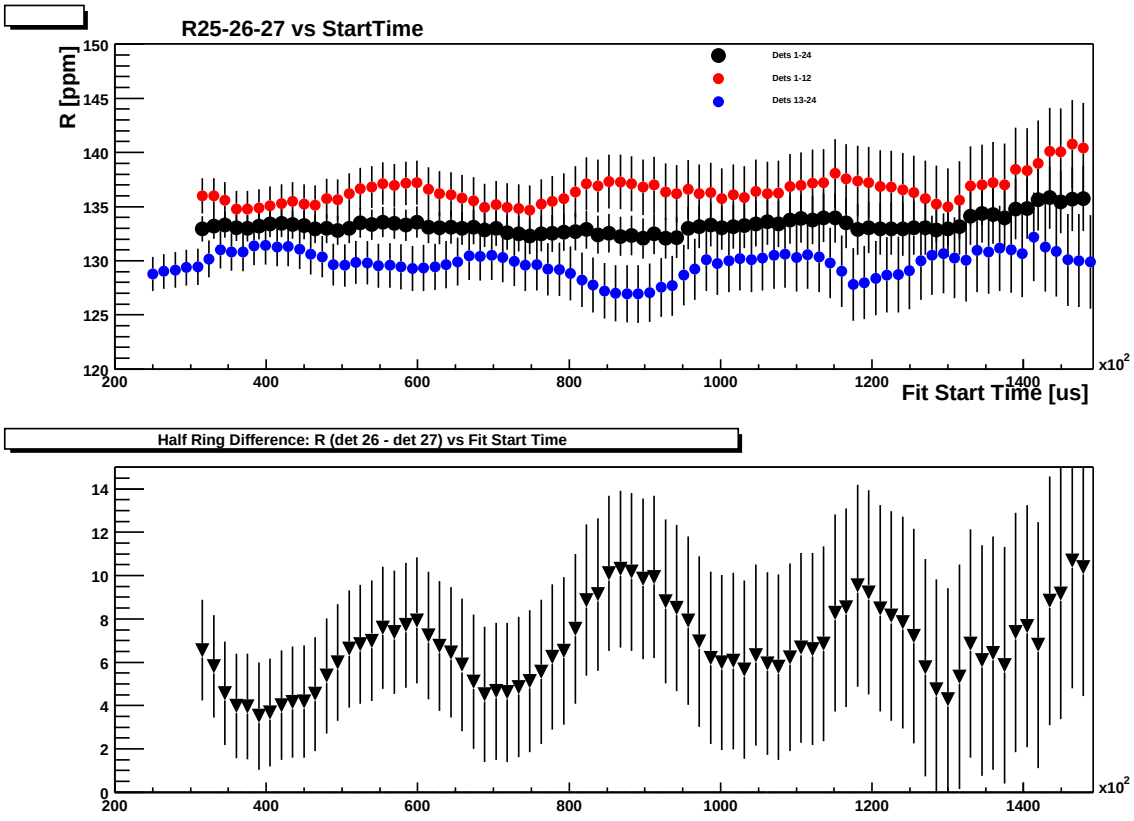

Figure 42: R (3 par) for the sum of 23 detectors (black points), first (red) and second (blue) halves of the ring versus fit start time (high n).

R value for 3-parameter fit of the sum of 23 detectors (low and high n data sets together) is shown in Fig. 43 versus fit start time. This plot clear demonstrates the additional benefit of adding all data sets together. The R variations for low and high n data sets are opposite in phase. So, combined data looks more stable versus fit start time. The same effect was seen for Monte-Carlo simulated data. See appropriat Sec. below.

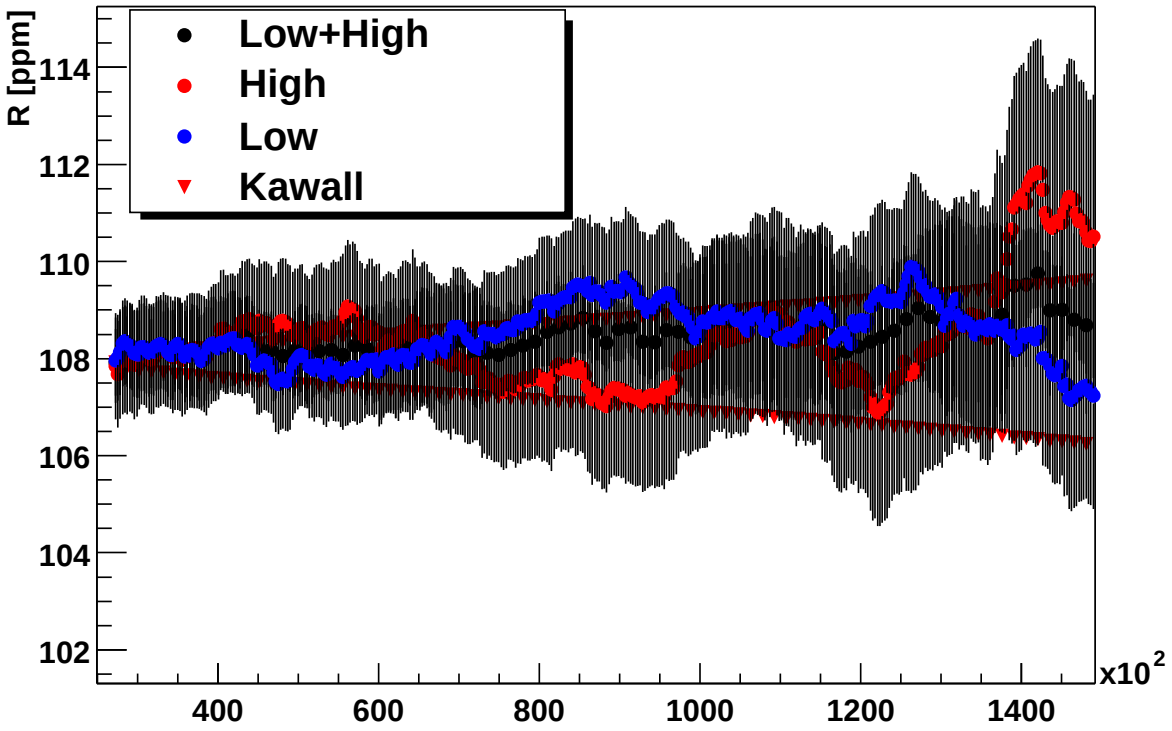

Figure 43: R(3-parameter) versus fit start time for sum of 23 detectors. Low n, high n and combined data sets are shown. Kawall 1σ band for the sum of 23 detectors is shown.

3.4 Results versus detector

In this section, 3-parameter fit results are presented by plotting fit returned values versus detector number. Figs. 44, 45, and 46 show the behavior of R, asymetry and phase across detectors, taken at 31.7 μs for all data sets, low and high n data respectively.

The effect of the CBO is demonstrated in the sinusoidal variation in R values across detectors, the so-called half-ring effect.

Note here that the amplitude of the halfring effect is 0.8 ppm for all data sets combined.

In Fig. 44, the χ^2/Ndf distributions at 31.7 μs are plotted versus detector and fitted to a constant.

Fig. 45 shows R, asymmetry, phase and χ^2/Ndf plotted versus detector at 31.7 μs for the low n data. The spread in A distribution reflects the fact that I do not fix the asymmetry to a particular value when performing my endpoint energy calibration.

Fig. 46 shows R, asymmetry, phase and χ^2/Ndf plotted versus detector at 31.7 μs for the high n data.

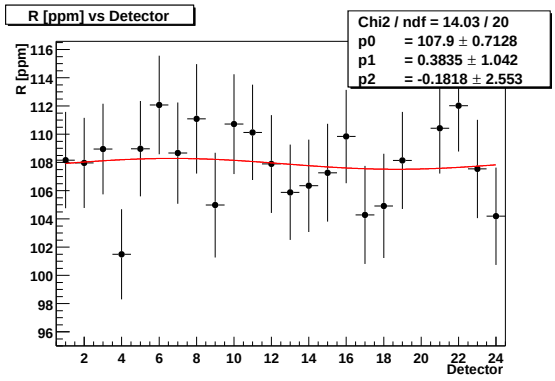

(a) R fit by sine

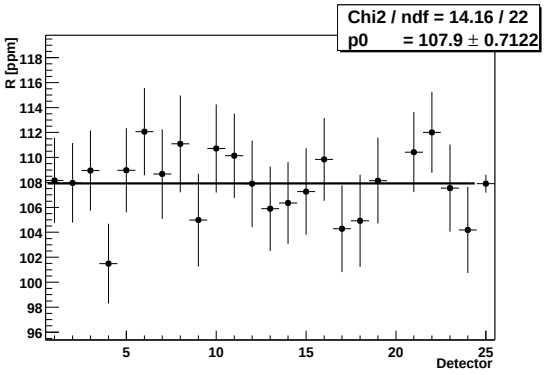

(b) R fit by constant

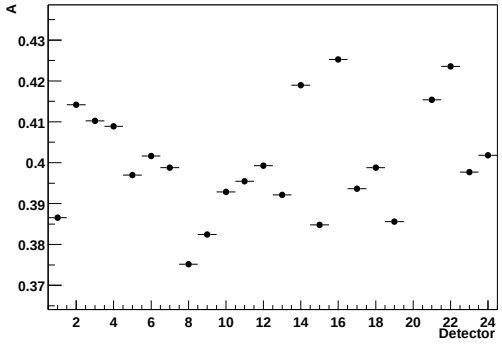

(c) Asymetry 3-parameter fit

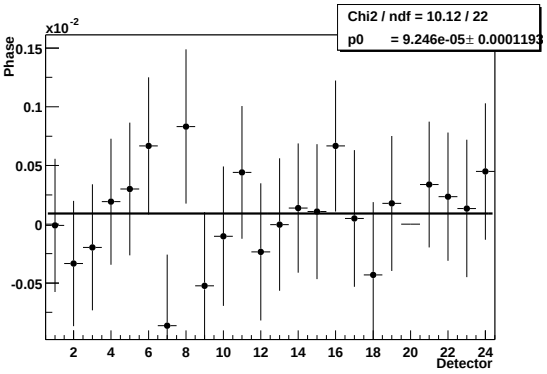

(d) Phase 3-parameter fit

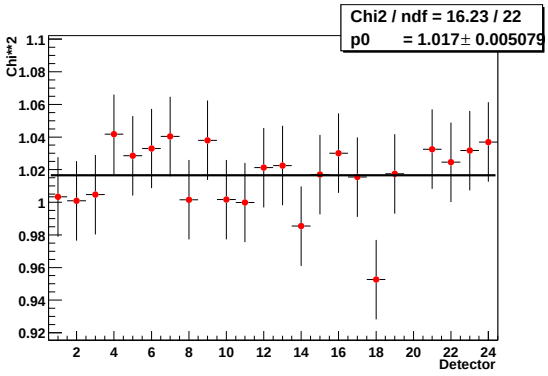

(e) χ^2/Ndf

Figure 44: R versus detector at 31.7 μs, fit to a constant (left top) or a sinusoidal function (right top). Asymetry and phase across detectors are plotted bottom left and right respectively. All run data sets together.

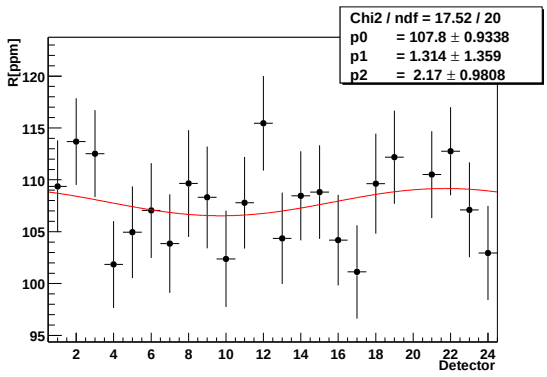

(a) R fit by sine

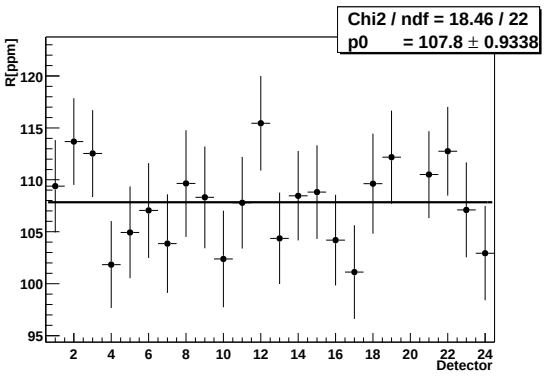

(b) R fit by constant

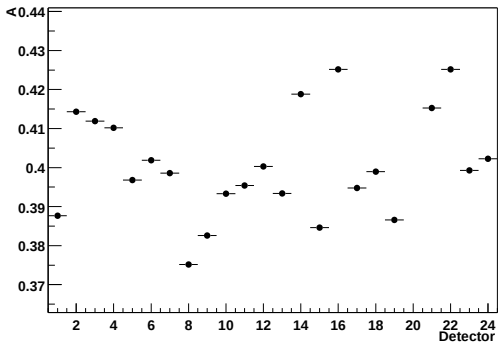

(c) Asymetry

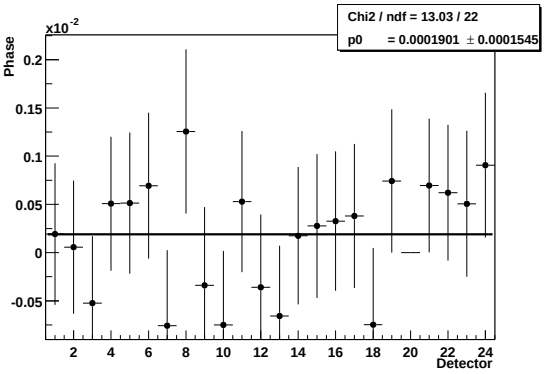

(d) Phase

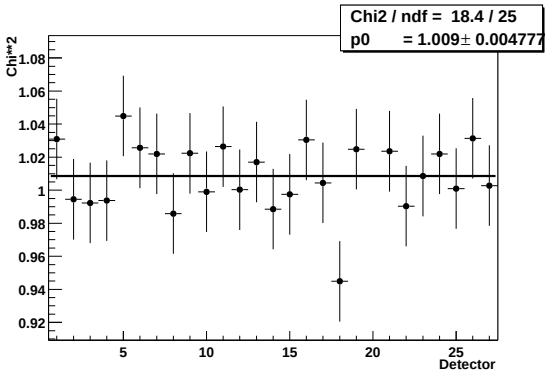

(e) χ^2/Ndf

Figure 45: R versus detector at 31.7 μs, fit to a constant (left top) or a sinusoidal function (right top). Asymetry and phase across detectors are plotted bottom left and right respectively. Results of 3-parameter fit for low n data.

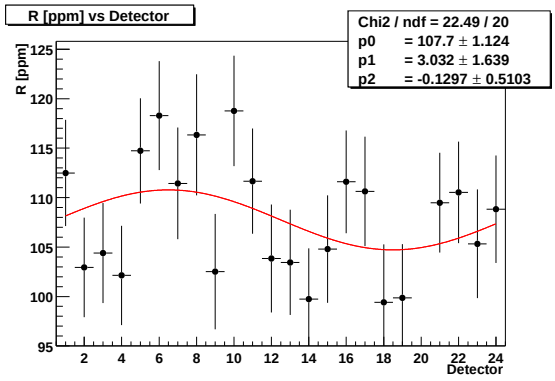

(a) R fit by sine

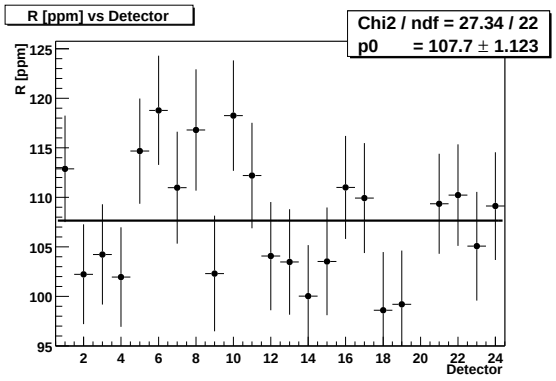

(b) R fit by constant

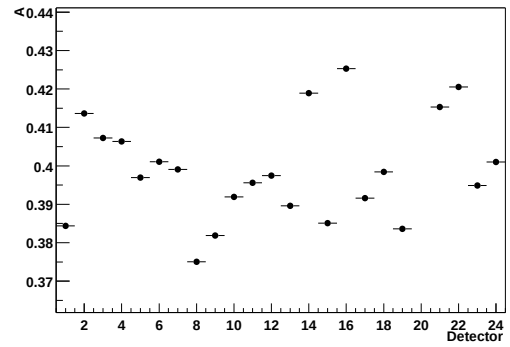

(c) Asymetry

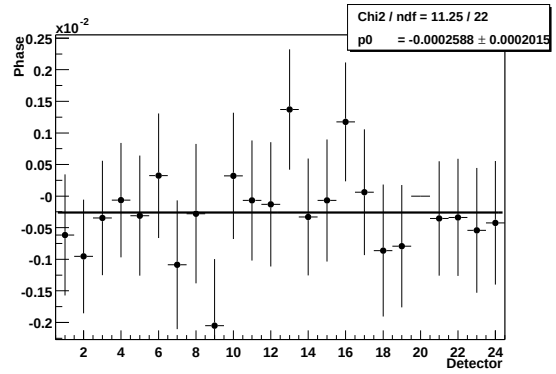

(d) Phase

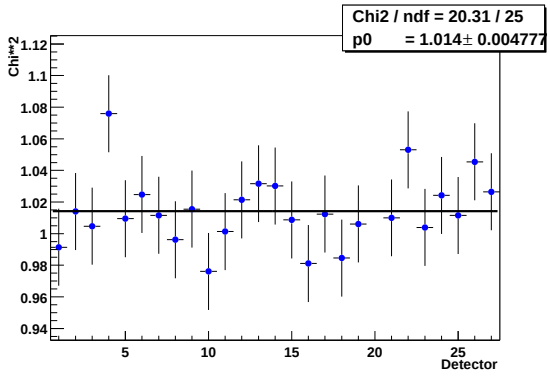

(e) χ^2/Ndf

Figure 46: R versus detector at 31.7 μs, fit to a constant (left top) or a sinusoidal function (right top). Asymetry and phase across detectors are plotted bottom left and right respectively. Results of 3-parameter fit for high n data.

3.5 Results for 7-parameter fit function. CBO sidebands included in fit.

The following functional form of the ratio method has been used to fit for the CBO, so-called 7-parameter fit function:

$$\begin{aligned} r(t) &= A\cos(\omega_a t+\phi)+0.000287 \\ &+ e^{-t/\tau_{cbo}}[A_1\cos(\omega_1 t)+B_1\sin(\omega_1 t)+A_2\cos(\omega_2 t)+B_2\sin(\omega_2 t)]. \end{aligned} \quad (6)$$

Here $\omega_1 = \omega_{cbo} - \omega_a$ and $\omega_2 = \omega_{cbo} + \omega_a$ are sidebands frequencies. In my fits, the CBO frequency, $\omega_{cbo} = 2\pi/f_{cbo}$, and exponential CBO lifetime were fixed. The numerical value depends on the quad voltage settings. 2001 data can be divided into two data sets with different CBO frequencies and lifetimes. For low n data $f_{cbo} = 418.5$ kHz ; $\tau_{cbo} = 90.0$ μs, and $f_{cbo} = 490.6$ kHz ; $\tau_{cbo} = 120.5$ μs for high n data respectively (see Chris, Jon, Mario and Xiaobo reports). This functional form take into account only sidebands frequencies. Another 7 parameters functional form (Including main CBO grequency) was used for CBO systematic study (see later).

The fit results of using 7-parameters function are plotted in Figs. 47-49 and in Figs. 48-50.

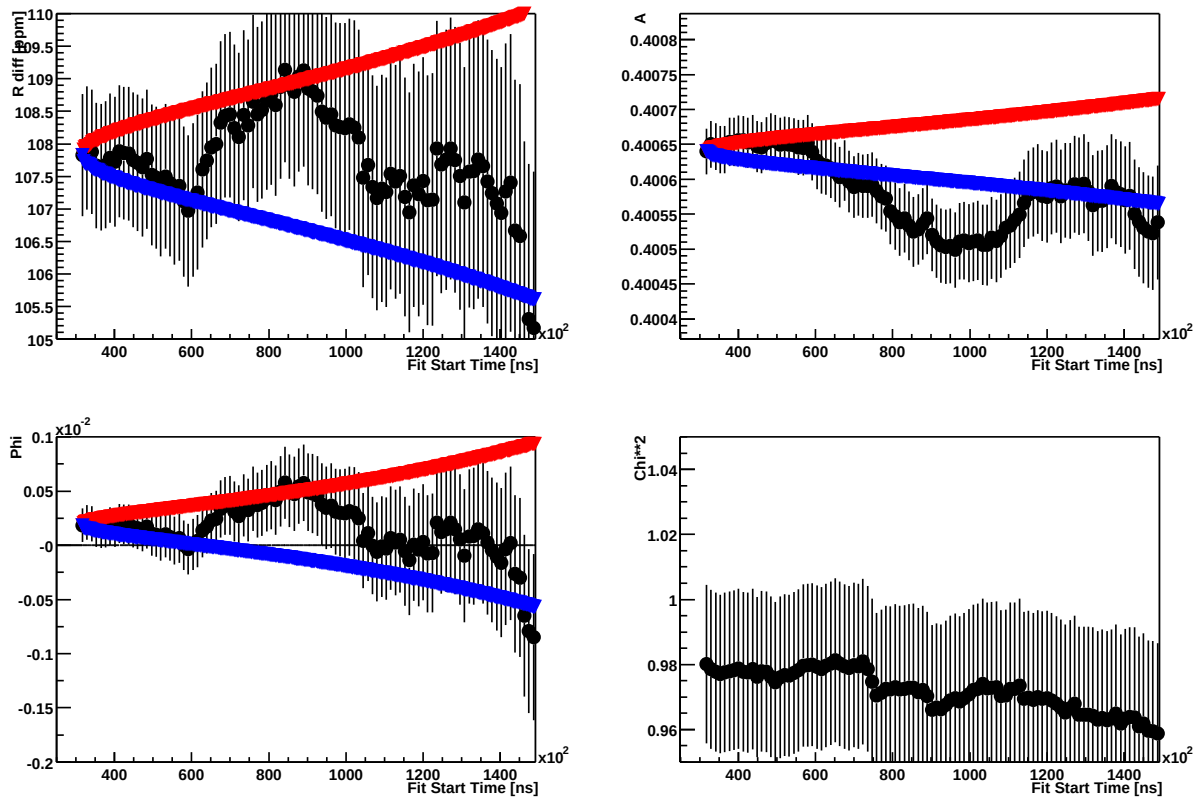

Figure 47: R for the sum of 23 detectors (top right), asymetry (top left) phase (bottom right) and χ^2/Ndf versus 7-parameter fit start time (for low n data set).

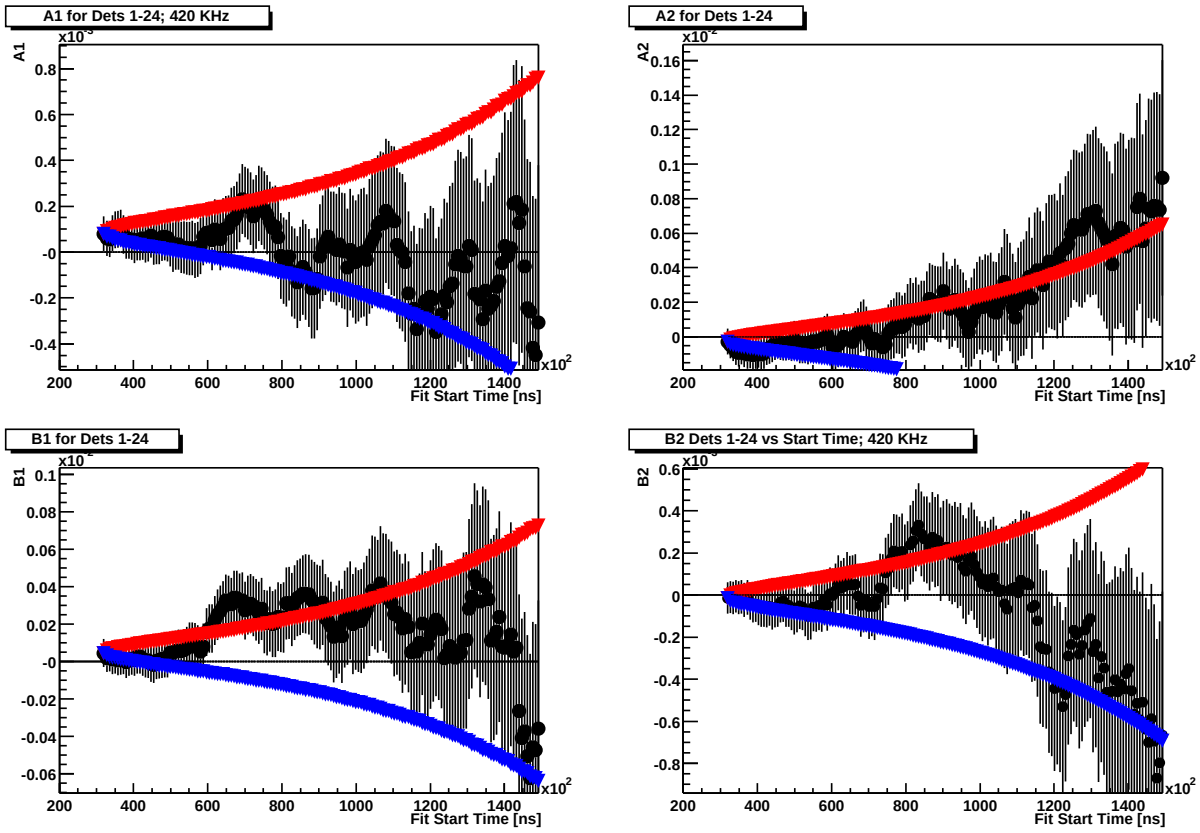

Figure 48: CBO parameters : A1 (top right), A2 (top left), B1 (bottom right) and B2 versus 7-parameter fit start time (low n data set).

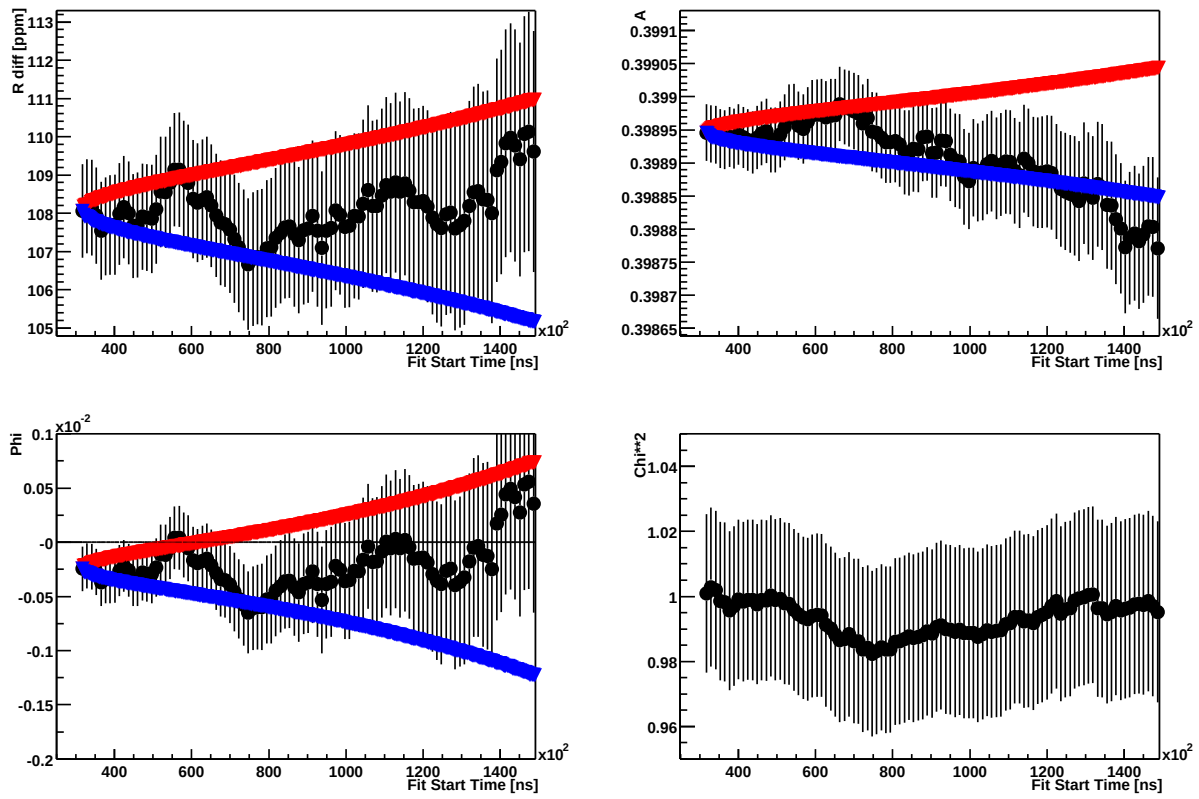

Figure 49: R for the sum of 23 detectors (top right), asymetry (top left) phase (bottom right) and χ^2/Ndf versus 7-parameter fit start time (high n data set).

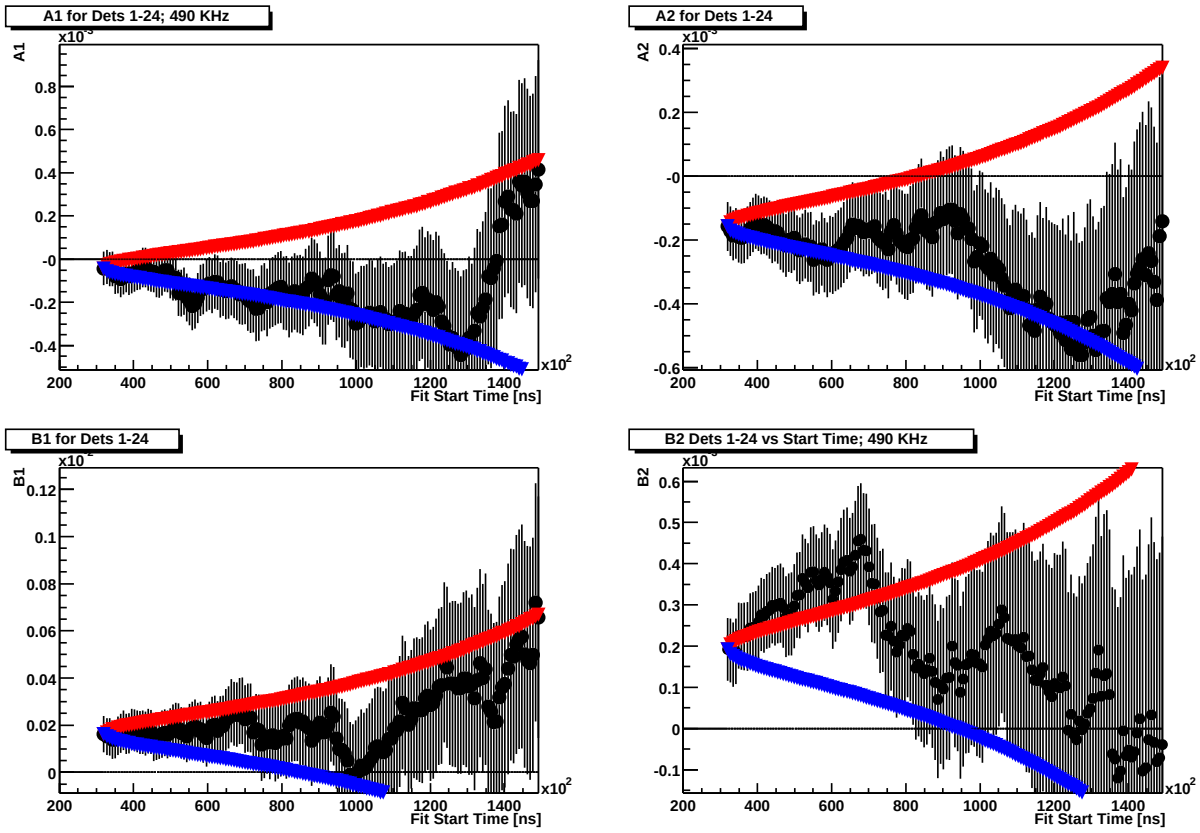

Figure 50: CBO parameters : A1 (top right), A2 (top left), B1 (bottom right) and B2 versus 7-parameter fit start time (high n data set).

The difference of the results when 3 or 7-parameter fit functions was found to be small (see in Table 5). So, I used 3-parameter fit function to obtain my final results and estimate systematic unceratinties associated with neglecting CBO terms. There are no benefits to use more complicated fit function since the systematic uncertainty associated with CBO is small for 2001 data.

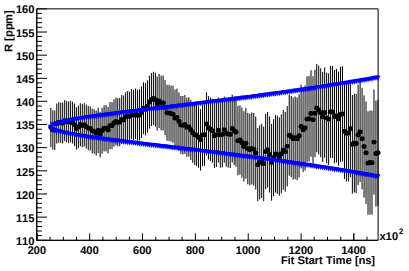

(a) R for detector 1

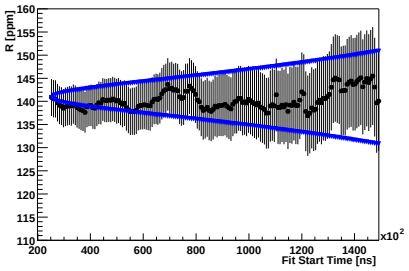

(b) R for detector 2

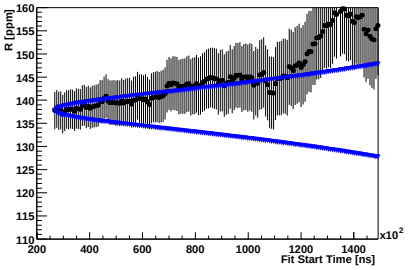

(c) R for detector 3

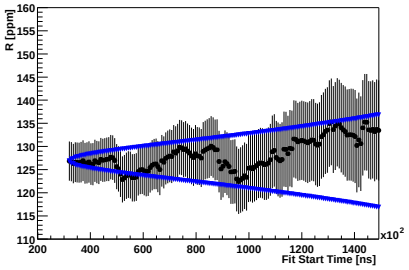

(d) R for detector 4

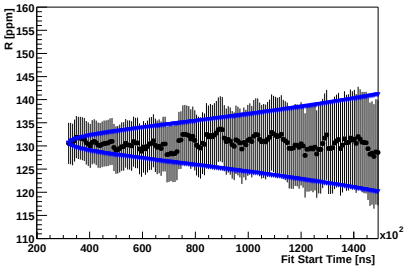

(e) R for detector 5

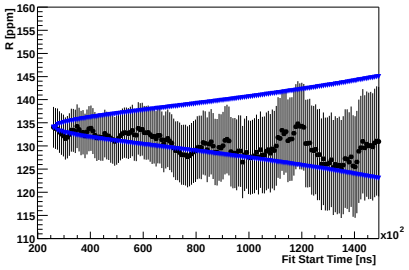

(f) R for detector 6

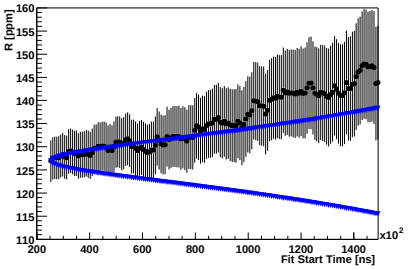

(g) R for detector 7

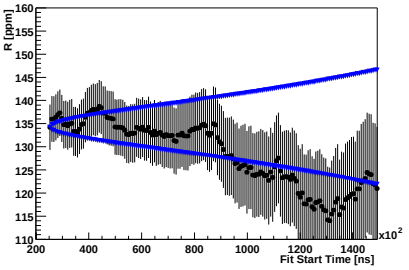

(h) R for detector 8

Figure 51: R for 7-parameter fit function versus fit start time for detectors 1-8 low n data set.

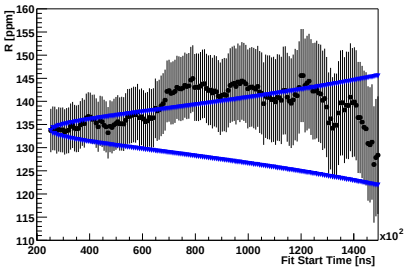

(a) R for detector 9

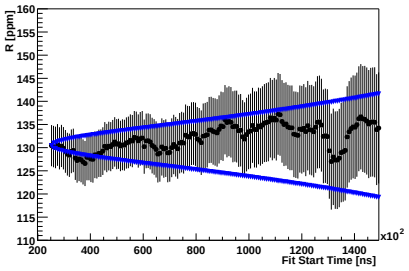

(b) R for detector 10

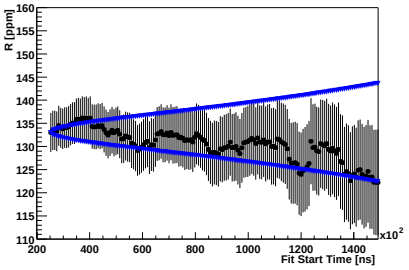

(c) R for detector 11

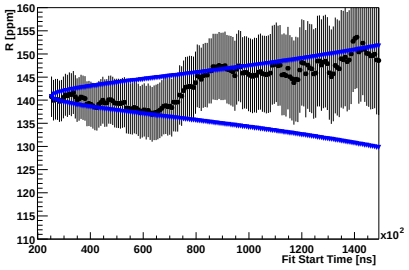

(d) R for detector 12

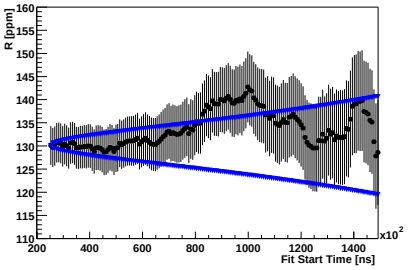

(e) R for detector 13

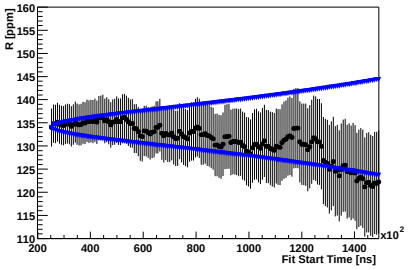

(f) R for detector 14

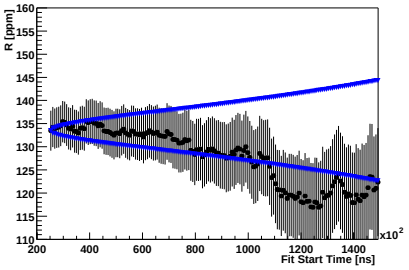

(g) R for detector 15

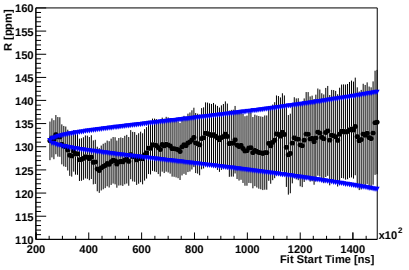

(h) R for detector 16

Figure 52: R for 7-parameter fit function versus fit start time for detectors 9-16 low n data set.

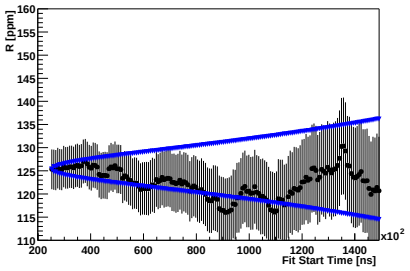

(a) R for detector 17

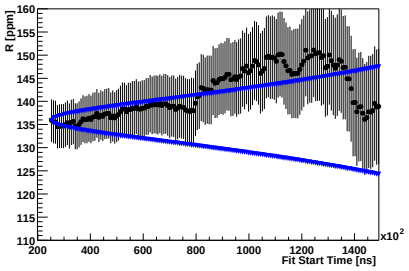

(b) R for detector 18

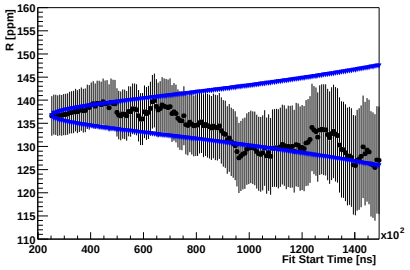

(c) R for detector 19

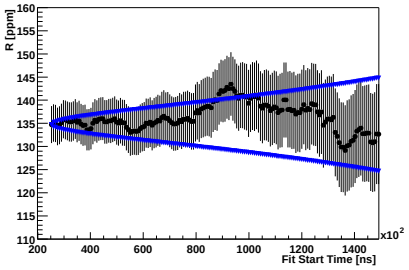

(d) R for detector 21

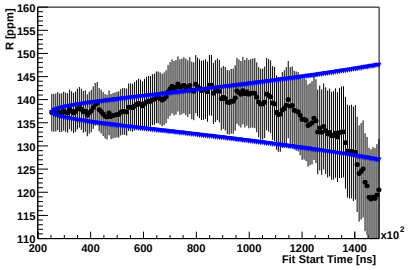

(e) R for detector 22

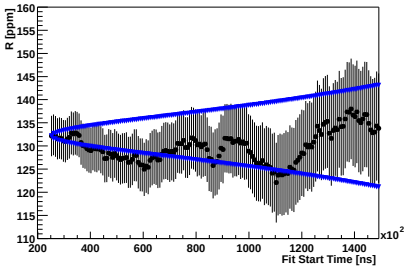

(f) R for detector 23

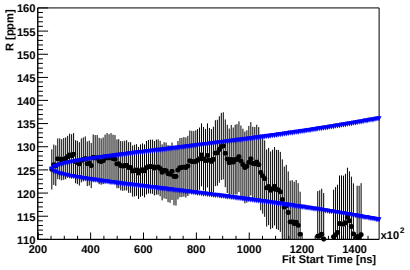

(g) R for detector 24

Figure 53: R for 7-parameter fit function versus fit start time for detectors 17-24 low n data set.

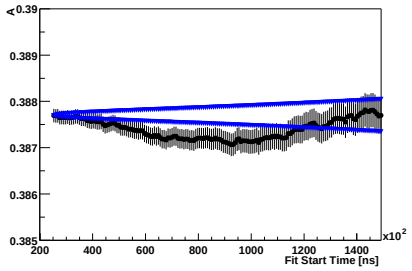

(a) A for detector 1

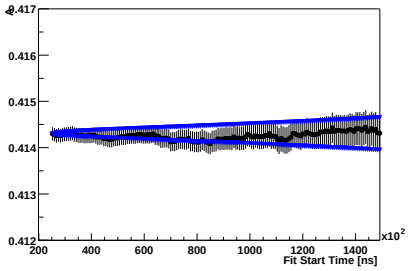

(b) A for detector 2

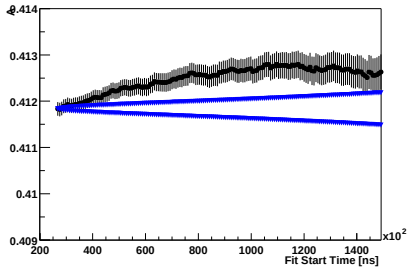

(c) A for detector 3

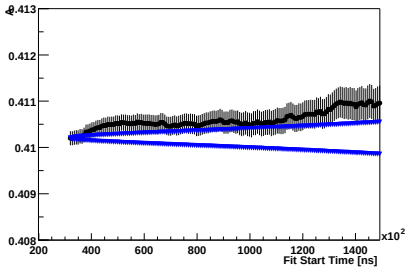

(d) A for detector 4

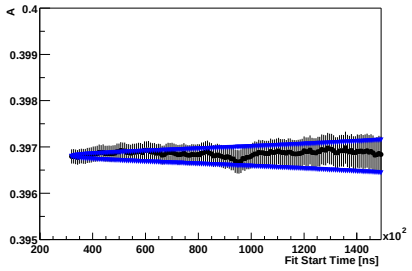

(e) A for detector 5

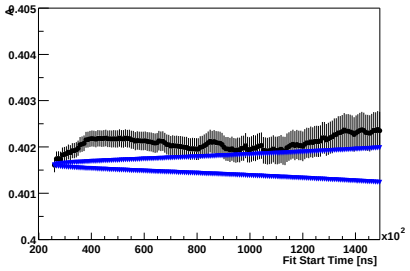

(f) A for detector 6

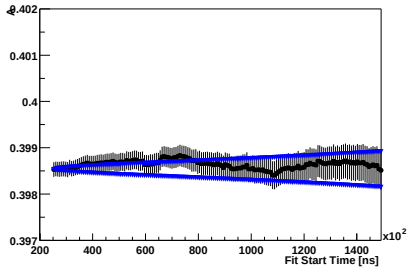

(g) A for detector 7

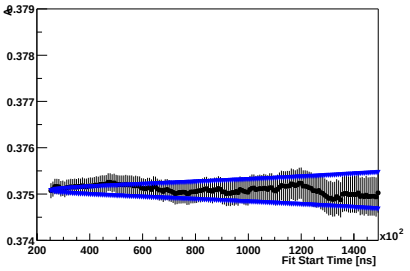

(h) A for detector 8

Figure 54: A for 7-parameter fit function versus fit start time for detectors 1-8 low n data set.

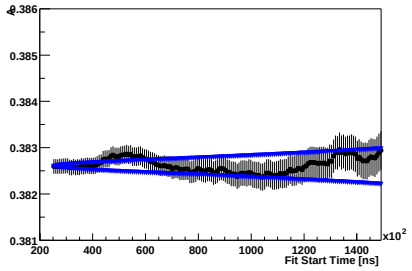

(a) A for detector 9

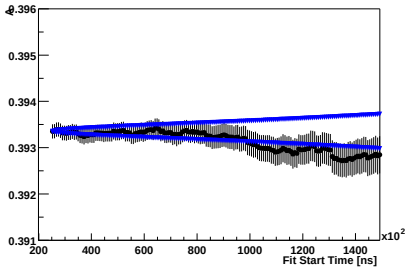

(b) A for detector 10

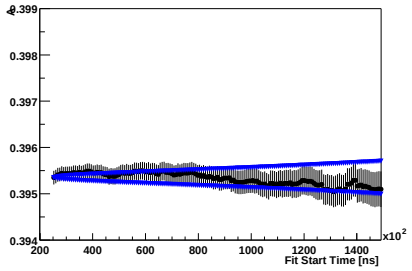

(c) A for detector 11

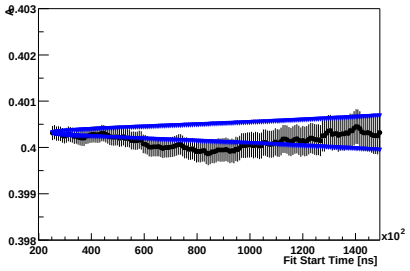

(d) A for detector 12

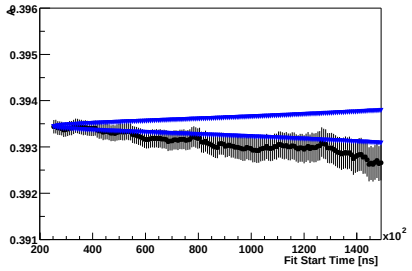

(e) A for detector 13

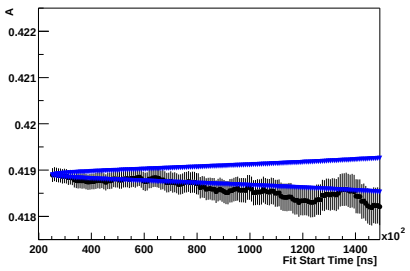

(f) A for detector 14

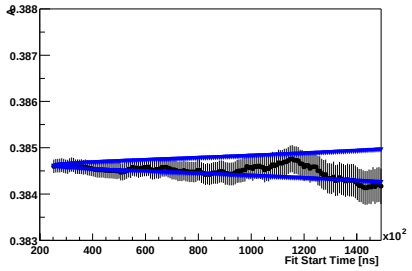

(g) A for detector 15

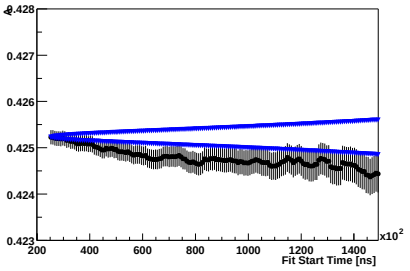

(h) A for detector 16

Figure 55: A for 7-parameter fit function versus fit start time for detectors 9-16 low n data set.

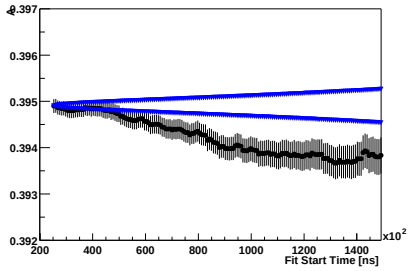

(a) A for detector 17

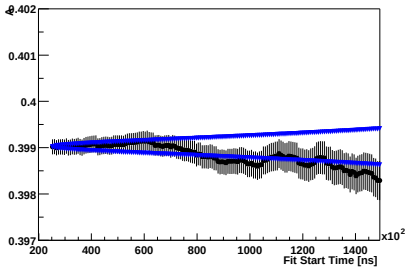

(b) A for detector 18

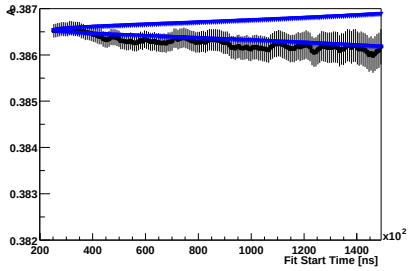

(c) A for detector 19

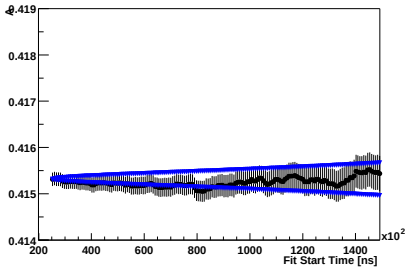

(d) A for detector 21

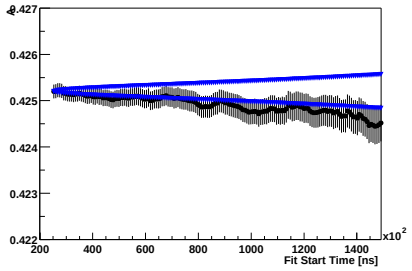

(e) A for detector 22

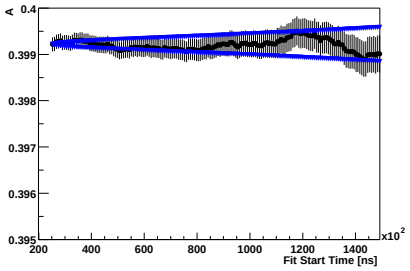

(f) A for detector 23

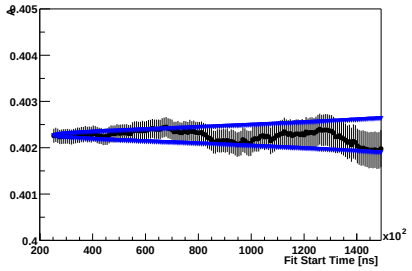

(g) A for detector 24

Figure 56: A for 7-parameter fit function versus fit start time for detectors 17-24 low n data set.

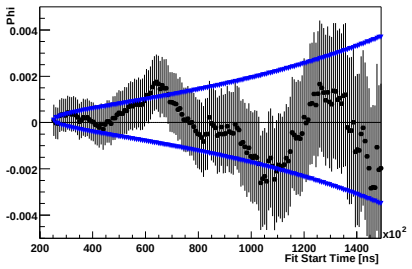

(a) G-2 ϕ for detector 1

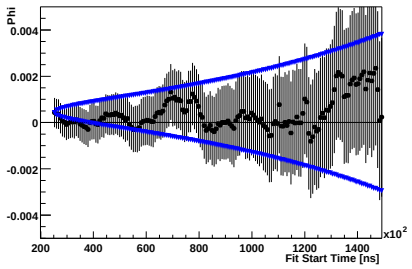

(b) G-2 ϕ for detector 2

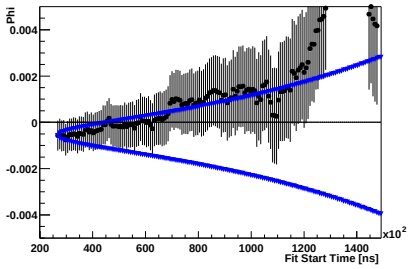

(c) G-2 ϕ for detector 3

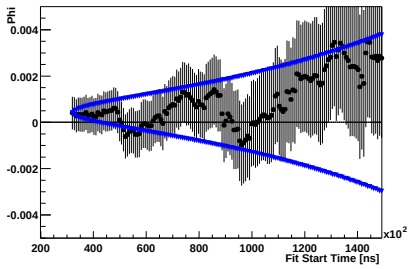

(d) G-2 ϕ for detector 4

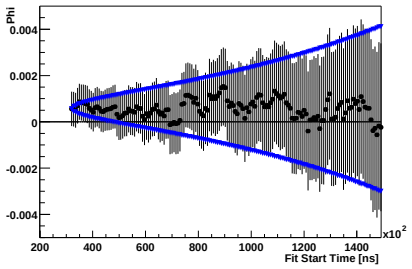

(e) G-2 ϕ for detector 5

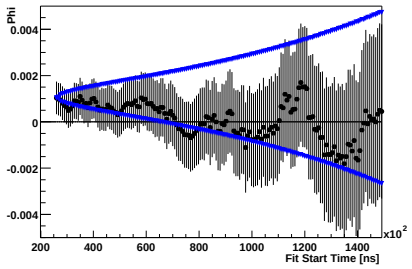

(f) G-2 ϕ for detector 6

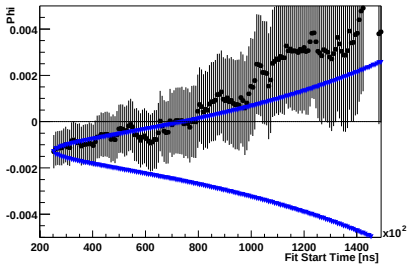

(g) G-2 ϕ for detector 7

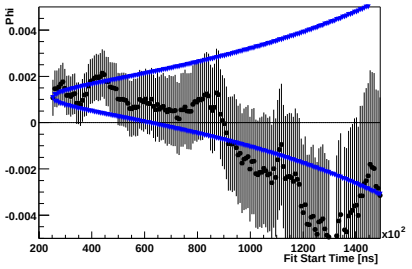

(h) G-2 ϕ for detector 8

Figure 57: G-2 ϕ for 7-parameter fit function versus fit start time for detectors 1-8 low n data set.

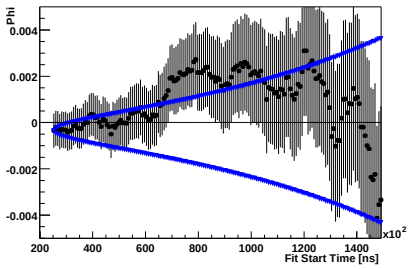

(a) ϕ for detector 9

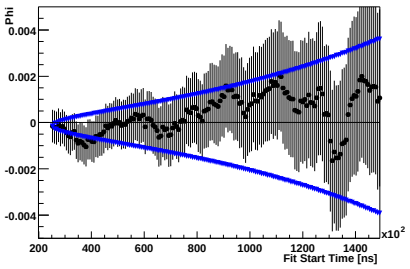

(b) ϕ for detector 10

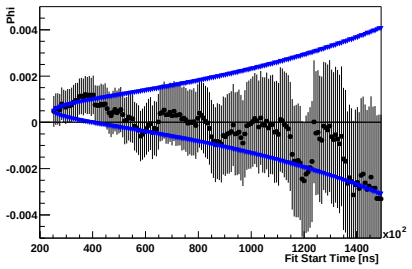

(c) ϕ for detector 11

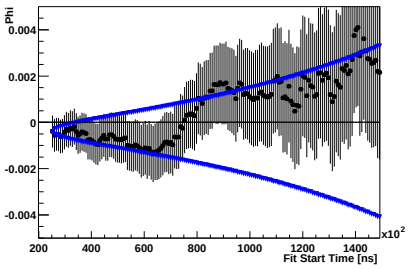

(d) ϕ for detector 12

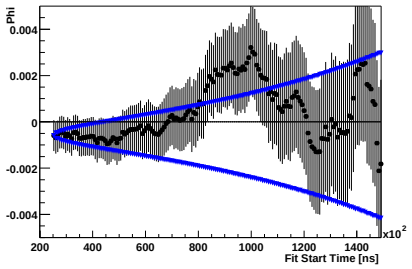

(e) ϕ for detector 13

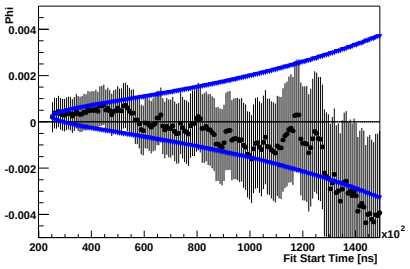

(f) ϕ for detector 14

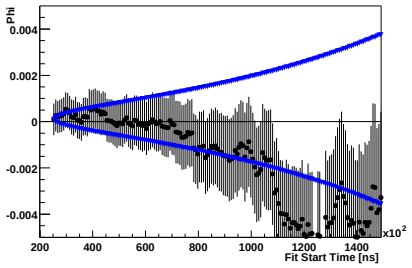

(g) ϕ for detector 15

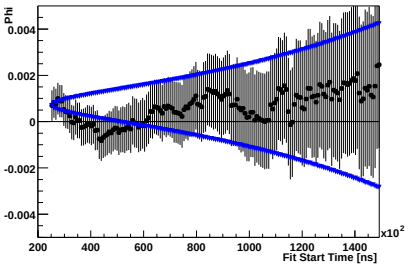

(h) ϕ for detector 16

Figure 58: G-2 ϕ for 7-parameter fit function versus fit start time for detectors 9-16 low n data set.

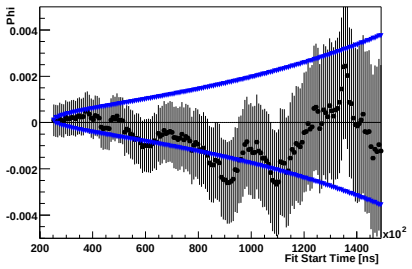

(a) ϕ for detector 17

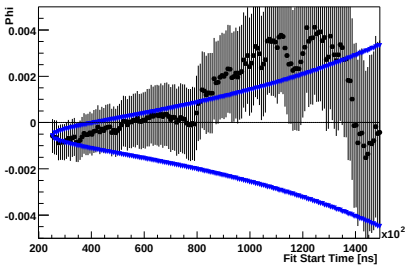

(b) ϕ for detector 18

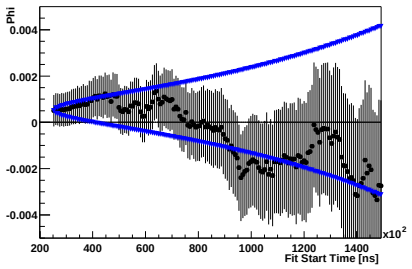

(c) ϕ for detector 19

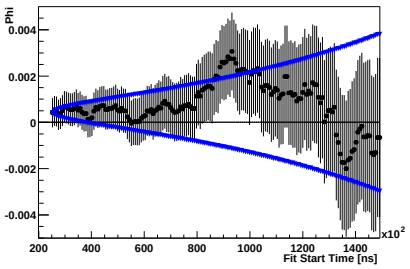

(d) ϕ for detector 21

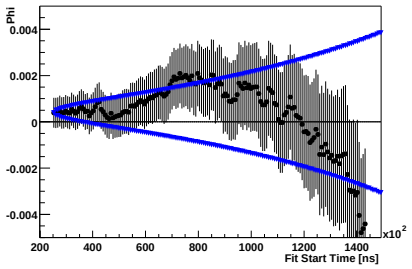

(e) ϕ for detector 22

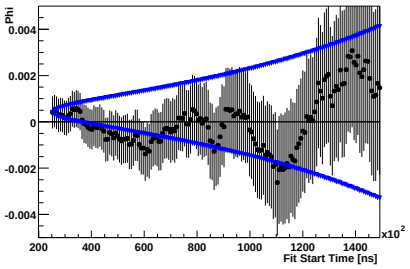

(f) ϕ for detector 23

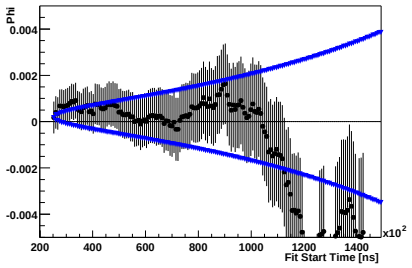

(g) ϕ for detector 24

Figure 59: G-2 ϕ for 7-parameter fit function versus fit start time for detectors 17-24 low n data set.

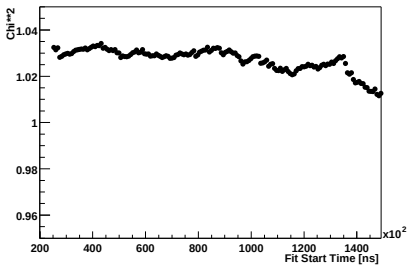

(a) χ^2/Ndf for detector 1

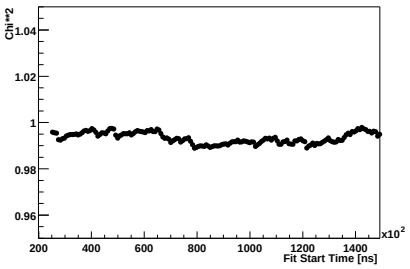

(b) χ^2/Ndf for detector 2

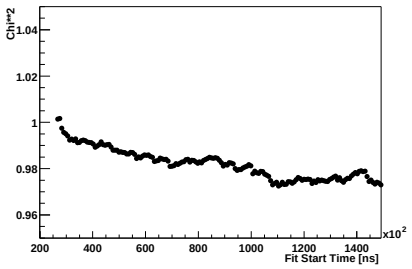

(c) χ^2/Ndf for detector 3

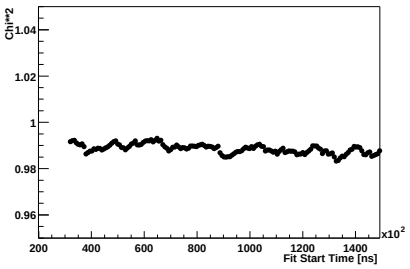

(d) χ^2/Ndf for detector 4

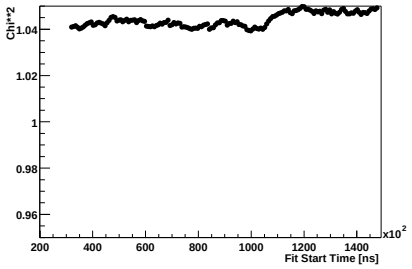

(e) χ^2/Ndf for detector 5

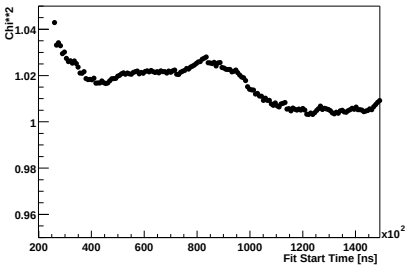

(f) χ^2/Ndf for detector 6

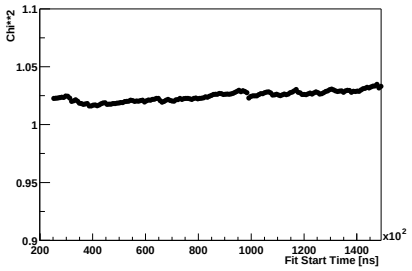

(g) χ^2/Ndf for detector 7

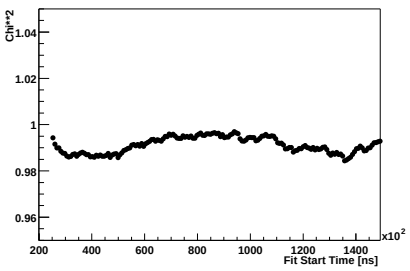

(h) χ^2/Ndf for detector 8

Figure 60: χ^2/Ndf for 7-parameter fit function versus fit start time for detectors 1-8 low n data set.

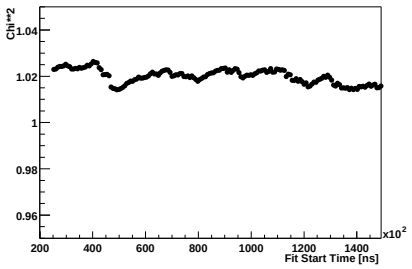

(a) χ^2/Ndf for detector 9

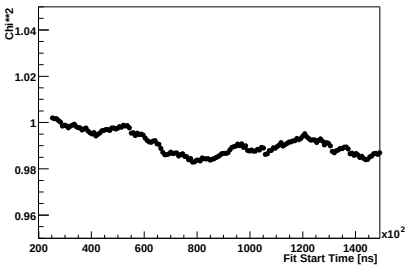

(b) χ^2/Ndf for detector 10

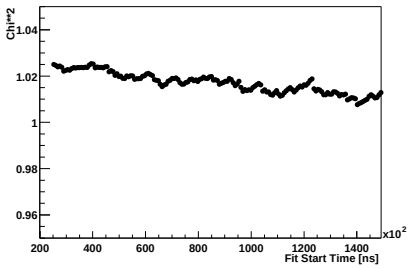

(c) χ^2/Ndf for detector 11

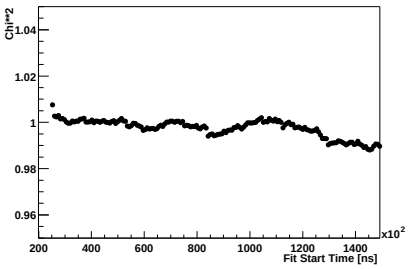

(d) χ^2/Ndf for detector 12

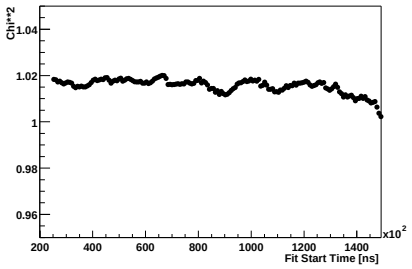

(e) χ^2/Ndf for detector 13

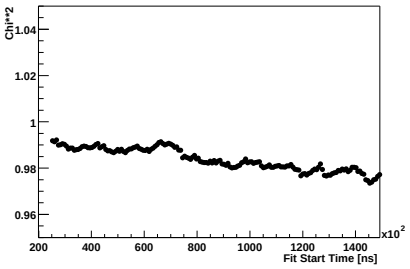

(f) χ^2/Ndf for detector 14

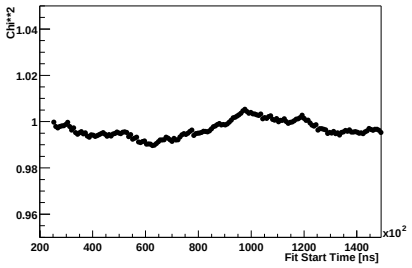

(g) χ^2/Ndf for detector 15

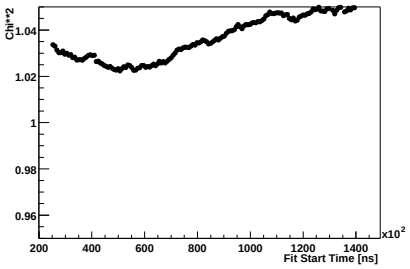

(h) χ^2/Ndf for detector 16

Figure 61: χ^2/Ndf for 7-parameter fit function versus fit start time for detectors 9-16 low n data set.

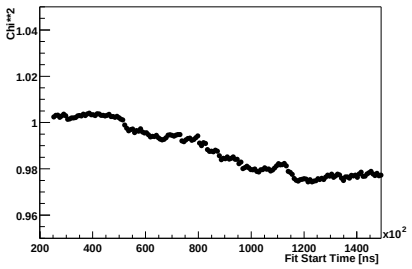

(a) χ^2/Ndf for detector 17

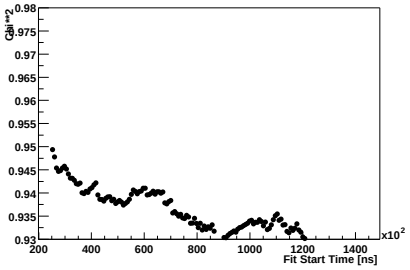

(b) χ^2/Ndf for detector 18

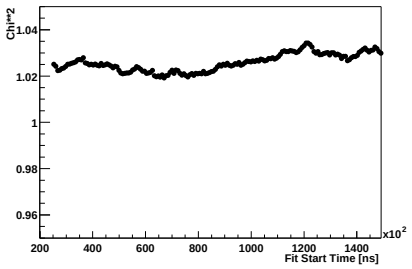

(c) χ^2/Ndf for detector 19

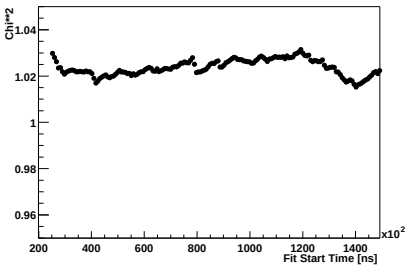

(d) χ^2/Ndf for detector 21

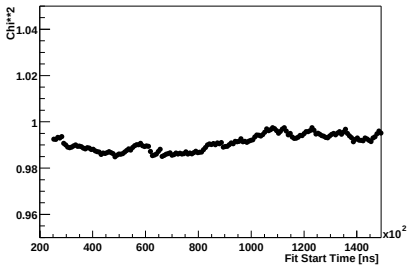

(e) χ^2/Ndf for detector 22

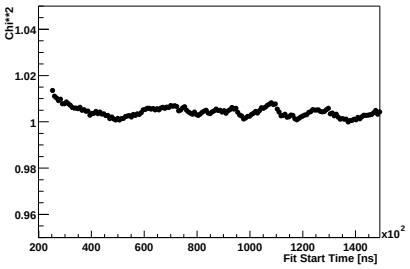

(f) χ^2/Ndf for detector 23

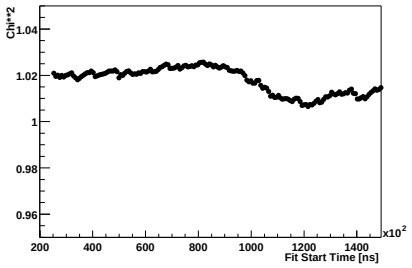

(g) χ^2/Ndf for detector 24

Figure 62: χ^2/Ndf for 7-parameter fit function versus fit start time for detectors 17-24 low n data set.

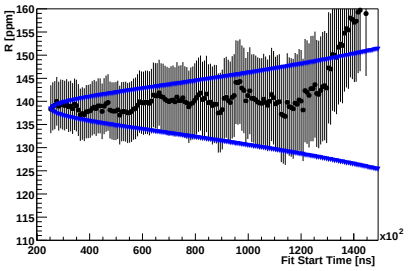

(a) R for detector 1

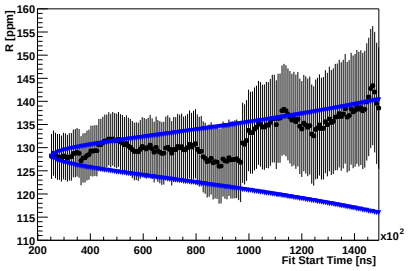

(b) R for detector 2

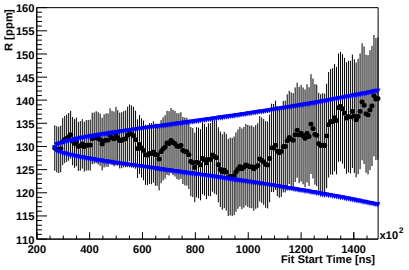

(c) R for detector 3

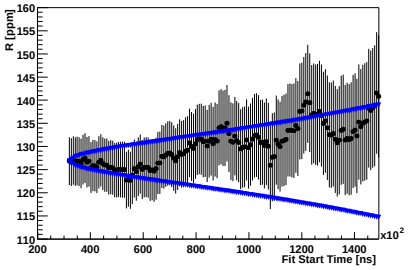

(d) R for detector 4

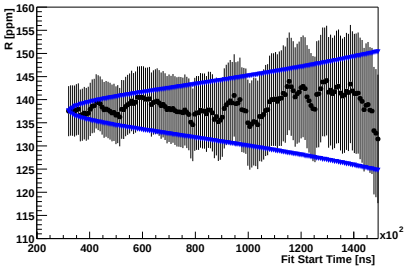

(e) R for detector 5

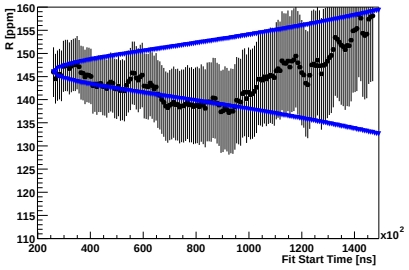

(f) R for detector 6

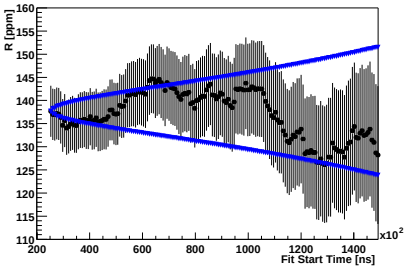

(g) R for detector 7

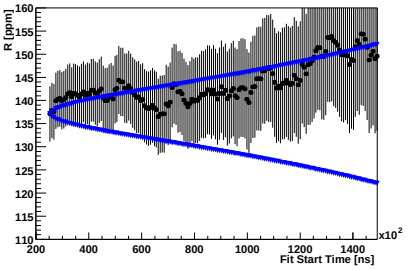

(h) R for detector 8

Figure 63: R for 7-parameter fit function versus fit start time for detectors 1-8 high n data set.

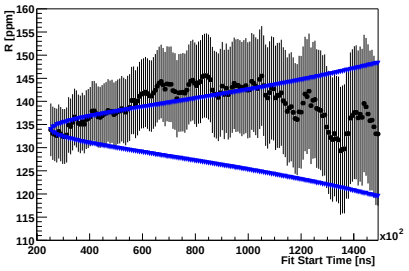

(a) R for detector 9

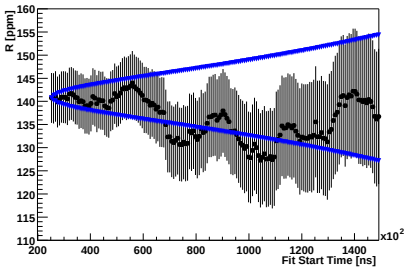

(b) R for detector 10

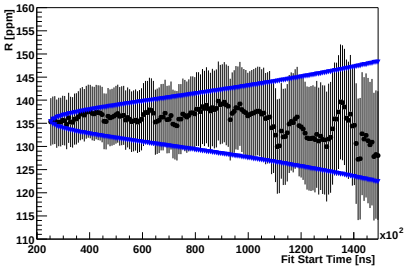

(c) R for detector 11

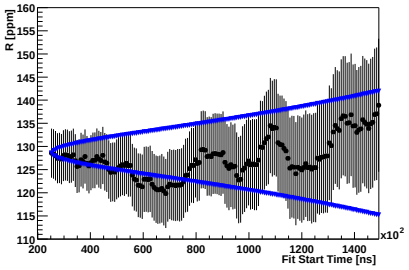

(d) R for detector 12

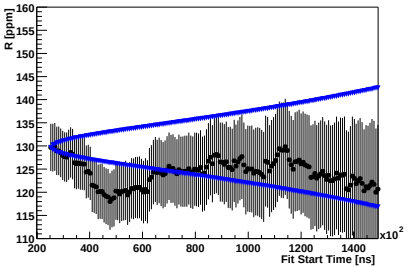

(e) R for detector 13

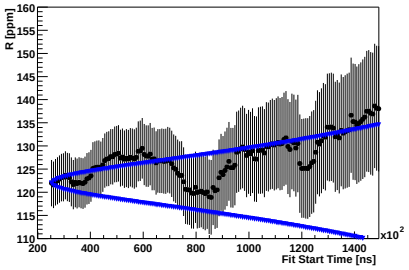

(f) R for detector 14

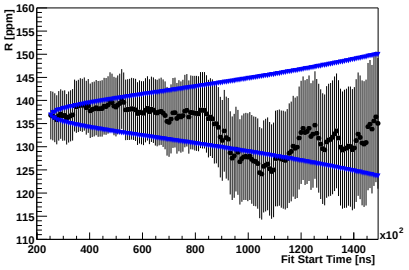

(g) R for detector 15

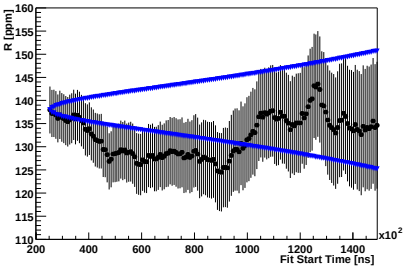

(h) R for detector 16

Figure 64: R for 7-parameter fit function versus fit start time for detectors 9-16 high n data set.

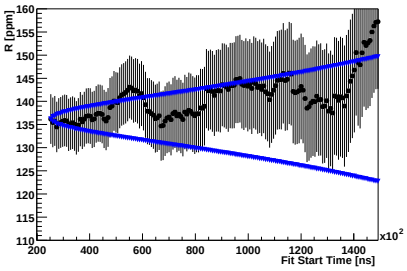

(a) R for detector 17

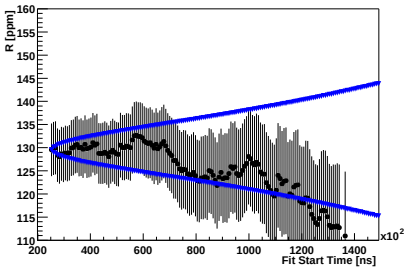

(b) R for detector 18

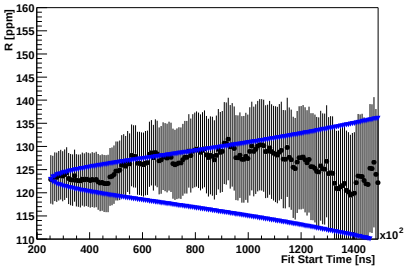

(c) R for detector 19

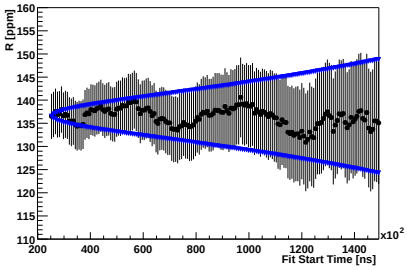

(d) R for detector 21

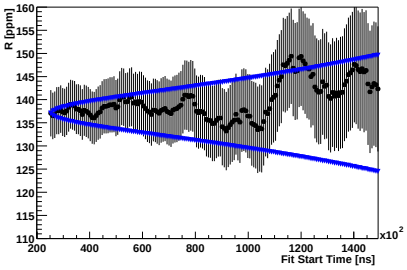

(e) R for detector 22

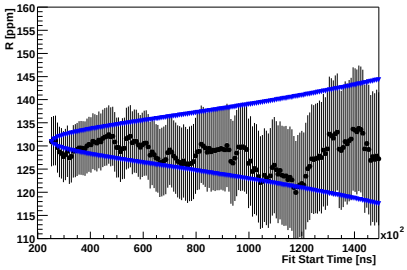

(f) R for detector 23

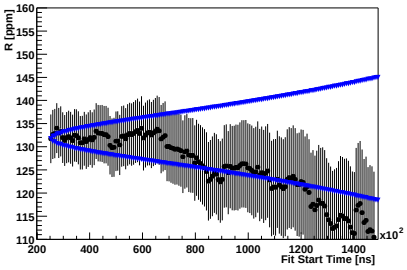

(g) R for detector 24

Figure 65: R for 7-parameter fit function versus fit start time for detectors 17-24 high n data set.

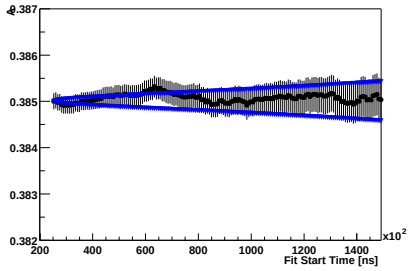

(a) A for detector 1

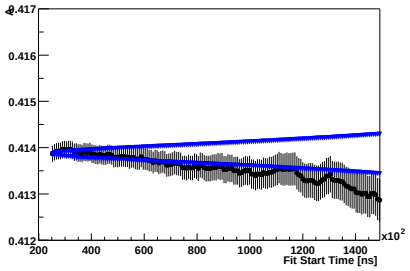

(b) A for detector 2

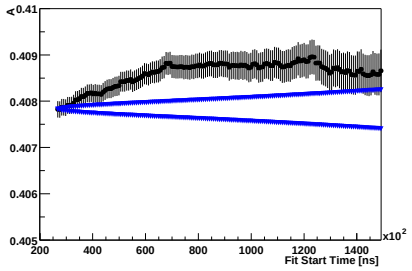

(c) A for detector 3

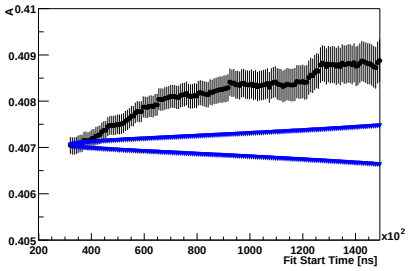

(d) A for detector 4

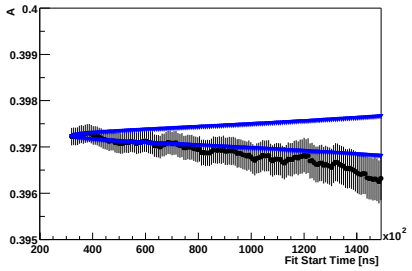

(e) A for detector 5

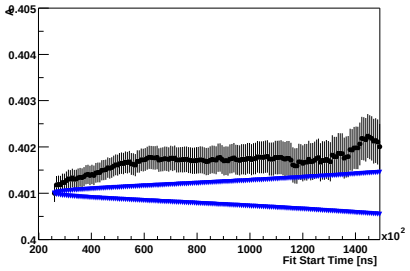

(f) A for detector 6

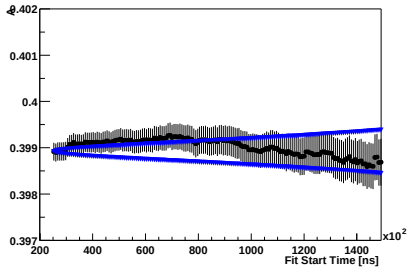

(g) A for detector 7

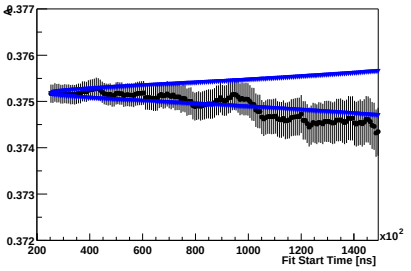

(h) A for detector 8

Figure 66: A for 7-parameter fit function versus fit start time for detectors 1-8 high n data set.

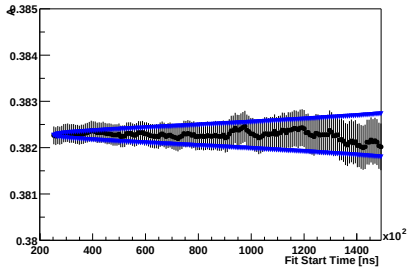

(a) A for detector 9

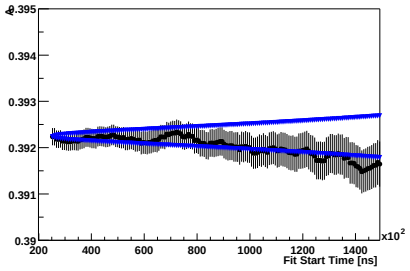

(b) A for detector 10

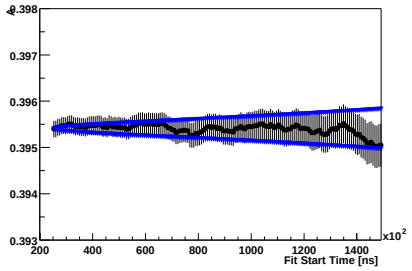

(c) A for detector 11

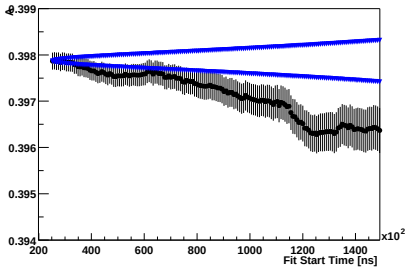

(d) A for detector 12

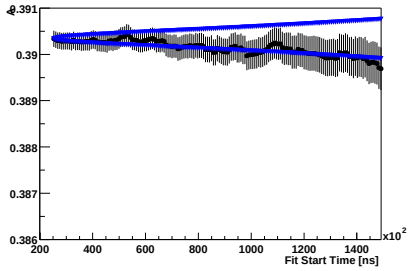

(e) A for detector 13

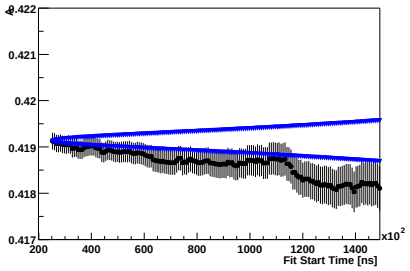

(f) A for detector 14

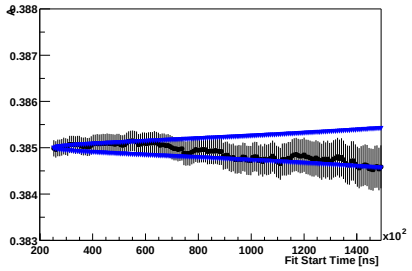

(g) A for detector 15

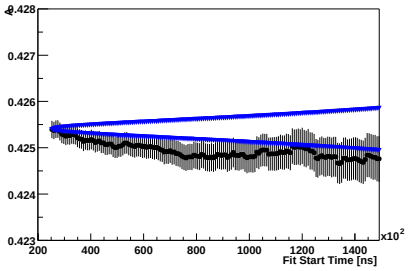

(h) A for detector 16

Figure 67: A for 7-parameter fit function versus fit start time for detectors 9-16 high n data set.

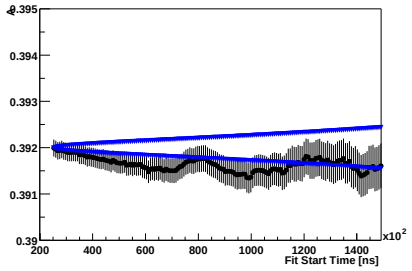

(a) A for detector 17

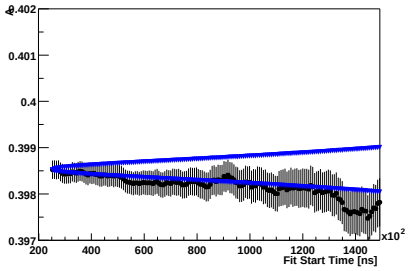

(b) A for detector 18

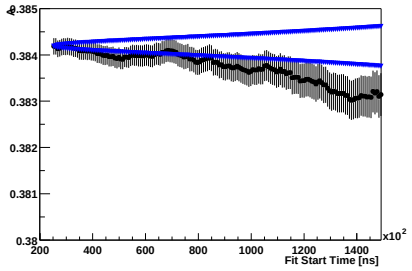

(c) A for detector 19

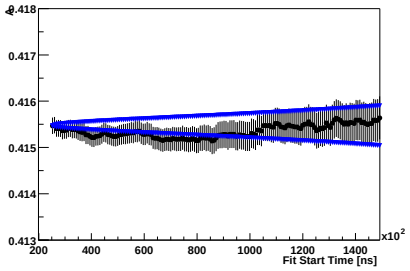

(d) A for detector 21

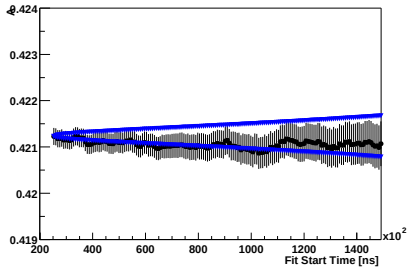

(e) A for detector 22

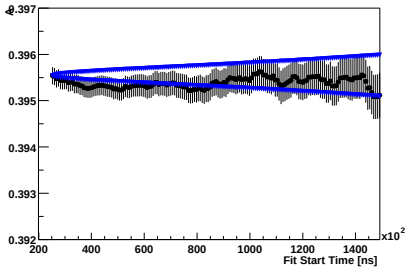

(f) A for detector 23

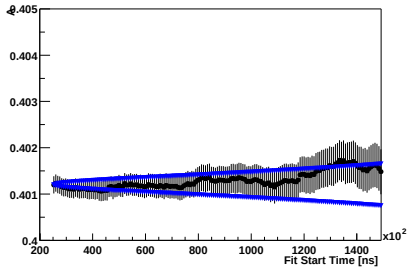

(g) A for detector 24

Figure 68: A for 7-parameter fit function versus fit start time for detectors 17-24 high n data set.

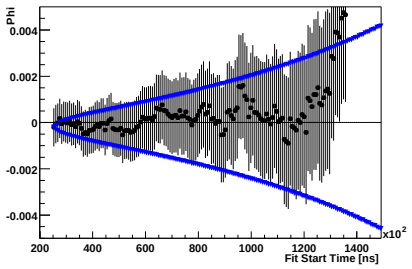

(a) G-2 ϕ for detector 1

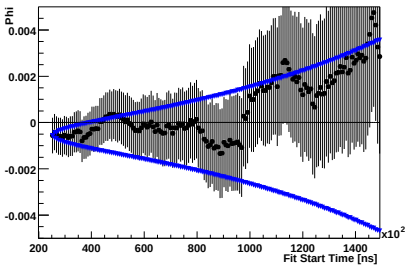

(b) G-2 ϕ for detector 2

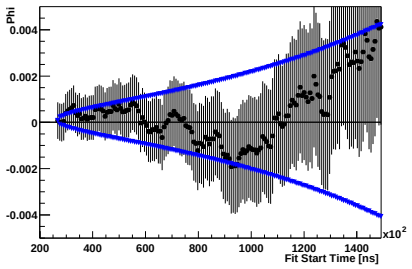

(c) G-2 ϕ for detector 3

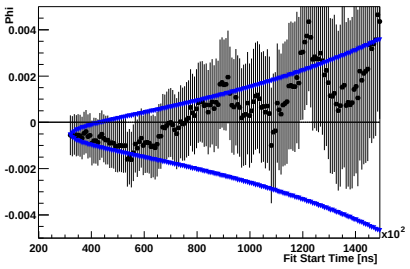

(d) G-2 ϕ for detector 4

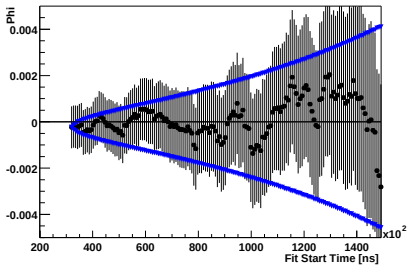

(e) G-2 ϕ for detector 5

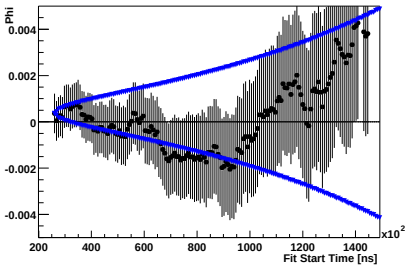

(f) G-2 ϕ for detector 6

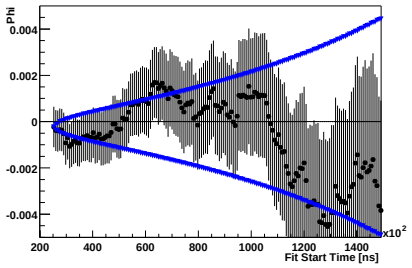

(g) G-2 ϕ for detector 7

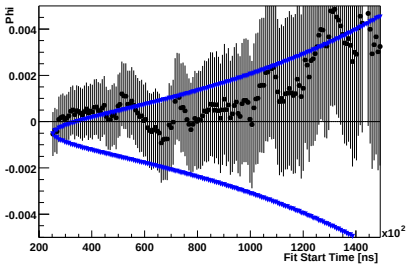

(h) G-2 ϕ for detector 8

Figure 69: G-2 ϕ for 7-parameter fit function versus fit start time for detectors 1-8 high n data set.

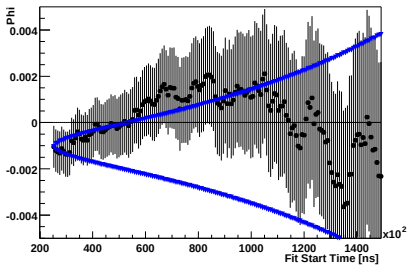

(a) ϕ for detector 9

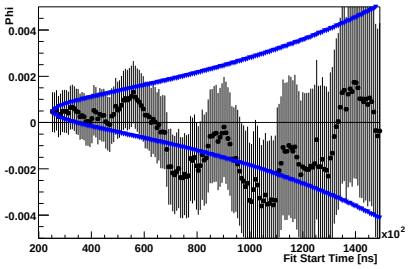

(b) ϕ for detector 10

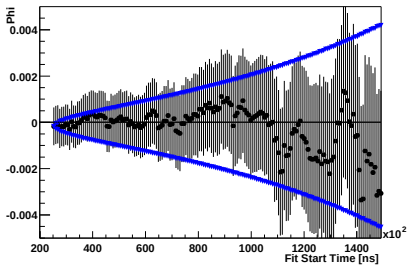

(c) ϕ for detector 11

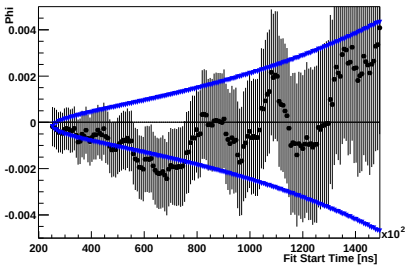

(d) ϕ for detector 12

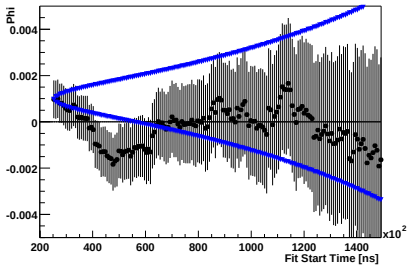

(e) ϕ for detector 13

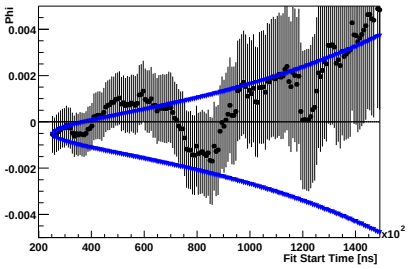

(f) ϕ for detector 14

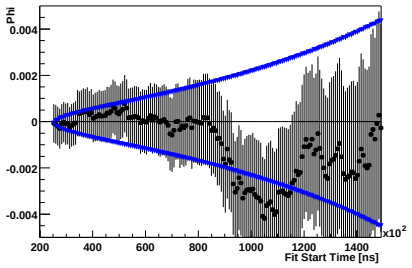

(g) ϕ for detector 15

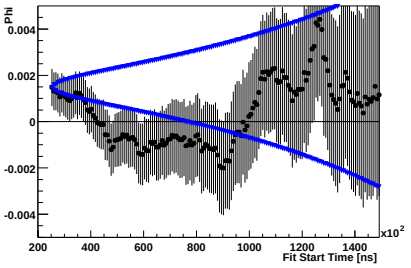

(h) ϕ for detector 16

Figure 70: G-2 ϕ for 7-parameter fit function versus fit start time for detectors 9-16 high n data set.

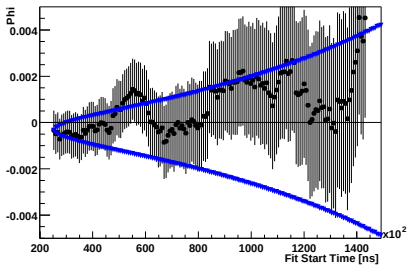

(a) ϕ for detector 17

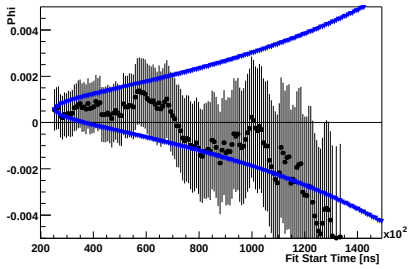

(b) ϕ for detector 18

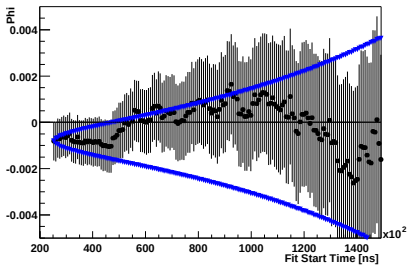

(c) ϕ for detector 19

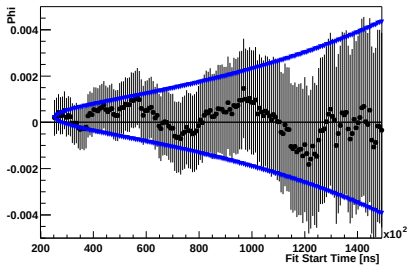

(d) ϕ for detector 21

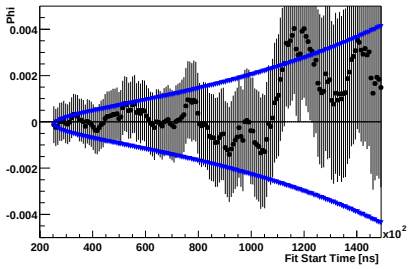

(e) ϕ for detector 22

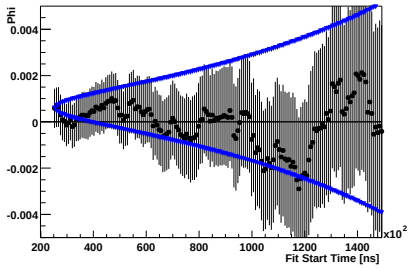

(f) ϕ for detector 23

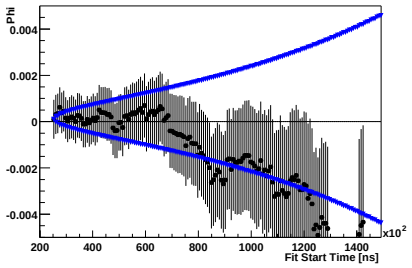

(g) ϕ for detector 24

Figure 71: G-2 ϕ for 7-parameter fit function versus fit start time for detectors 17-24 high n data set.

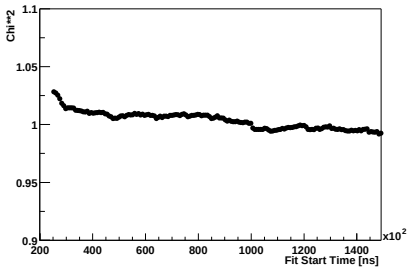

(a) χ^2/Ndf for detector 1

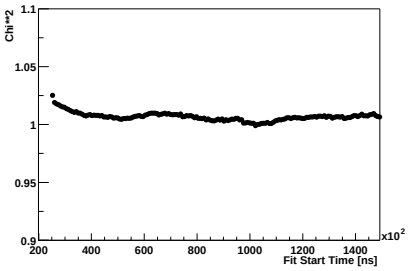

(b) χ^2/Ndf for detector 2

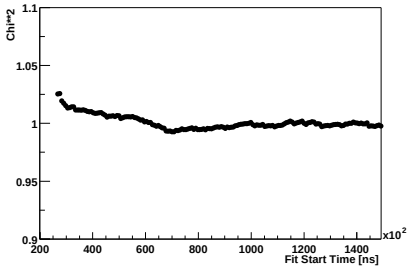

(c) χ^2/Ndf for detector 3

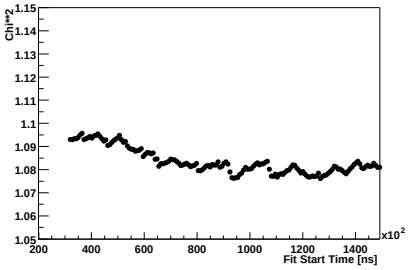

(d) χ^2/Ndf for detector 4

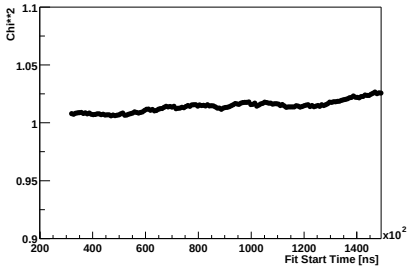

(e) χ^2/Ndf for detector 5

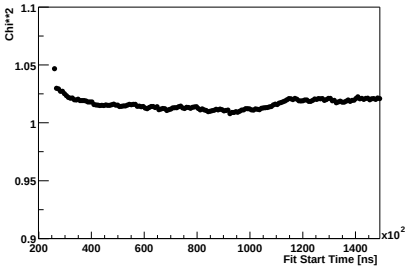

(f) χ^2/Ndf for detector 6

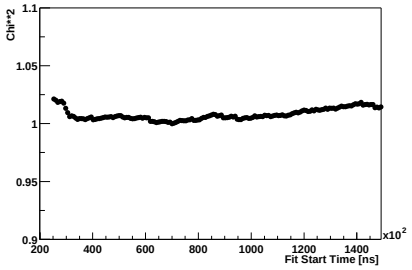

(g) χ^2/Ndf for detector 7

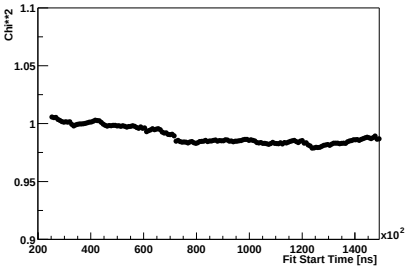

(h) χ^2/Ndf for detector 8

Figure 72: χ^2/Ndf for 7-parameter fit function versus fit start time for detectors 1-8 high n data set.

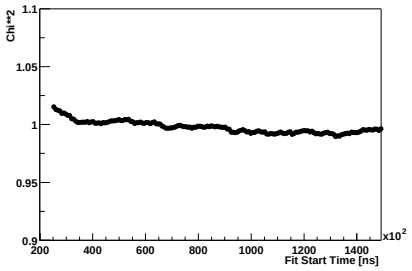

(a) χ^2/Ndf for detector 9

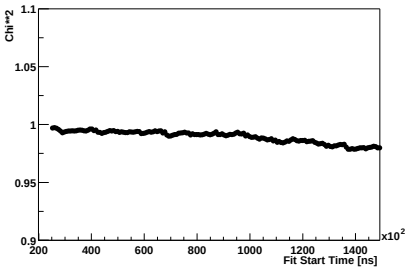

(b) χ^2/Ndf for detector 10

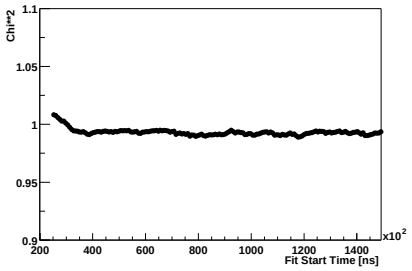

(c) χ^2/Ndf for detector 11

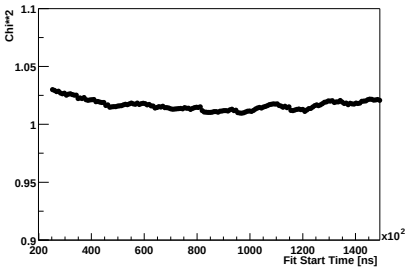

(d) χ^2/Ndf for detector 12

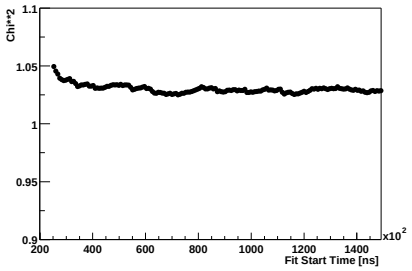

(e) χ^2/Ndf for detector 13

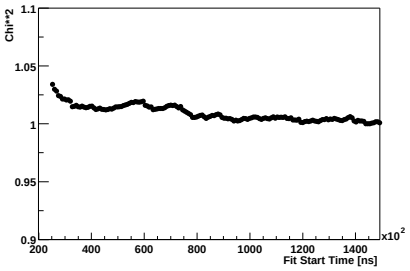

(f) χ^2/Ndf for detector 14

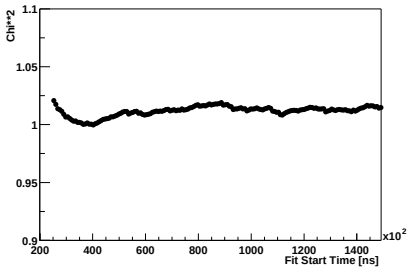

(g) χ^2/Ndf for detector 15

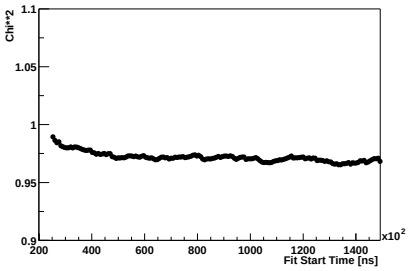

(h) χ^2/Ndf for detector 16

Figure 73: χ^2/Ndf for 7-parameter fit function versus fit start time for detectors 9-16 high n data set.

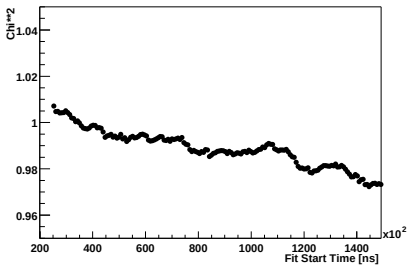

(a) χ^2/Ndf for detector 17

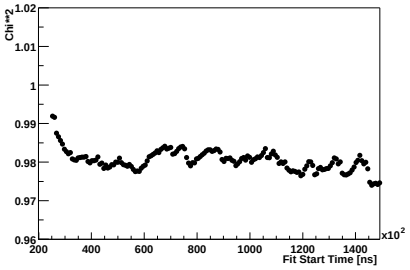

(b) χ^2/Ndf for detector 18

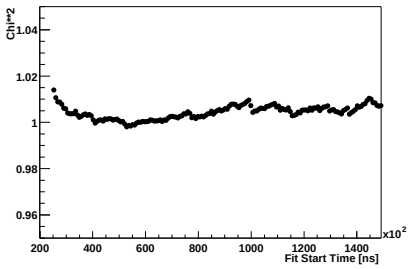

(c) χ^2/Ndf for detector 19

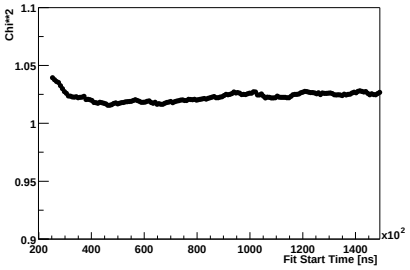

(d) χ^2/Ndf for detector 21

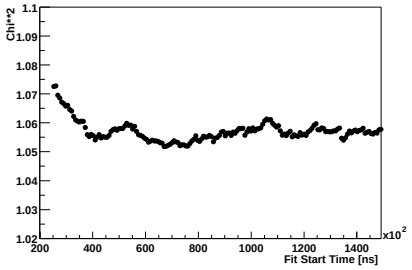

(e) χ^2/Ndf for detector 22

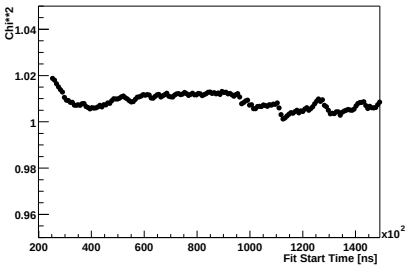

(f) χ^2/Ndf for detector 23

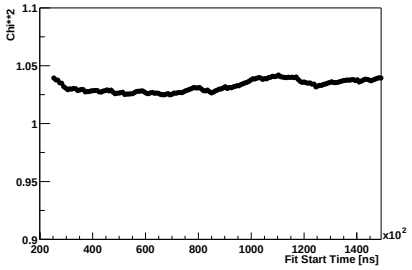

(g) χ^2/Ndf for detector 24

Figure 74: χ^2/Ndf for 7-parameter fit function versus fit start time for detectors 17-24 high n data set.

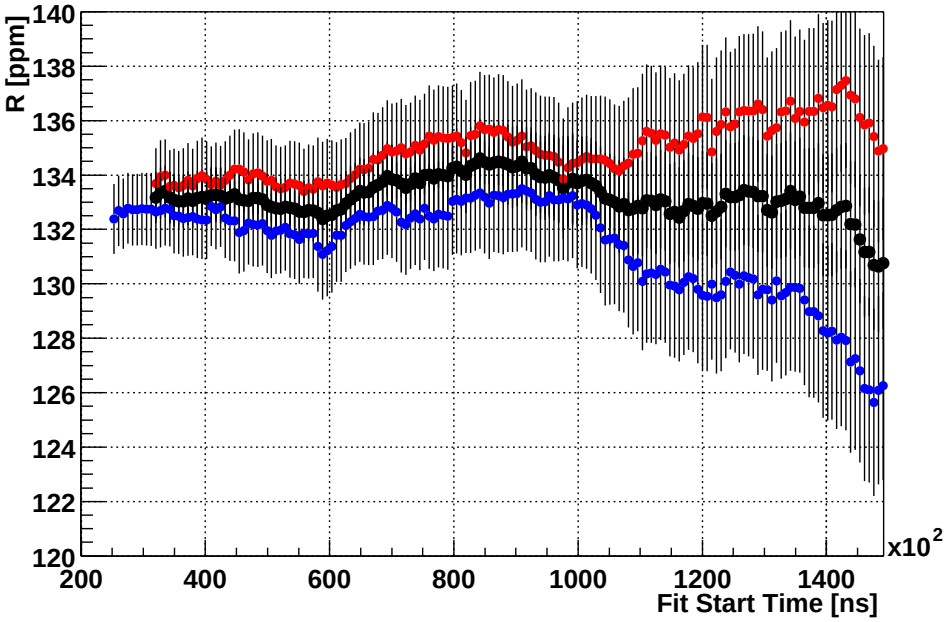

Figure 75: R values for 7-parameter fit function. Black points - value for the sum of 23 detectors. Red points - first half of the ring, blue - second half. Low n data set.

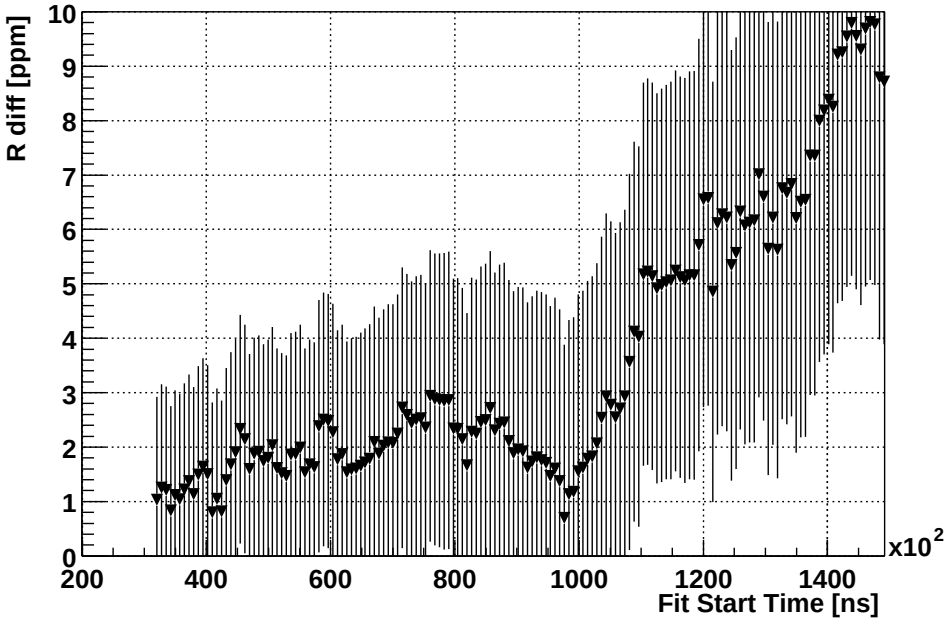

Figure 76: Difference of R values (7-parameter fit function) for the first and second halves of the ring. Low n data set.

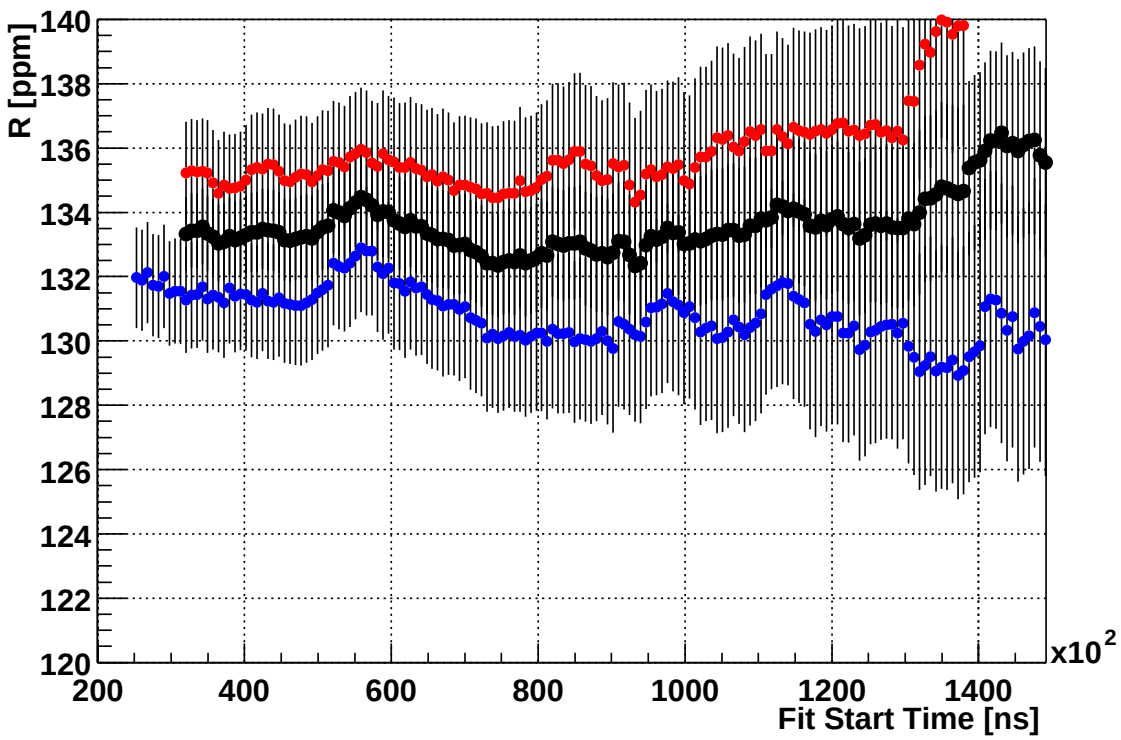

Figure 77: R values (7-parameter fit function) for the sum of 23 detectors (black points) first (red points) and second (blue points) halves of the ring. High n data set.

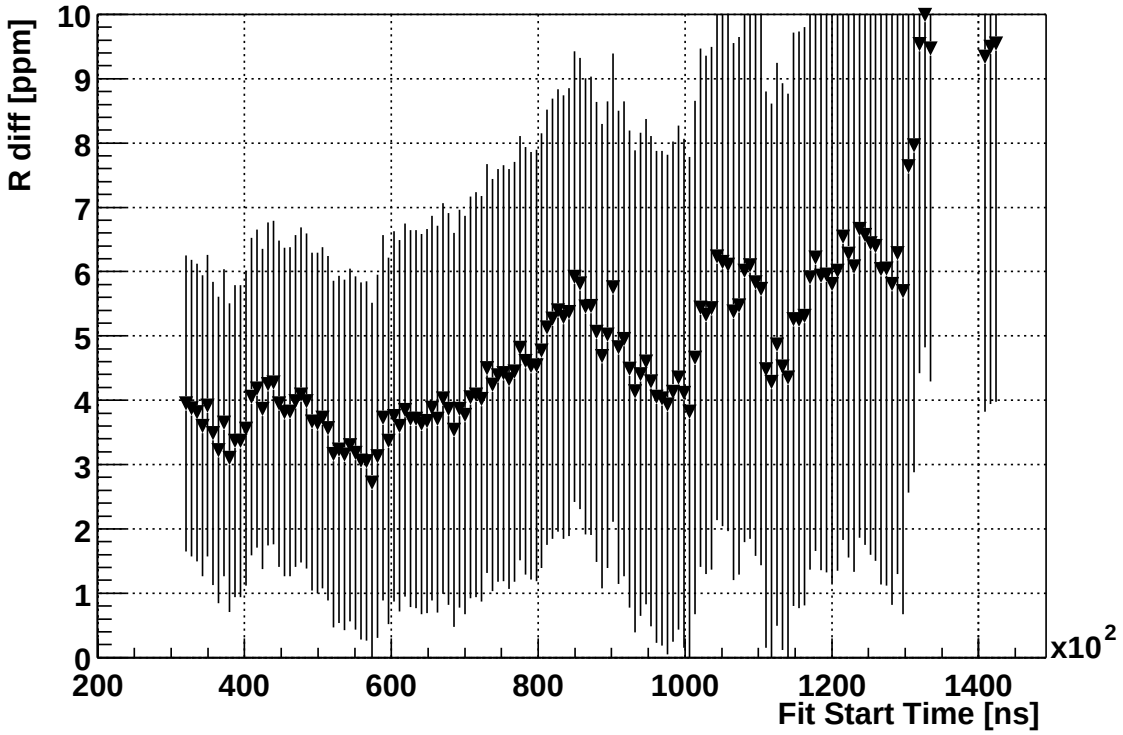

Figure 78: Difference of R values (7-parameter fit function) for the first and second halves of the ring. High n data set.

3.6 Short summary

Summary of the results are shown in Table 5 provides a comparison of R values obtained. More details will be included later.

Table 5: Summary table of fit results at a fit start time of 27.5 μs.

Data Set		3-parameter	31.7 μs	Weighted average	Centroid
low n	R	107.97 ± 0.886	107.94 ± 0.92	107.85 ± 0.881	107.84 ± 0.873
	χ^2/Ndf	0.978 ± 0.005	1.003 ± 0.005	1.008 ± 0.005	
high n	R	107.85 ± 1.095	108.30 ± 1.12	108.08 ± 1.102	108.02 ± 1.10
	χ^2/Ndf	1.012 ± 0.005	1.014 ± 0.005	1.008 ± 0.005	
Low+High	R	107.95 ± 0.686	108.14 ± 0.71	107.85 ± 0.69	107.80 ± 0.69
	χ^2/Ndf	1.006 ± 0.005		1.017 ± 0.005	

4 Systematic Studies

4.1 Ratio Method/Fitting Procedure

In his thesis [1], Long cited a systematic uncertainty of 0.05 ppm for the ratio method. This conservative upper limit accounts for all uncertainties in the fitting procedure, including those due to the choices of binwidth and how to select the value of $r(t)$ within a given time bin.

The error resulting from an uncertainty in the guessed value of the $g-2$ period, T_a, (used to shift the electron time spectra for the ratio method) was studied using Monte Carlo simulated and real data.

MC data were created for each detector using the function:

$$n(t) = N_\circ[i_{det}] \times e^{-t/\tau_\mu} \times (1 - A[i_{det}] \times \cos(\omega_a t + \phi)) \tag{7}$$

Here, $N_\circ[i_{det}]$ and $A[i_{det}]$ are the distributions across detectors of electron number and (g-2) asymmetry observed in the 2001 data, $g-2$ period, $T_a = 4365.4$ ns.

Electron time spectra were randomly splitted into 4 subsets (one shifted in time by $+\ T_a/2$; one by - $T_a/2$; and two not shifted). The value of the time shift T was differed from the $g-2$ period T_a by 50 ppm. The $r(t)$ was constructed using ratio method procedure the same as for the measured data.

The sum of 23 detectors (detector 20 excluded) was fitted using 3 parameter ratio fit function. The difference in R(fit-input) is plotted versus fit start time in Fig. 79.

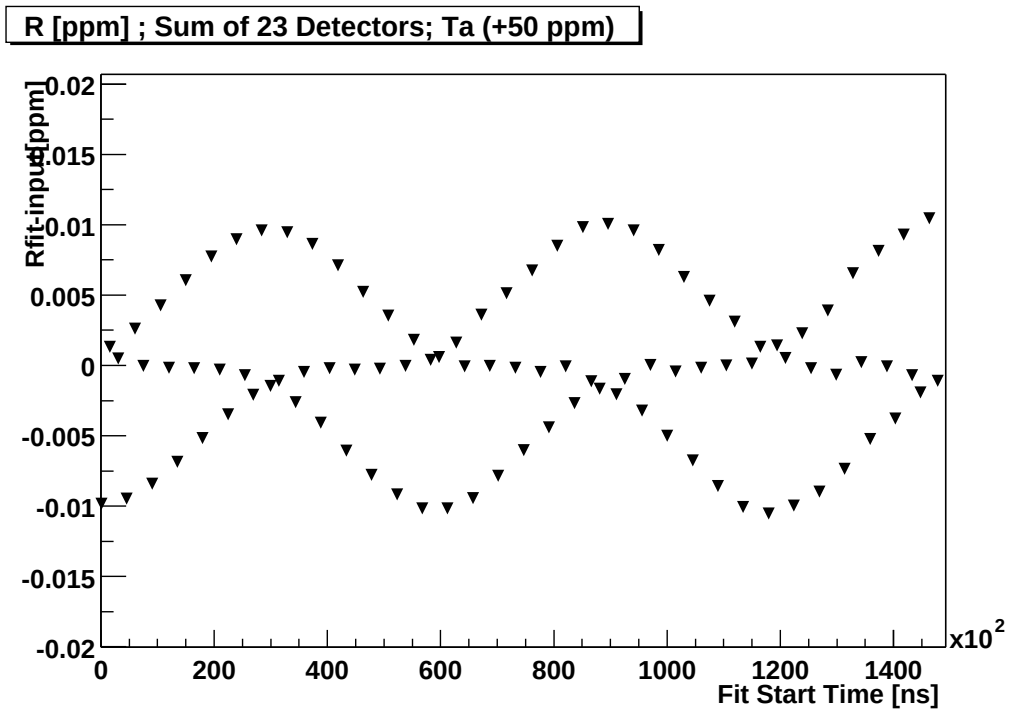

Figure 79: Difference in R between MC input and 3-parameter ratio fit result (sum of 23 detectors) versus fit start time.

The amplitude of the uncertainty oscillations is 0.01 ppm.

Decay electrons time spectra were reproduced using real data for 4 different sets of time shifts: T_a +/- 5 ppm and T_a +/- 10 ppm. The result for 3 parameter fit function of the sum of 23 detectors versus time shift T variation is shown in Fig. 80. The maximum difference is 0.04 ppm and is considered to be the statistical variation due to the random data splitting into 4 subsets.

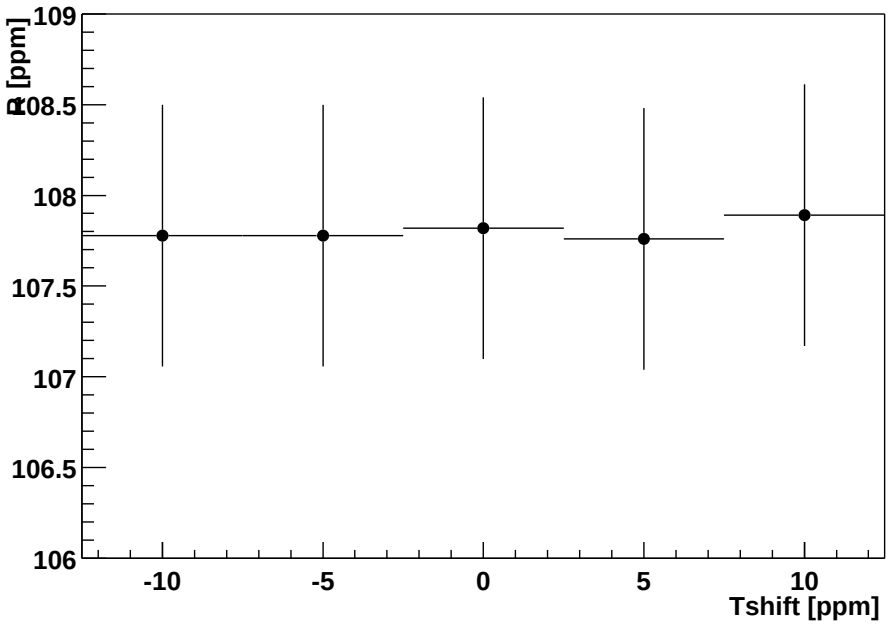

Figure 80: R (3-parameter ratio fit result; sum of 23 detectors) versus variation in T_a.

4.2 Fill randomization

The shifting of electron times in the fill randomization procedure introduces statistical fluctuations in ω_a as well as in the χ^2/Ndf of the fit. In 1999, Long established that for the ratio method the error in R due to randomization is approximately 0.1 times the level of statistics. Averaging over n randomized data sets reduces this error so that $\Delta R = \frac{0.1\sigma_R}{\sqrt{n-1}}$. Assuming a statistical uncertainty of 0.686 ppm, the error in R is 0.03 ppm for 6 random seeds. After fill randomization, the structure of the residual fast rotation leads to a background term in the ratio function. Neglecting this term entirely causes an error of 0.02 ppm [1]. Combining these errors in quadrature yields 0.036 ppm as an estimate for the uncertainty in the fill randomization procedure.

4.3 Pileup subtraction

As a first step, I fitted pileup unsubtracted data. Fig. 83 plots the difference between 3-parameter ratio fit results to pileup subtracted and unsubtracted data for the sum of all detectors. The

maximum of this difference is 0.36 ppm at 31.7 and 0.45 ppm at 27.5 μs. The oscillation probably comes from the non-wiggling part of the pileup spectrum. From Fig. 83 the maximum error made if pile-up not subracted at all is 0.36(0.45) ppm.

In order to estimate the fraction of unsubtructed pileup events the study of the rate dependence of the pile-up fraction was performed. The constructed pile-up events number is proportional to the rate squared (as mostly doule event cases). The total number of events is proportional to the rate. So, the ratio of the number of pile-up events to the total should be proportional to rate. The ideally constructed pile-up should vanishs at zero rate. No muons in the ring - no pile-up events.

These simple assumption allows to check how accurate pile-up events are constructed. The rate value is defined as the mean number of detected electrons per one fill per detector. For each run the rate distribution were plotted and fitted by Gaussian. The fitted mean was used as the rate value for particular detector. The fraction of the pile-up events was measured for the same run. It is the ratio of the constructed pileup events to the total number of events. Bi-dimensional scatter plots were produced for each detector: Y - pile-up fraction; X - mean rate. In Fig. 84 plots for detectors 4, 7, 13 and 23 were shown. Correlation is clearly seen.

Plots were fitted using linear function:

$$PUfraction = A_o + A_1 \times rate \tag{8}$$

The results of fitting are shown in Fig. 85 for detectors 6, 17, 18 and 23. The values of Ao and A1 across detectors were plotted in Figs. 86-87. The deviation of Ao value from zero defines how many pile-up events overconstructed or underconstructed. The value of misconstructed pileup fraction averaged over the all detectors is close to 10%. The slope value A1 is almost uniform across detectors. So, the pileup subtraction is effective to 90%, an error for residual pileup can be set at 0.36(0.45) ppm $\times$ 0.1 = 0.036(0.045) ppm.

The pile-up was constructed for different values of time offset T = 10, 20, 30, 40 and 50 ns. Pile-up subtracted data were fitted using 3-parameter fit function. The R value versus offset time is shown in Fig. 88. The rms of R distribution is 0.107 ppm including statistical fluctuation. This error is due to the statistical nature of the constructed pile-up. This error is added quadratically to the statistical uncertainty in R resulting 0.686 ppm statistical error instead of original 0.677 ppm.

Some uncertainty can be made in the constructed pile-up pulse energy too. To estimate the dependence of mean energy versus rate for the pile-up and normal events was studied. 1.8 GeV lower energy threshold was used. Mean energy versus rate was plotted for detectors 13 and 24 in Fig. 81. The mean energy versus rate was fitted using linear function. The slope and intersept versus detector plotted in Fig. 82.

The average difference in mean pile-up energy is 0.043 GeV leads to the uncertainty in number of pile-up events, asymetry and phase. Following the formalism developed in V.Logashenko note (conserning low energy pile-up) the estimate for resultant additional uncertainty is 0.042 ppm.

Combining two estimates in quadrature gives the total pile-up associated uncertainty of 0.06(0.07) ppm.

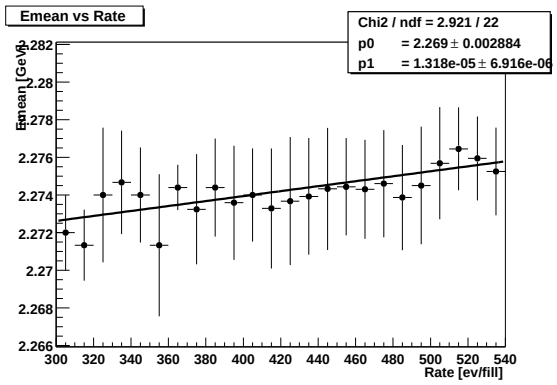

(a) det 13

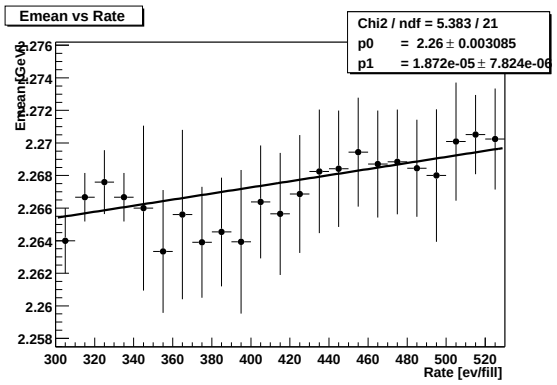

(b) det 24

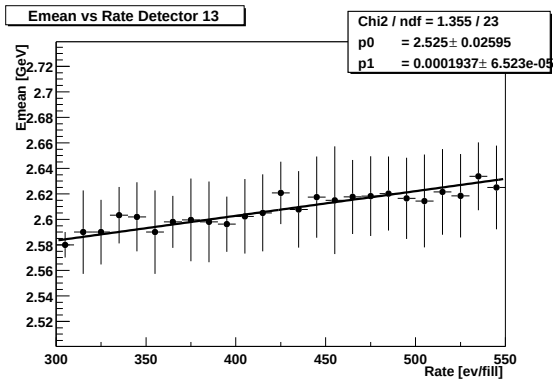

(c) det 13 Pile-up

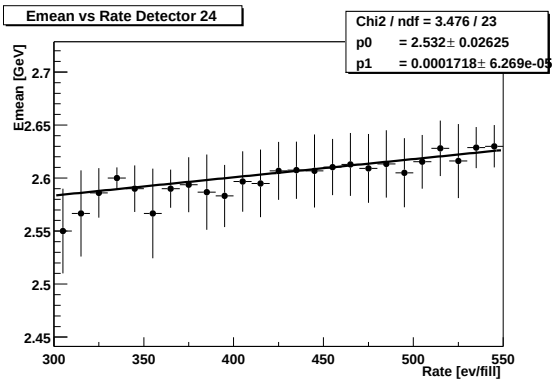

(d) det 24 Pile-up

Figure 81: Mean energy versus rate for normal and pile-up events for detectors 13 and 24. Two data sets together.

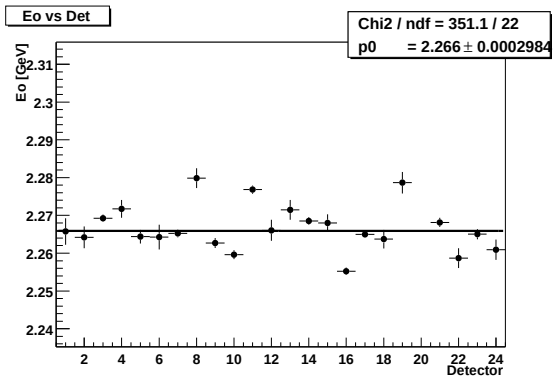

(a) normal events

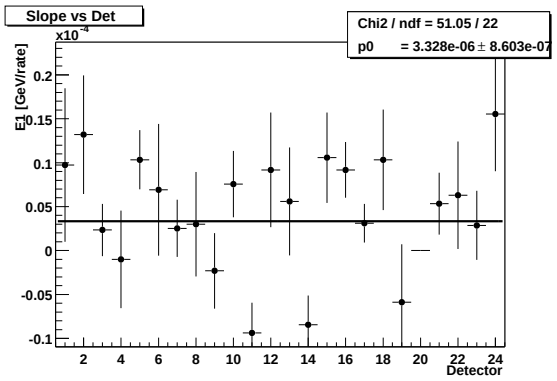

(b) normal events

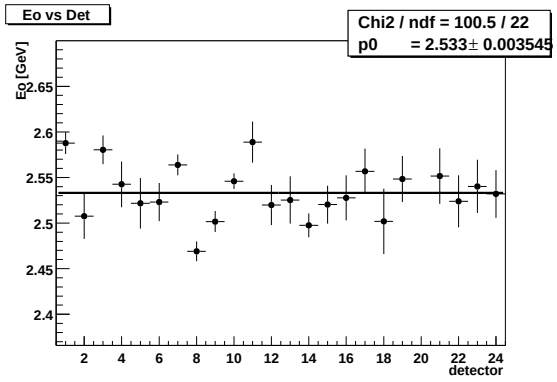

(c) pile-up

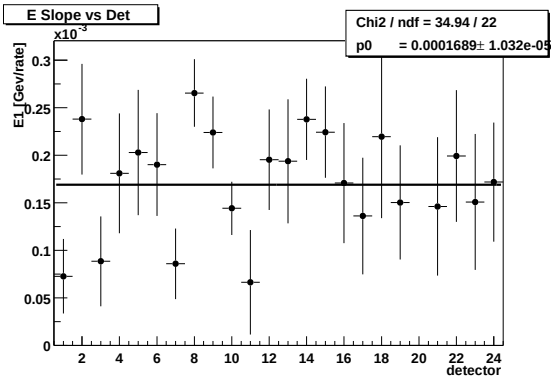

(d) pile-up

Figure 82: Intersept and slope of mean energy versus rate dependance fitted by linear function for normal and pile-up events versus detector. Two data sets together.

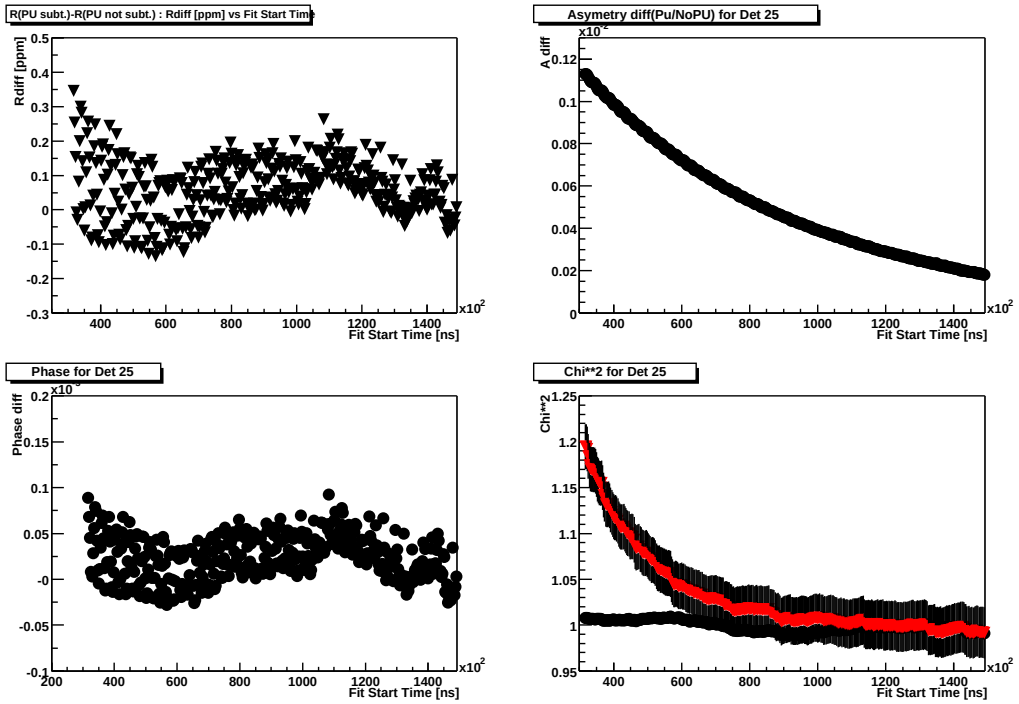

Figure 83: Difference between fitting pileup subtracted and unsubtracted data for the 3-parameter ratio fit (sum of all detectors). The R difference (top left) has a maximum of 0.36 ppm and max amplitude of 0.3 ppm. Asymetry and phase differences are plotted top right and bottom left. χ^2/Ndf difference is plotted bottom right.

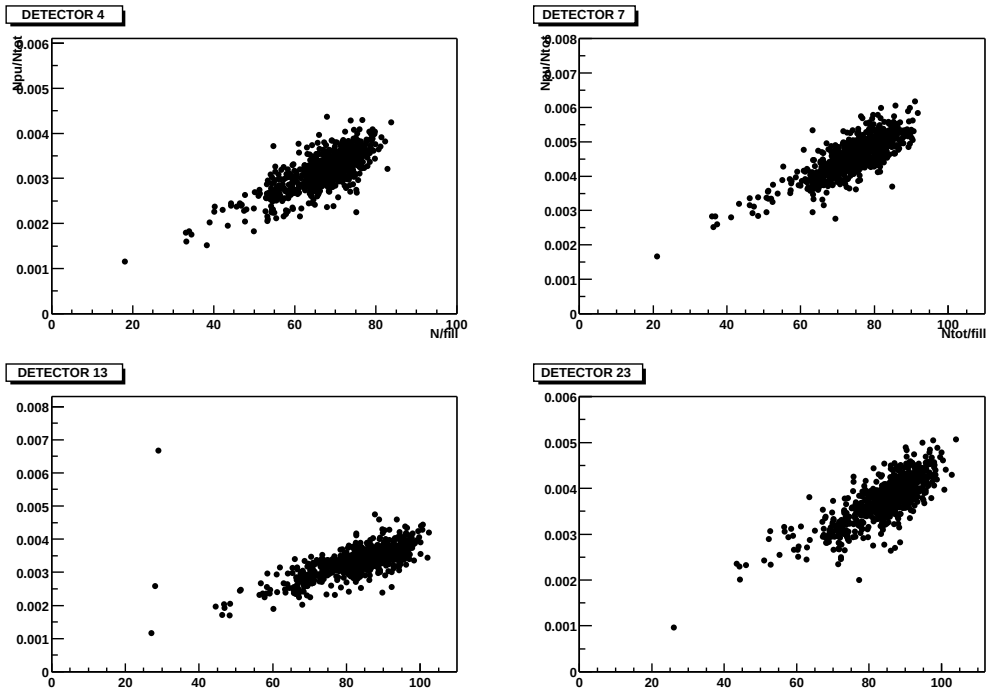

Figure 84: Two-dimensional plots of pile-up fraction (N_{pu}/N_{tot}) versus rate for detectors 4, 7, 13 and 23. Clear correlation seen.

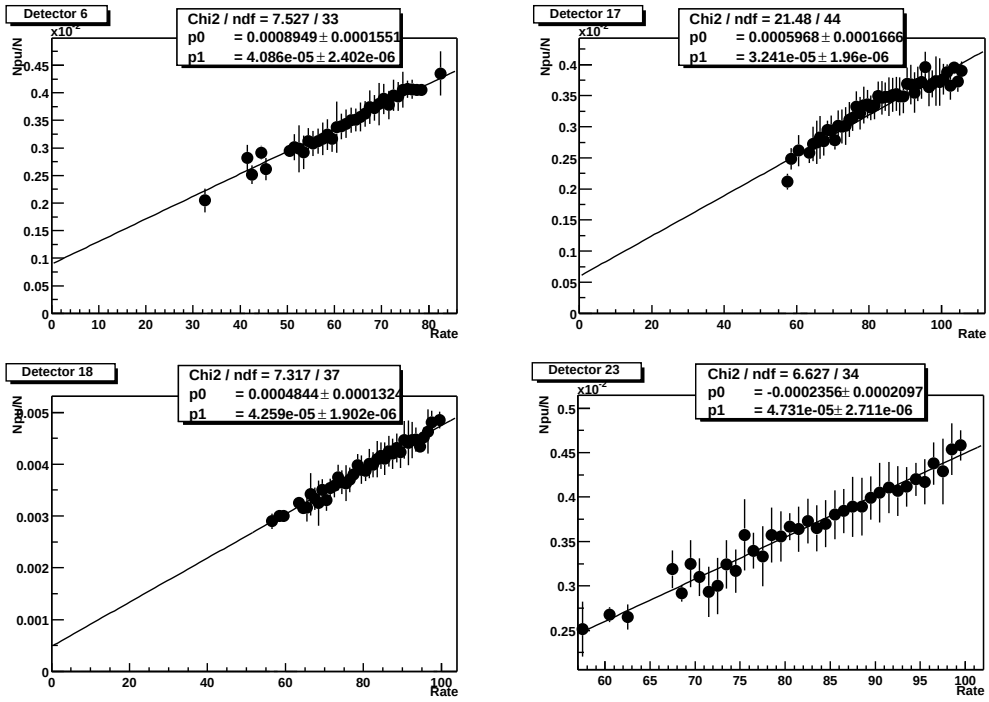

Figure 85: Linear fitting of pile-up fraction (N_{pu}/N_{tot}) versus rate for detectors 6, 17, 18 and 23.

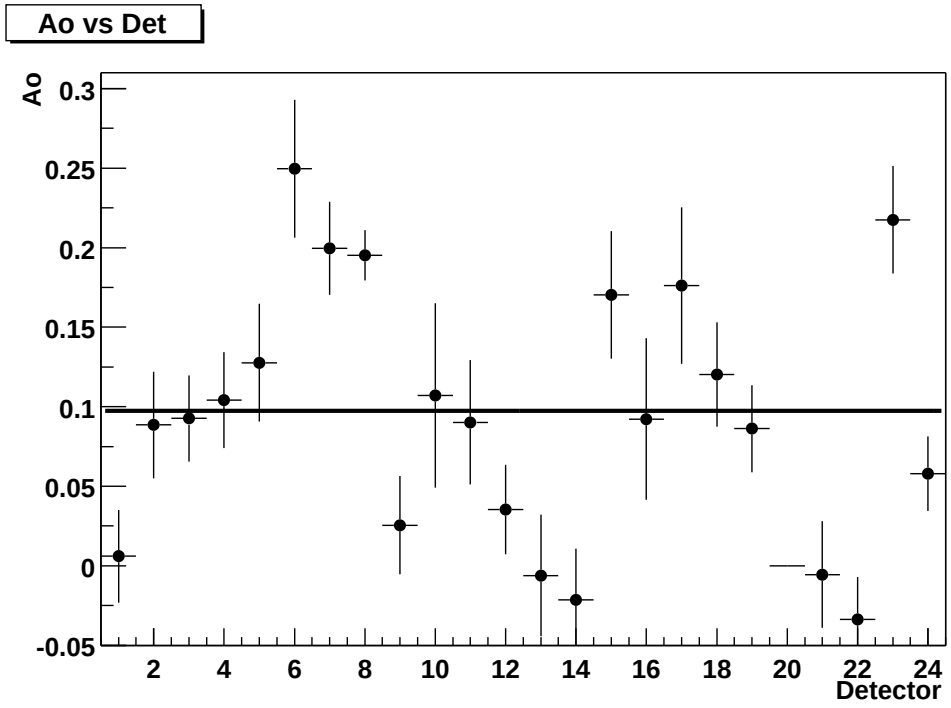

Figure 86: Linear fitting normalized Ao coefficient versus detector.

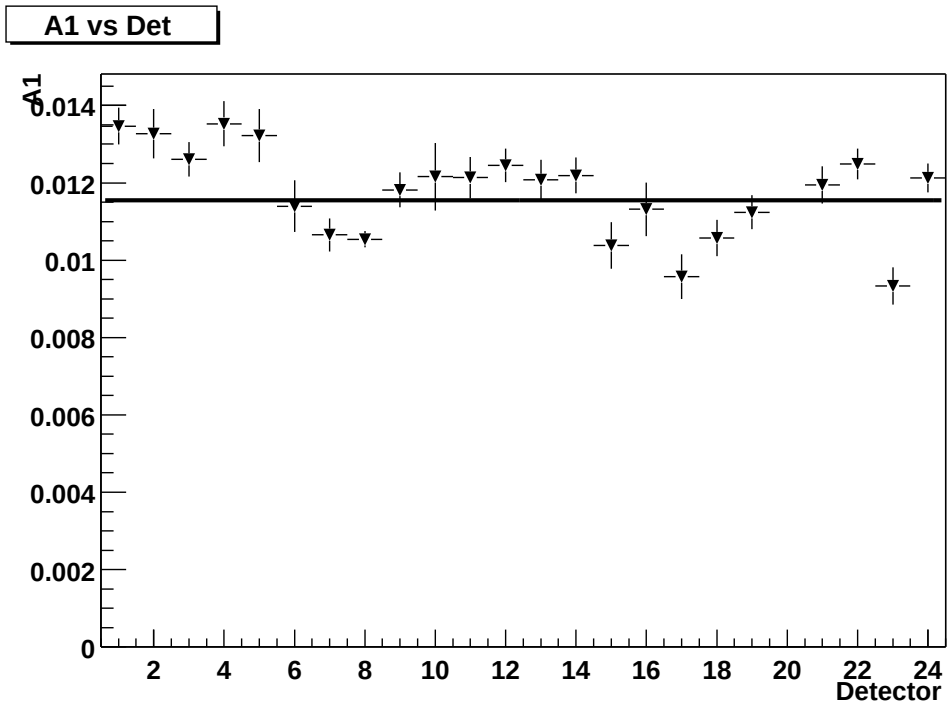

Figure 87: Linear fitting A1 coefficient versus detector.

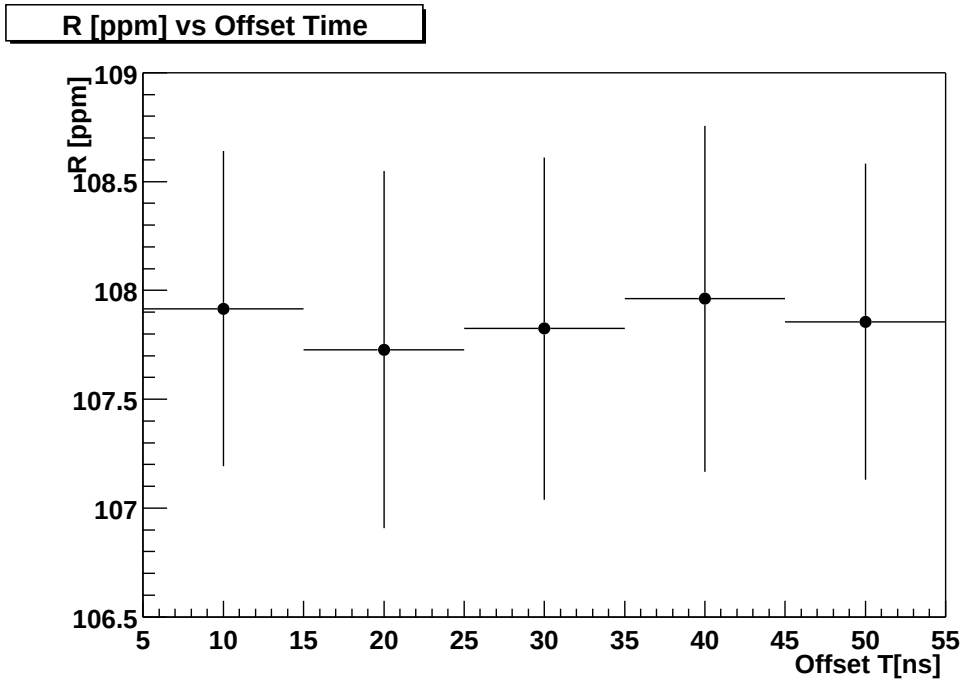

Figure 88: R versus constructed pile-up offset time T.

4.4 Energy threshold variation.

In this subsection, the fit results versus energy threshold variation were studied. The optimal subtraction of pile-up events requires the energy threshold to be applied to the data. To estimate the uncertainty associated with the energy threshold applied, the later was varied in the range of 1.7 - 2.2 GeV with 100 MeV step. The sum of 23 detectors (detector 20 excluded) was fitted using 3 parameter ratio fit function for each value of the threshold. The R (asymetry, phase and χ^2/Ndf) versus low energy threshold is plotted in Fig. 89. Six random seeds was used. The fit start time is 31.7 μs. The slope of R versus threshold is 0.973 ppm/GeV if fitted by linear fuction.

4.5 Gain Correction

R (3 parameter fit function) before and after gain correction and their differences versus detector are shown in Fig. 90.

The correlation between gain correction and pileup subtraction was plotted in Fig. 91. For each detector the difference between pileup subtracted and not subtracted values for R were plotted against difference in R before and after gain correction. The correlation coefficient C was calculated to be equal to -0.453.

Projection of the correlation plot on the gain axe is shown in Fig. 92.

Projection of the correlation plot on the pileup axe is shown in Fig. 93.

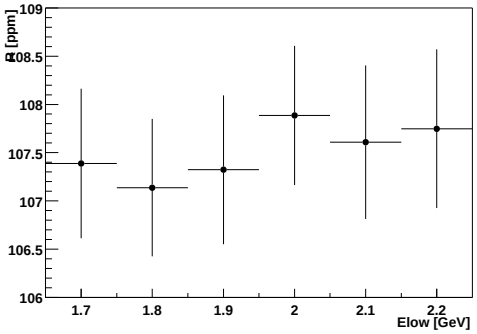

(a) R

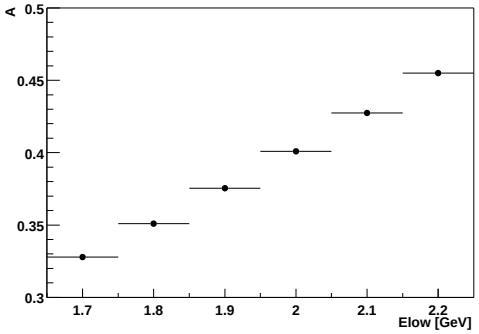

(b) A

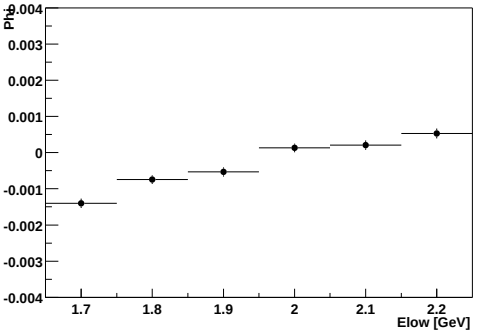

(c) Phase

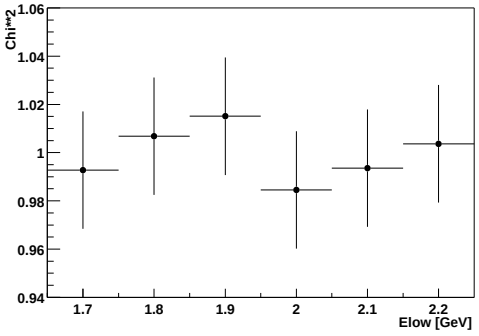

(d) χ^2/Ndf

Figure 89: R, asymetry A, phase and fit χ^2/Ndf versus low energy threshold at 31.7 μs. Results of 3 parameter fit function for the sum of 23 detectors. Two data sets together.

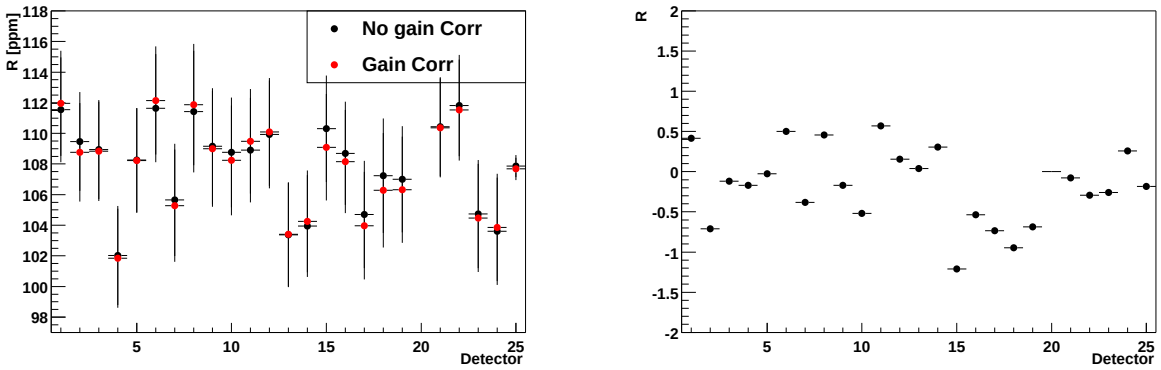

(a) R (b) Rdiff

Figure 90: R(3 par) versus Detector.

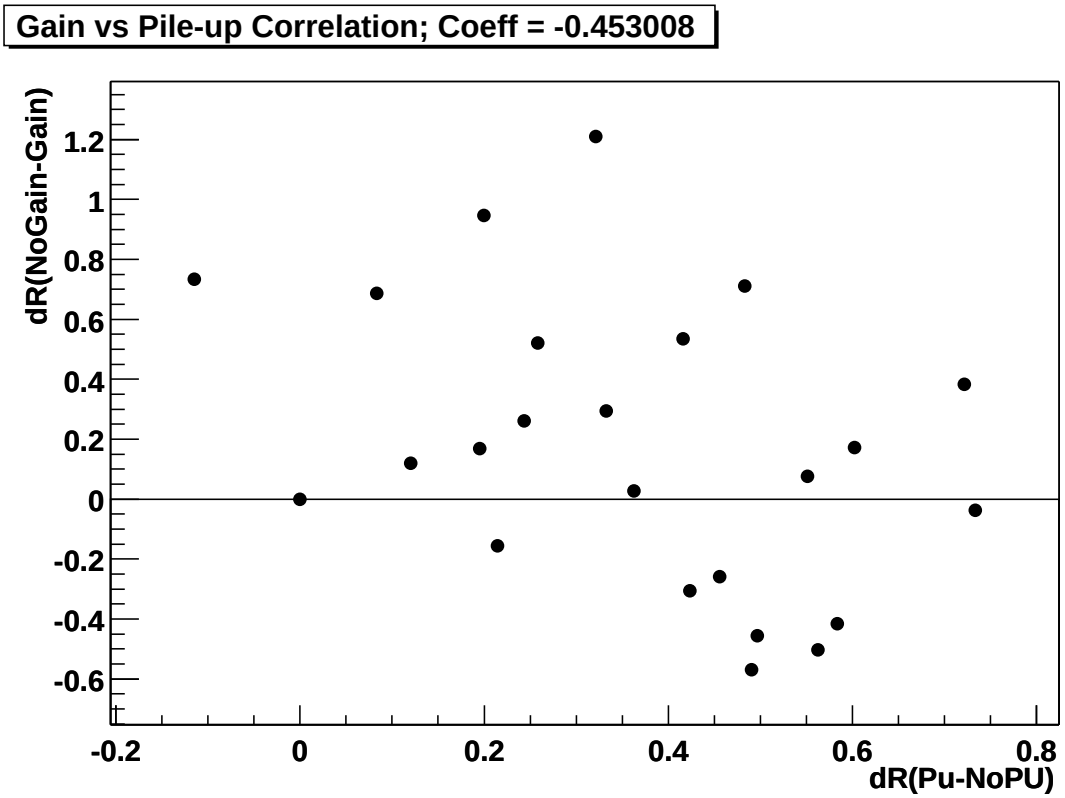

Figure 91: Correlation between Gain correction and Constructed Pile-Up subtraction.

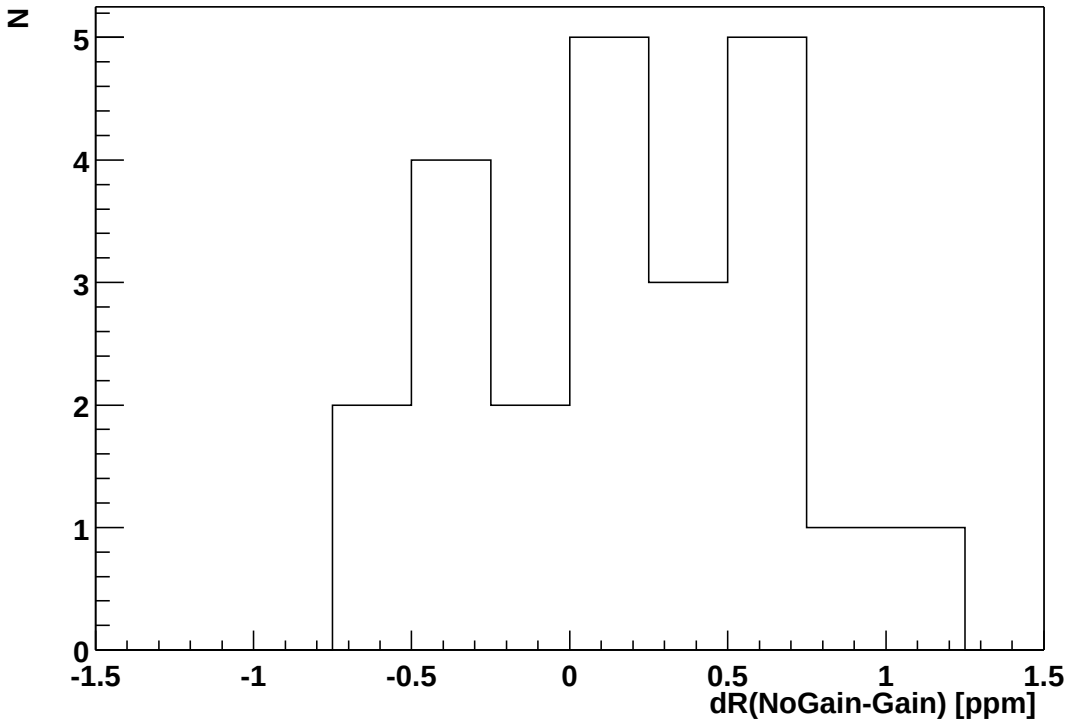

Figure 92: Difference in R [ppm] between gain not corrected and corrected data.

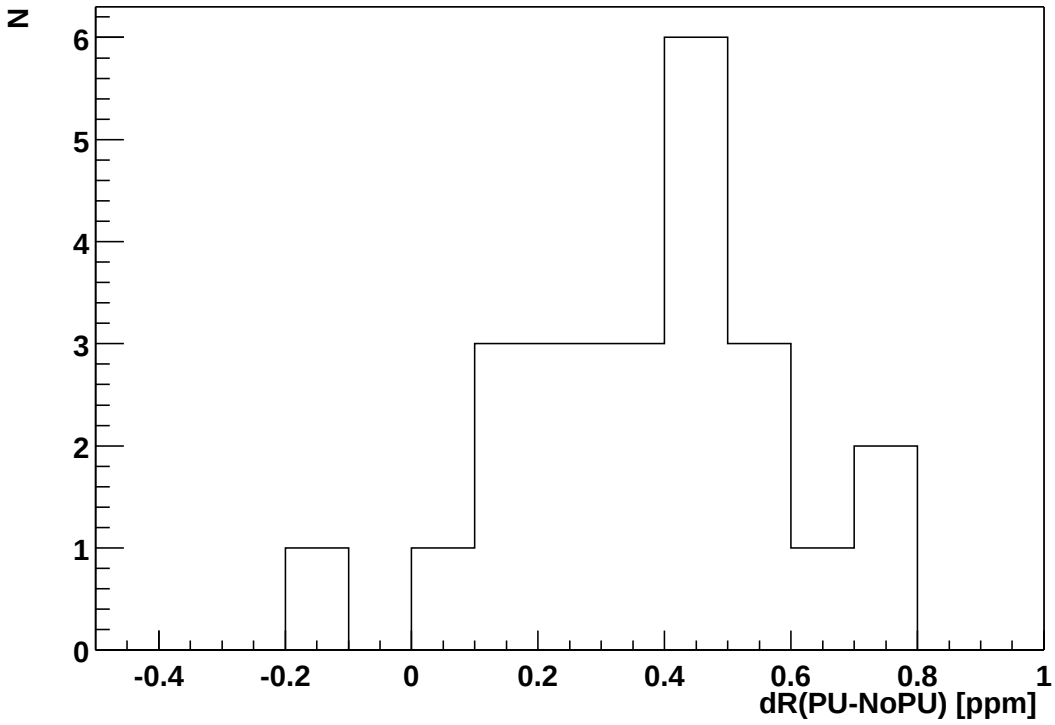

Figure 93: Difference in R [ppm] between Pile-up subtracted and not subtracted data.

In order to estimate gain systematic uncertainty different gain correction factors were applied. The factor 2 means that gain correction procedure was performed twice, gain factor -2 means that inverse gain correction were applied twice and etc.

The result of 3-par fitting for R plotted in Fig. 95 for start time 27.5 μs and in Fig. 94 for 31.7 μs . The uncertainty in gain is expected to be 40%. The resultant gain systematic uncertainty is 0.087 ppm.

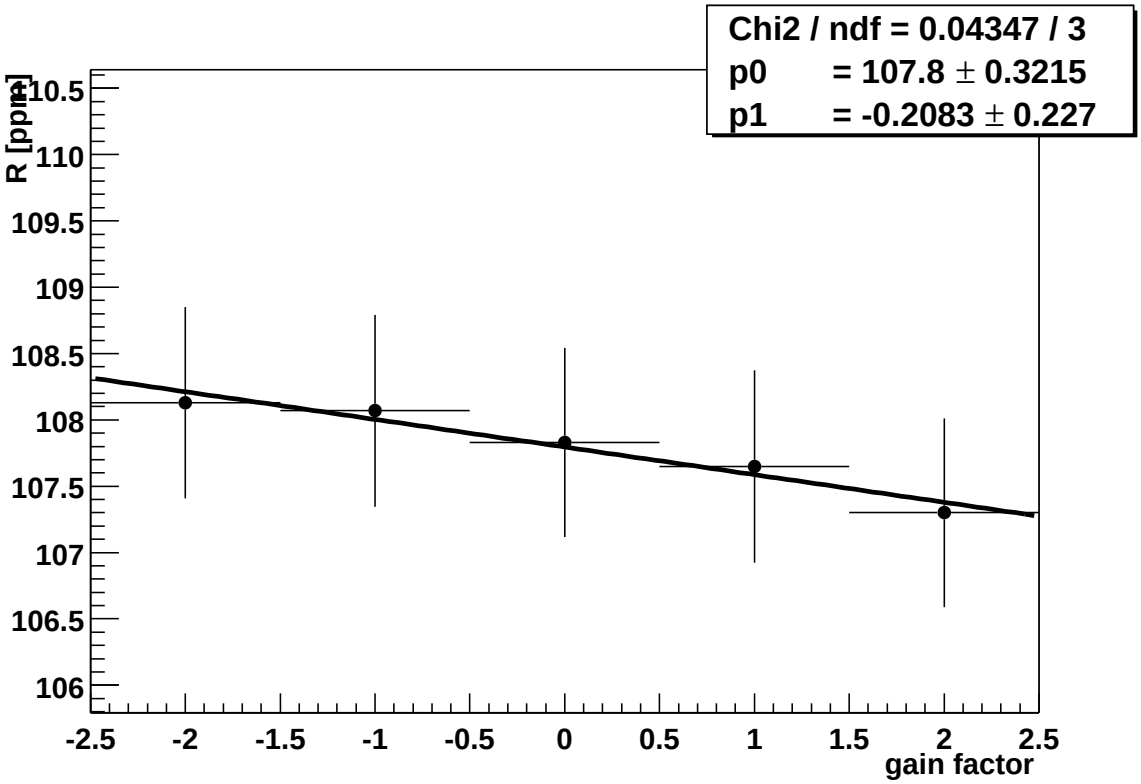

Figure 94: R versus gain factor. Fit start time 31.7 μs

4.6 $G2Too$ and $g2off$ comparison

In this section fit results for $G2Too$ and $g2off$ data are presented. The comparison between two different playbacks of the data provides the important check of the analysis. Fill randomization and pile-up subtraction were applied to the WFD reconstructed data prior to the ratio method fitting. The same fill randomization period of 149.185 ns was used for $G2Too$ and $g2off$ data. Fill randomization procedure introduces small uncertainty in the fitted values of R, A and phase. To reduce this uncertainty multiple random seeds were used. Four sets (random seeds) of the pseudorandom numbers were used for $G2Too$ and the same number of seeds for $g2off$. In all histograms 149.185 ns bin width was used. All fits stopped at 500 μs to guarantee the Gaussian events distribution for all the bins used. The same earliest fit start times were used for $G2Too$ and $g2off$.

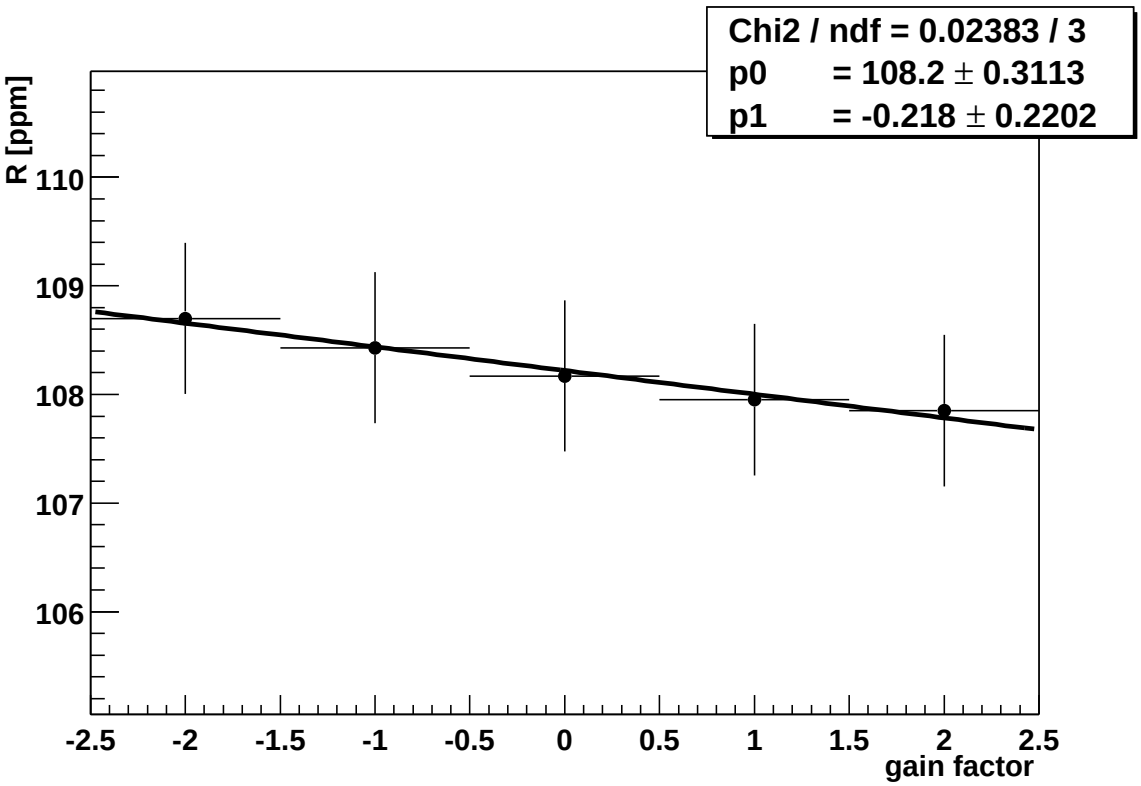

Figure 95: R versus gain factor. Fit start time 27.5 μs

As for the pile-up construction, the same Mediterranean method was used for both data. The time offset $T = 10$ ns and time window width $T_w = 5$ ns were used for $G2Too$ data and $T = 15$ ns, $T_w = 2.9$ ns for $g2off$.

Golden runlist was used for the run selection for both data. For $g2off$ data some runs presented for $G2Too$ were missing: 9472-9479, 10560, 10825-10837, 11226, 11381. Totally 15 runs missing for $g2off$.

The results are presented for low and high n data subsets separately.

For the $G2Too$ and $g2off$ results comparison the data overlap is important. The right way to do data overlap measurement is pulse-by-pulse comparison. But it seems posssible to estimate data overlap using relatively easy procedure.

For each run and each detector the difference in number of events detected by $G2Too$ and $g2off$ were measured. Because of different the pile-up events representaion for $G2Too$ and $g2off$ (10 ns offset for $G2Too$ and 15 ns for $g2off$) data the number of pile-up events were added to the calculated difference. The resultant absolute value was plotted versus run number. The integrated difference was accumulated for each detector. Since the sum of 23 detectors were used to obtain the results for R the accumulated differences for all 23 detectors were added to produce the summary difference. So, the ratio of the accumulated number of events to the total event number gives the estimation of two productions data overlap.

In Fig. 96 the number of events versus detector was plotted for low n data. The data overlap is

estimated to be 93.4%.

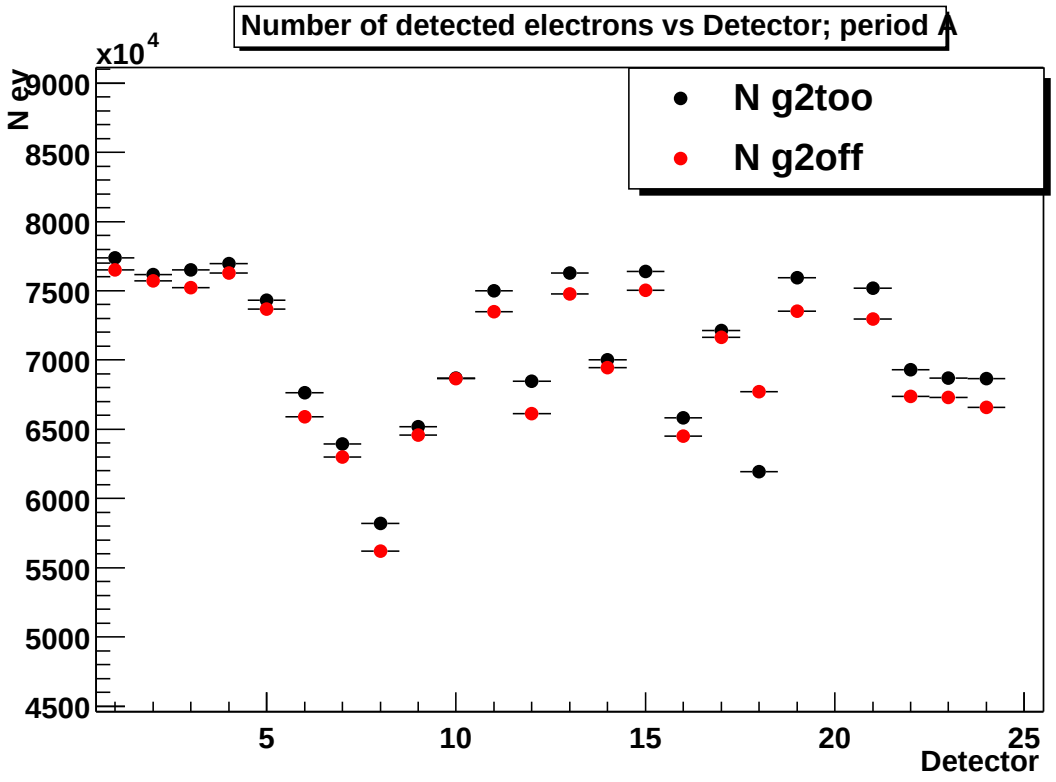

Figure 96: Number of events versus detector for $G2Too$ and $g2off$. Low n data.

In Figs. 97-99 R, asymetry A and χ^2/Ndf for the sum of 23 detectors versus fit start time were plotted for low n data. All the results obtained at fit start time 31.7 μs.

In Figs. 100-102 R, asymetry A and χ^2/Ndf versus detector were plotted for low n data. Detector 25 is the sum of 23 detector, detector 26 is the sum for detectors 1-12 and detector 27 - sum of detectors 13-24.

χ^2/Ndf averaged across 23 detectors gives:

$G2Too$ - 1.011 ± 0.005 , $g2off$ - 0.998 ± 0.004.

In Fig. 103 the number of events versus detector was plotted for high n data. The data overlap is estimated to be 94.7%.

In Figs. 104-106 R, asymetry A and χ^2/Ndf for the sum of 23 detectors versus fit start time were plotted for high n data.

In Figs. 107-109 R, asymetry A and χ^2/Ndf versus detector were plotted for high n data. Detector 25 is the sum of 23 detector, detector 26 is the sum for detectors 1-12 and detector 27 - sum of detectors 13-24.

χ^2/Ndf averaged across 23 detectors gives:

$G2Too$ - 1.013 ± 0.0055 , $g2off$ - 1.011 ± 0.005.

Summary of the $G2Too$ and $g2off$ comparison results are shown in Table 6. Where δR is the difference between $g2off$ and $G2Too$ at 31.7 μs, δ allowable variation of R calculated according to

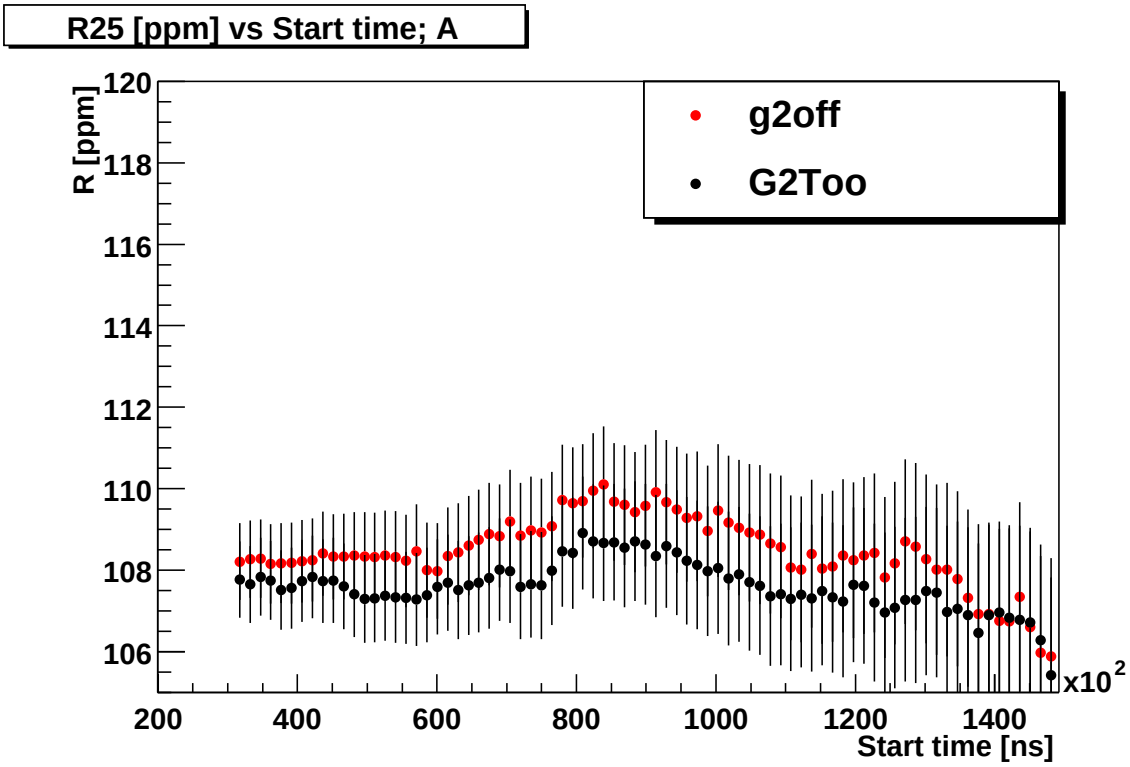

Figure 97: R for the sum of 23 detectors versus fit start time for $G2Too$ and $g2off$. Low n data.

data overlap.

For low n data the difference in R between $G2Too$ and $g2off$ δR is compatible with the allowable variation δ.

For high n data set the difference in R between $G2Too$ and $g2off$ δR is much higher then allowable variation δ.

Table 6: Summary table of $G2Too$ and $g2off$ 3 parameter ratio fit results at a fit start time of 31.7 μs.

Data Set		R $G2Too$ [ppm]	R $g2off$ [ppm]	δR [ppm]	δ [ppm]
low n	R	107.83 ± 0.93	108.21 ± 0.94	0.38	0.39
high n	R	108.06 ± 1.12	108.92 ± 1.13	0.86	0.38

4.7 Muon losses/AGS flashlets

Not studied. The estimation is 0.08 ppm for losses and 0.01 ppm for flashlets (taken from Jon's report).

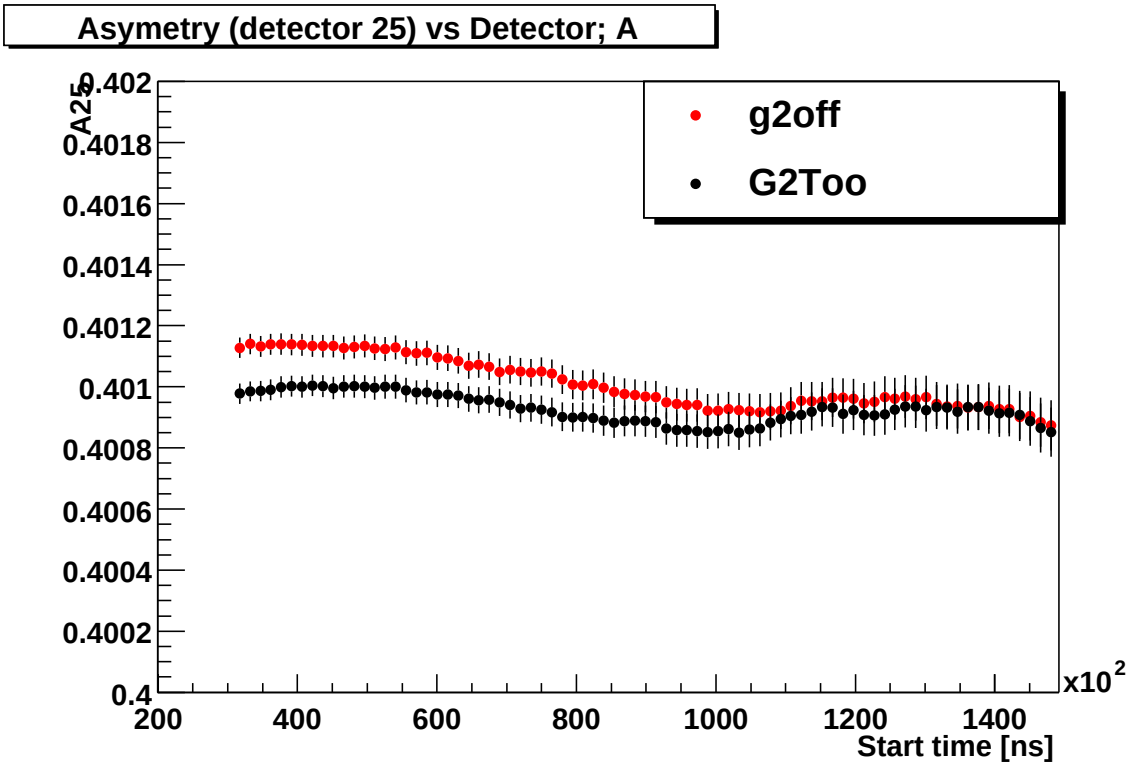

Figure 98: Asymetry for the sum of 23 detectors versus fit start time for $G2Too$ and $g2off$. Low n data.

4.8 Coherent Betatron Oscillations (CBO)

The error in R associated with coherent betatron oscillations (CBO) is due to the beating between ω_{cbo} and $2\omega_a$. In 2001, g-2 experiment ran with the quad tunings that set ω_{cbo} far beyond $2\omega_a$. As a result, the systematic errors due to CBO effect are much smaller than in 2000. In order to quantify the CBO related errors, Monte Carlo data was created in an attempt to reproduce the observed characteristics of the CBO in the 2001 data set. This section describes in detail the simulation studies which were carried out.

Monte Carlo data were created without statistical fluctuations. 1000 data sets were produced to simulate real data runs. The CBO was introduced in each set by including both the asymmetry and phase modulations :

$$N_{cbo} = N' \times e^{-t/\tau_{cbo}} \times \cos(\omega_{cbo}t + \phi_{cbo}) \tag{9}$$

$$A_{cbo} = 0.005 \times e^{-t/\tau_{cbo}} \times \cos(\omega_{cbo}t + \phi_{cbo}) \tag{10}$$

$$\Phi_{cbo} = 0.003 \times e^{-t/\tau_{cbo}} \times \cos(\omega_{cbo}t + \phi_{cbo}) \tag{11}$$

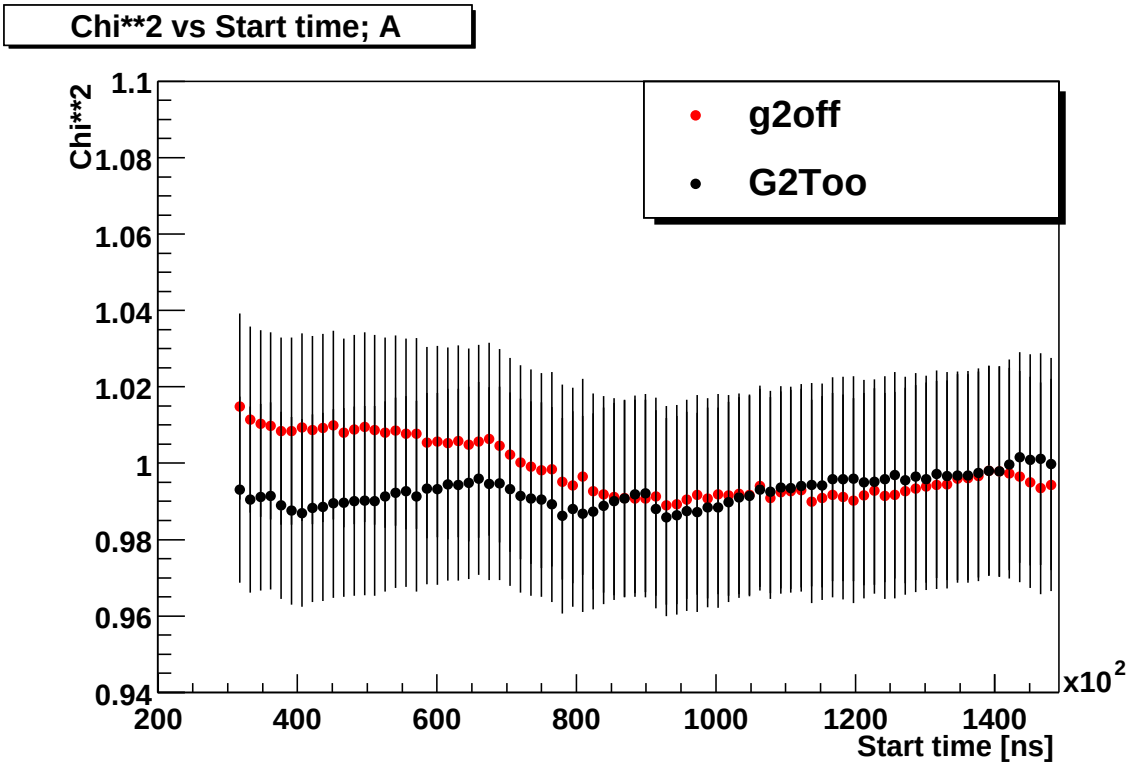

Figure 99: χ^2/Ndf for the sum of 23 detectors versus fit start time for $G2Too$ and $g2off$. Low n data.

where N' is 0.024 for detectors 7, 8, and 9, and 0.009 for the others. (These relative weightings were determined from the size of the peak in the FFT of the divided residuals from the fit to the data [3].) 700 runs were simulated for low CBO frequency (low n) and 300 run for high (high n).

The CBO phases for detectors were extracted from the 9-parameter ratio fit of the data. For each run, phases were simulated to be Gaussian distributed around the mean value with the width determined by the error in phase measurement. This was done to include phase uncertainty into the simulation process. Phases versus detector is plotted in Fig. 110 for low and high n data sets.

Bringing together these contributions yields the function that was used to create the data:

$$n(t) = N_\circ[i_{det}] \times (1 + N_{cbo}) \times e^{-t/\tau_\mu} \times (1 - A[i_{det}] \times (1 + A_{cbo}) \times \cos(\omega_a t + \phi + \Phi_{cbo}) \qquad (12)$$

Here, $N_\circ[i_{det}]$ and $A[i_{det}]$ are the distributions across detectors of electron number and (g-2) asymmetry observed in the 2001 data. Monte Carlo low and high n data were created as described above, with a CBO frequency given by $\omega_{cbo} = 2\pi f_{cbo}$ ($f_{cbo} = 418.5$ kHz for low n data, $f_{cbo} = 490.6$ kHz for high n data set) and an exponential lifetime of 90.5 μs and 125.0 μs. The binwidth was chosen to be 149.185 ns.

The runs were added together in the same manner as for the real data: low, high n and combined data sets.

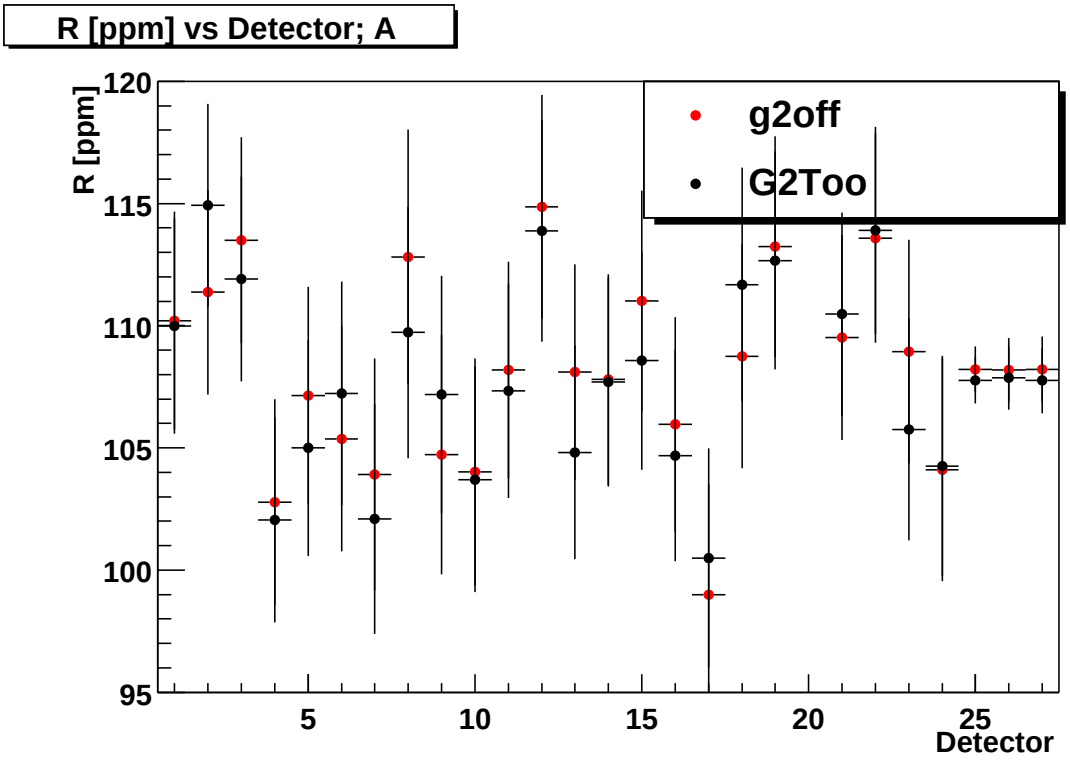

Figure 100: R versus detector for $G2Too$ and $g2off$. Low n data.

The data was fitted using 3-parameters functional form. The result for the difference in R between Monte Carlo input and fit output is plotted versus fit start time in Fig. 111 for the low n, high n and sum of two sets (combined data set). Note the realistic value of half-ring effect obtained for the appropriate run data sets simulation. For low n data set half-ring amplitude is 1.5 ppm, while for the high n - 2.0 ppm.

Table 7: Input parameters for CBO simulation.

Data set	N electrons, B	f_{cbo}(kHz)	τ_{cbo}(μs)
low n	2.78	419.1	130.0
high n	1.5	490.6	92.0

Fig. 112 shows the result of fitting combined simulated data set for the sum of 23 detectors.

The CBO concelation factor is 10 for the MC data close to the measured value.

As a cross check the data were fitted using modified 7 parameter fit function to include main CBO frequency. That functional form of the ratio method can be written:

$$r(t) \quad = \quad A(1 + e^{-t/\tau_{cbo}}[A_1 \cos(\omega_{cbo} t) + B_1 \sin(\omega_{cbo} t)])\ \cos(\omega_a t + \phi$$

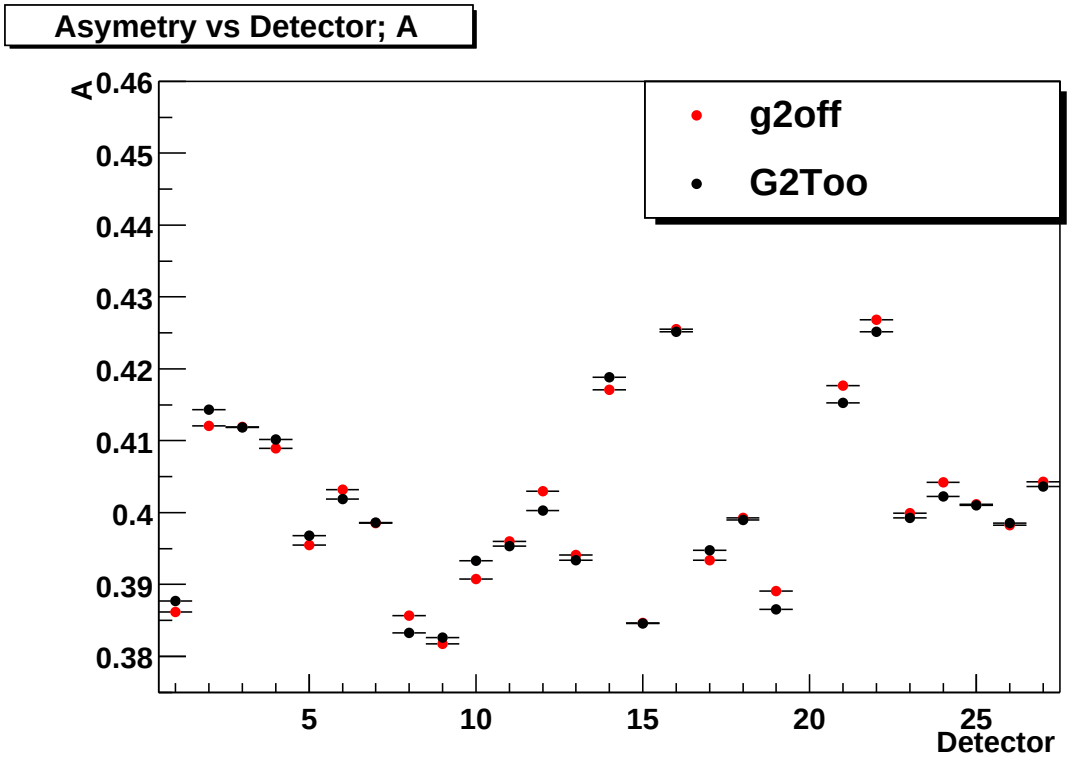

Figure 101: Asymetry A versus detector for $G2Too$ and $g2off$. Low n data.

$$+ \quad e^{-t/\tau_{cbo}}[A_2\cos(\omega_{cbo}t) + B_2\sin(\omega_{cbo}t)]) + 0.000287. \tag{13}$$

The CBO frequency, $\omega_{cbo} = 2\pi/f_{cbo}$, and exponential CBO lifetime were fixed. For low n data set $f_{cbo} = 419.1$ kHz ; $\tau_{cbo} = 92.0$ μs, and $f_{cbo} = 490.6$ kHz ; $\tau_{cbo} = 130.$ μs for high n data set respectively (see Jon's report).

The fit results of using modified 7-parameters function are plotted in Figs. 113-114 and in Figs. 48-50.

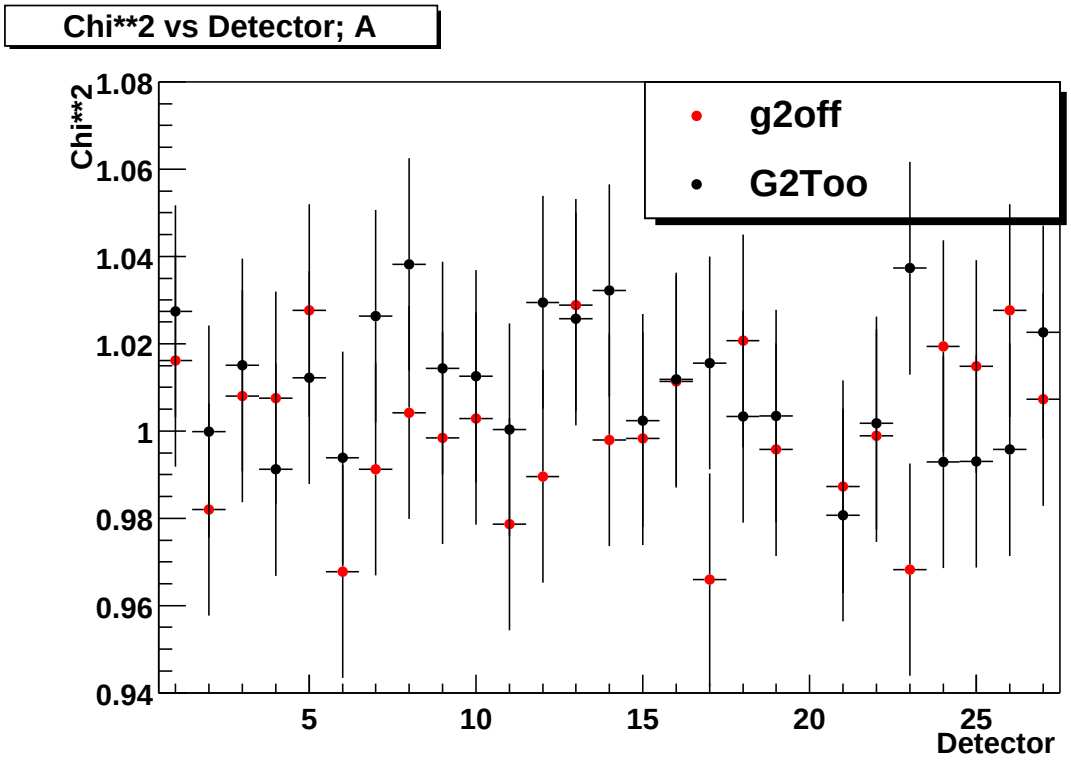

Figure 102: χ^2/Ndf versus detector for $G2Too$ and $g2off$. Low n data.

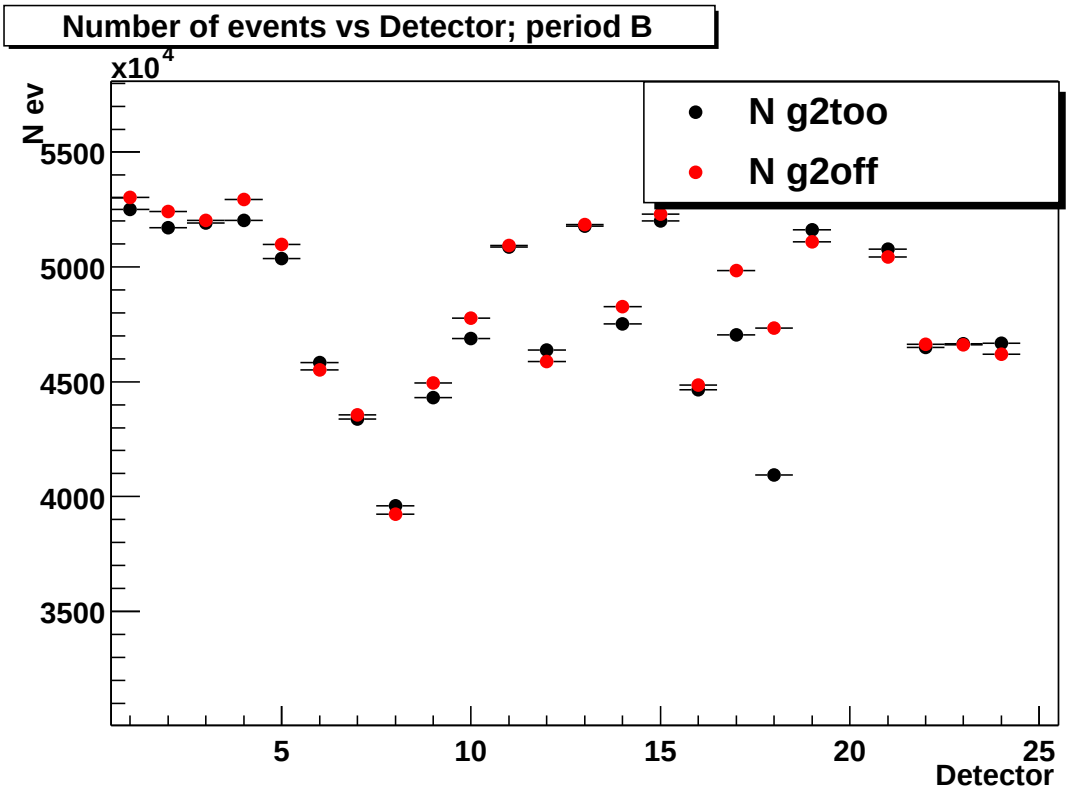

Figure 103: Number of events versus detector for $G2Too$ and $g2off$. High n data.

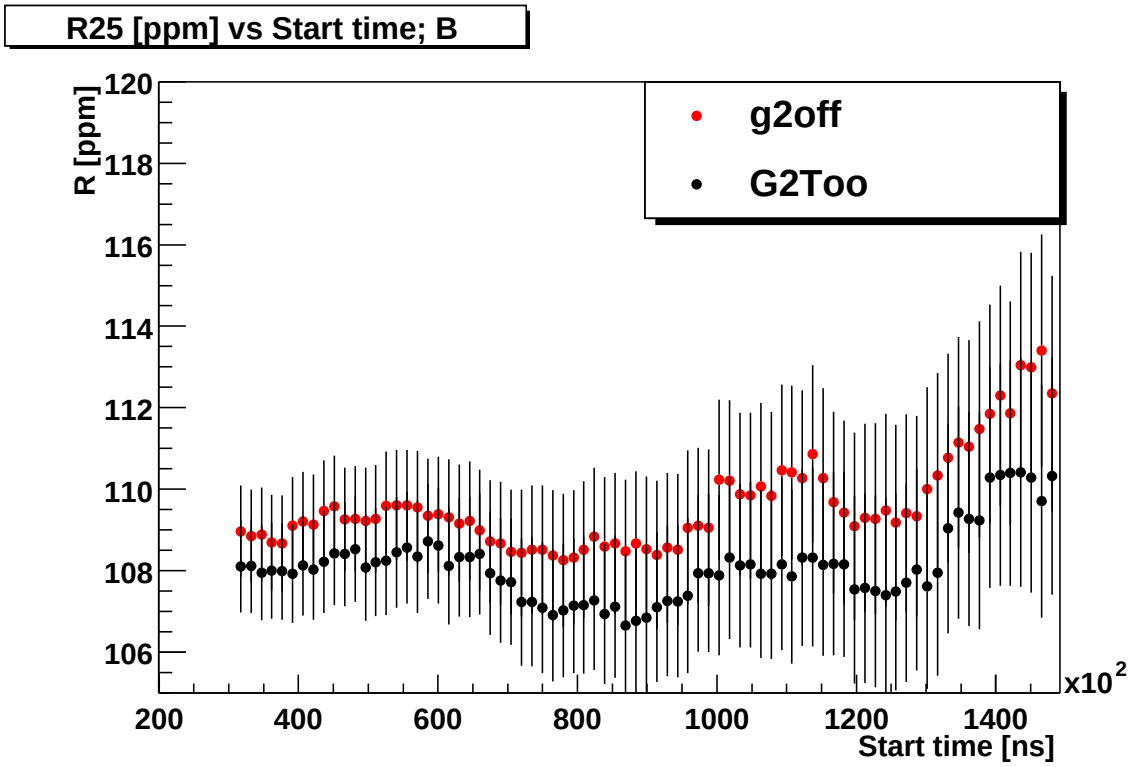

Figure 104: R for the sum of 23 detectors versus fit start time for $G2Too$ and $g2off$. High n data.

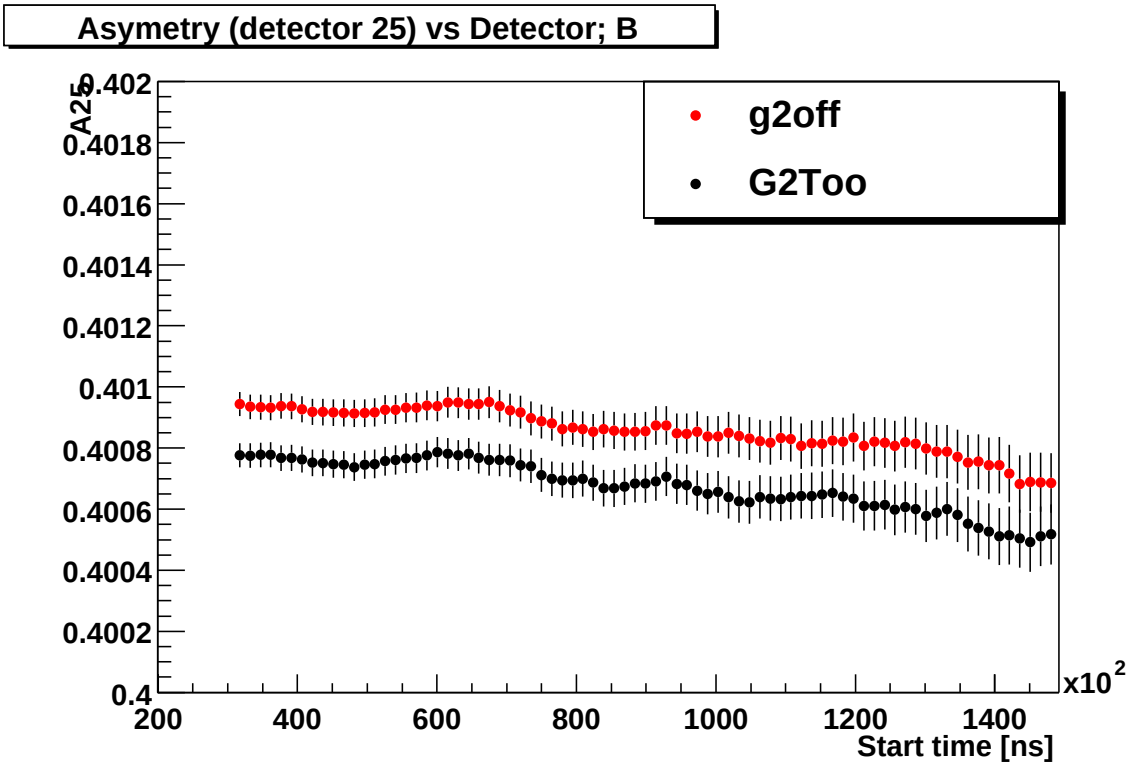

Figure 105: Asymetry for the sum of 23 detectors versus fit start time for $G2Too$ and $g2off$. High n data.

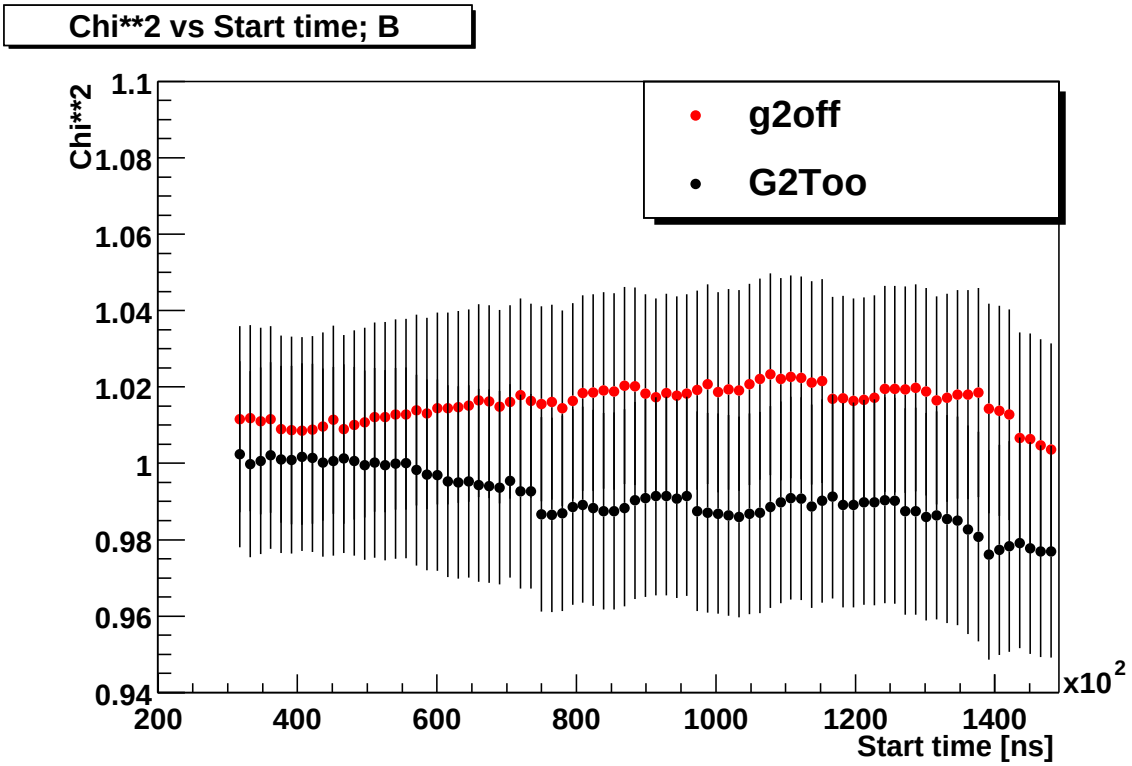

Figure 106: χ^2/Ndf for the sum of 23 detectors versus fit start time for $G2Too$ and $g2off$. High n data.

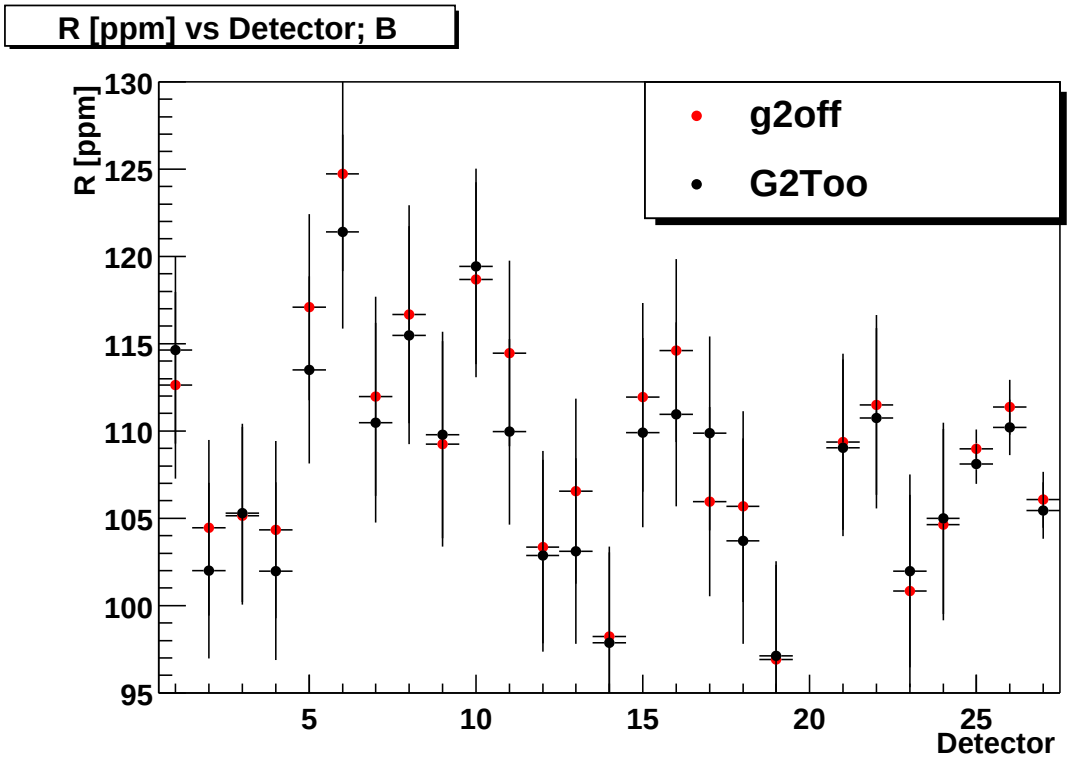

Figure 107: R versus detector for $G2Too$ and $g2off$. High n data.

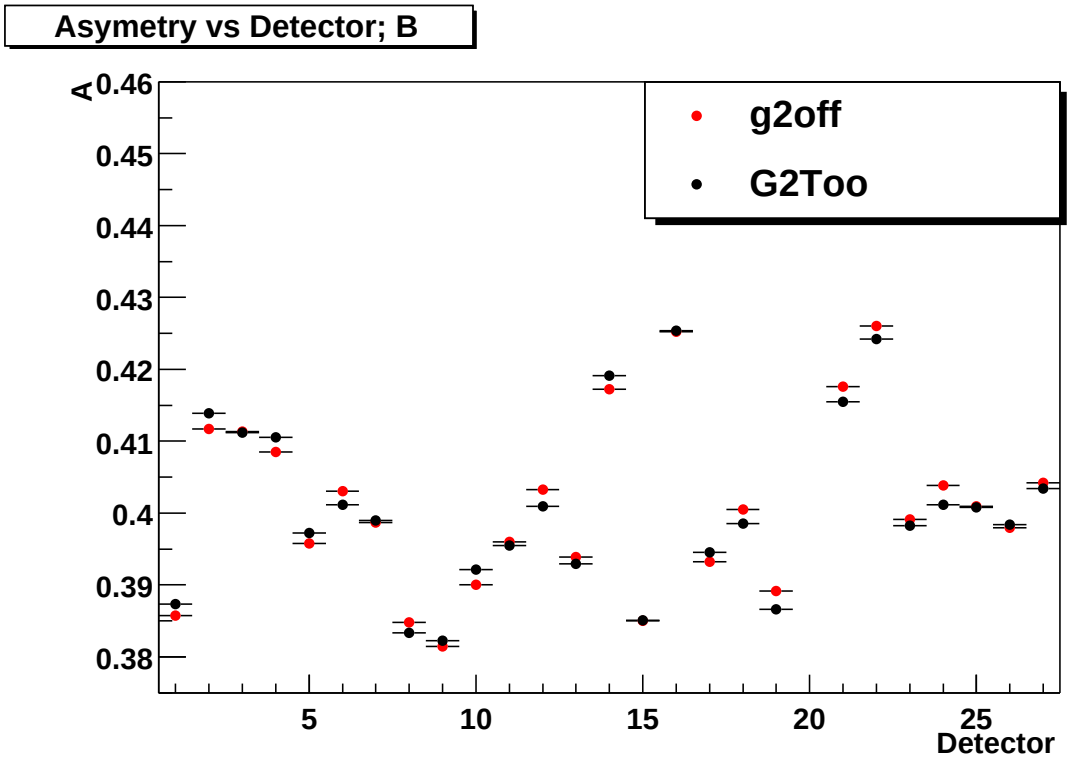

Figure 108: Asymetry A versus detector for $G2Too$ and $g2off$. High n data.

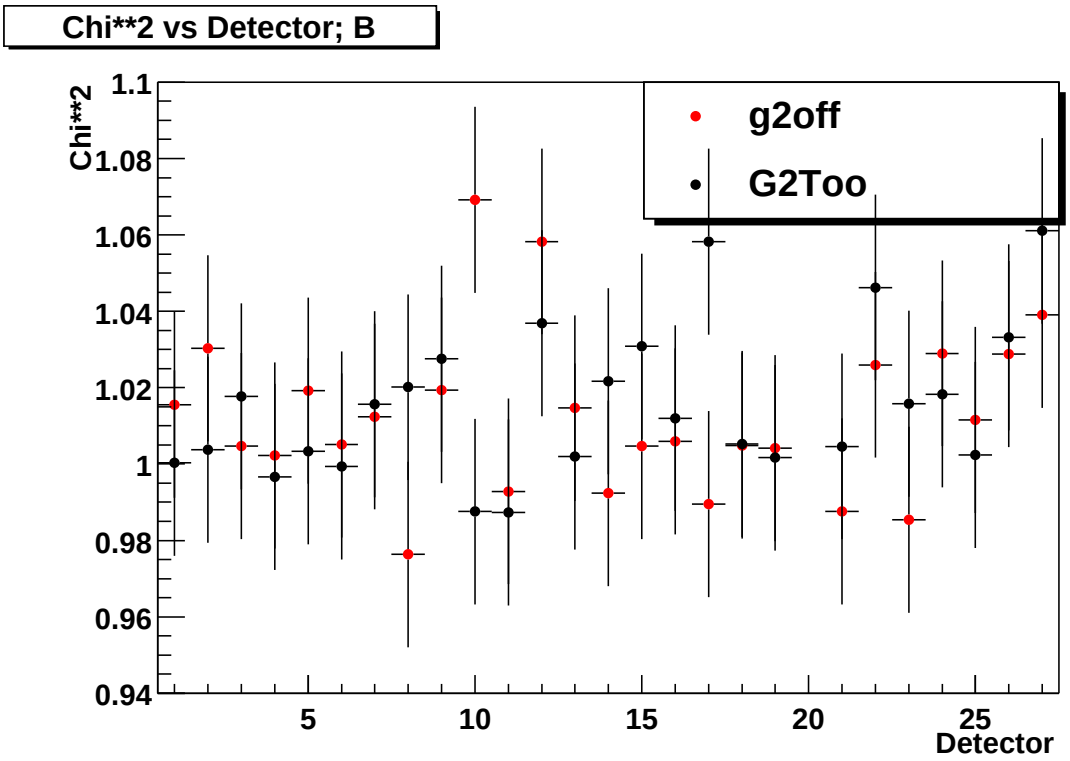

Figure 109: χ^2/Ndf versus detector for $G2Too$ and $g2off$. High n data.

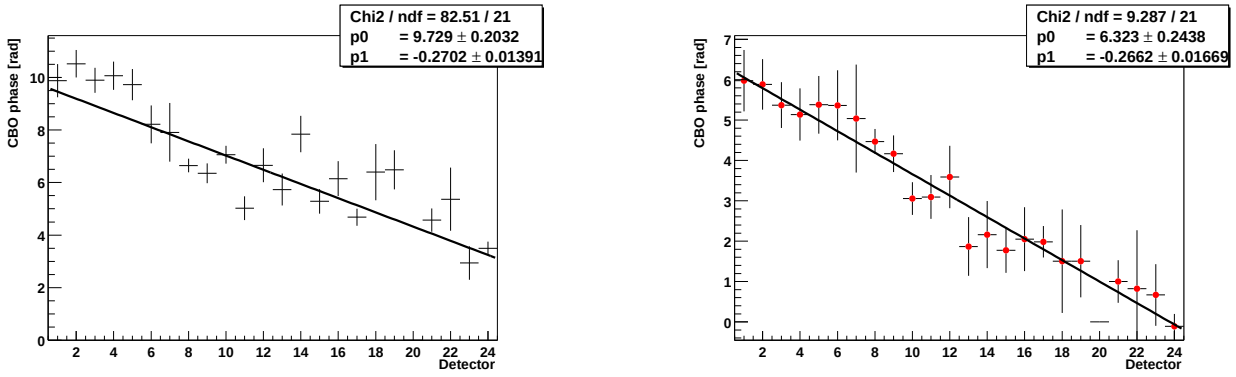

(a) (b)

Figure 110: (a) CBO phase versus detectors used to simulate the data for low. (b) CBO phase vs detector for the high n set.

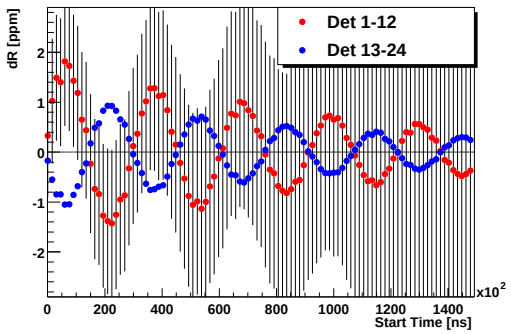

(a)

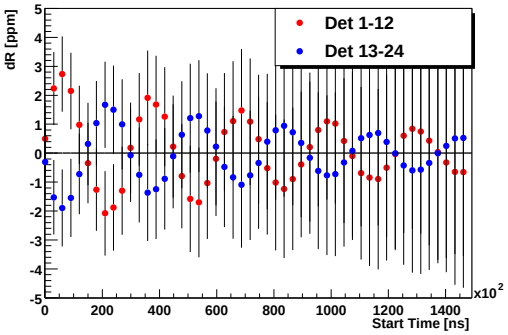

(b)

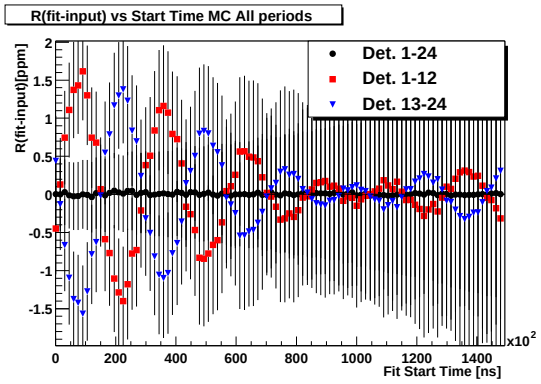

(c)

Figure 111: (a) R fit-input obtained from 3-paremeter fit of the low n set for the first (red) and second (blue) halves of the ring. (b) The same for the high n set. (c) R fit-input obtained for the combined data, the first (red) and second (blue) halves of the ring together with the sum of 23 detectors (black).

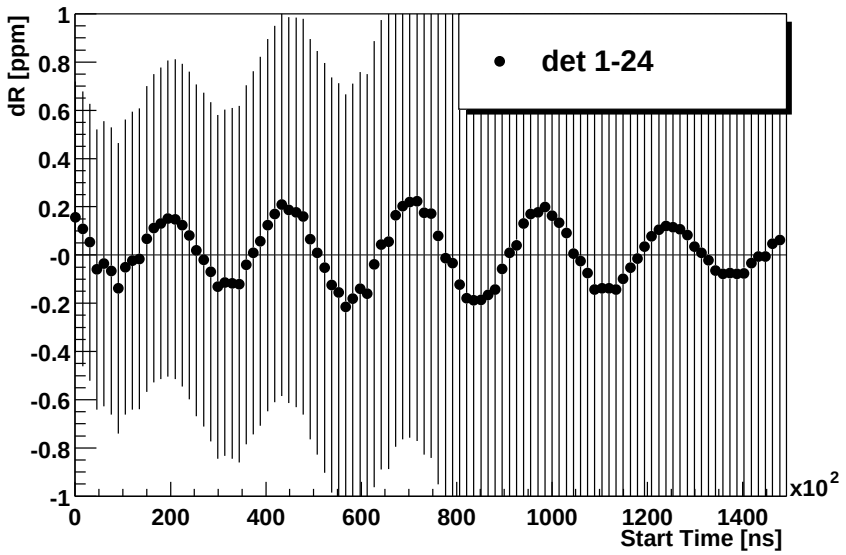

(a)

Figure 112: (a) R fit-input obtained from 3-paremeter fit of the combined data for the sum of 23 detectors.

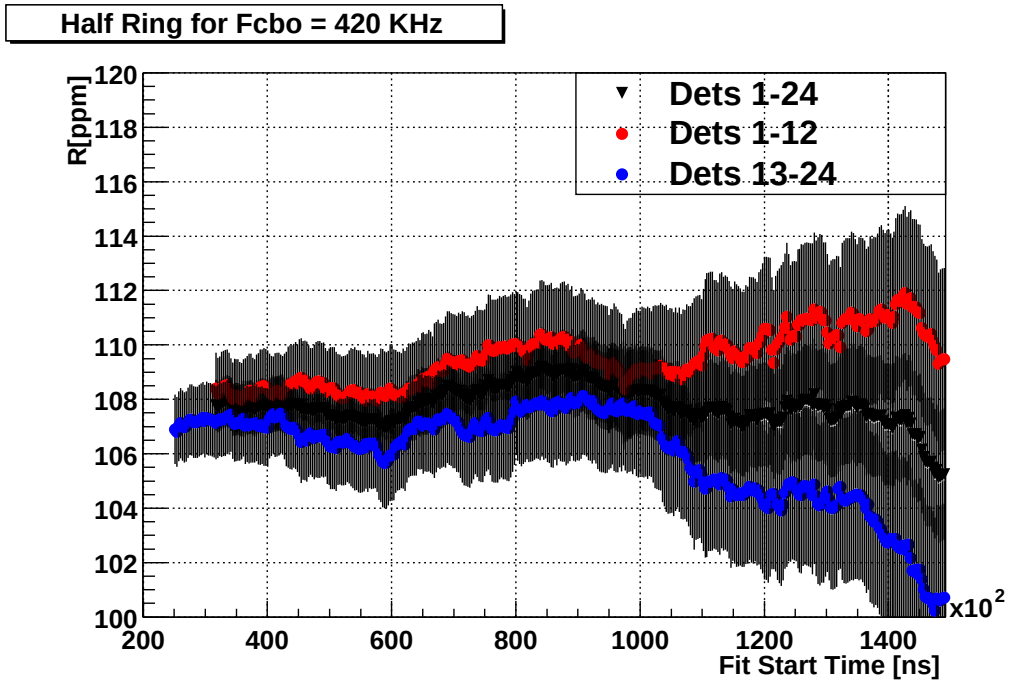

Figure 113: R values for the main CBO frequency 7-parameter fit function. Black points - value for the sum of 23 detectors. Red points - first half of the ring, blue - second half. Low n data set.

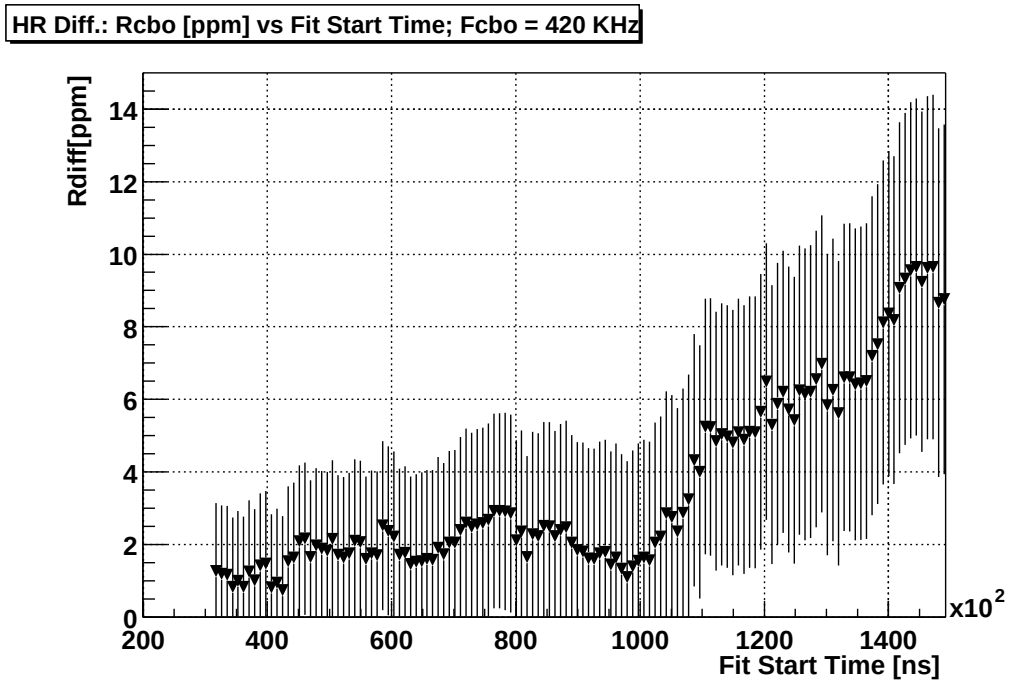

Figure 114: Difference of R values (main CBO 7-parameter fit function) for the first and second halves of the ring. Low n data set.

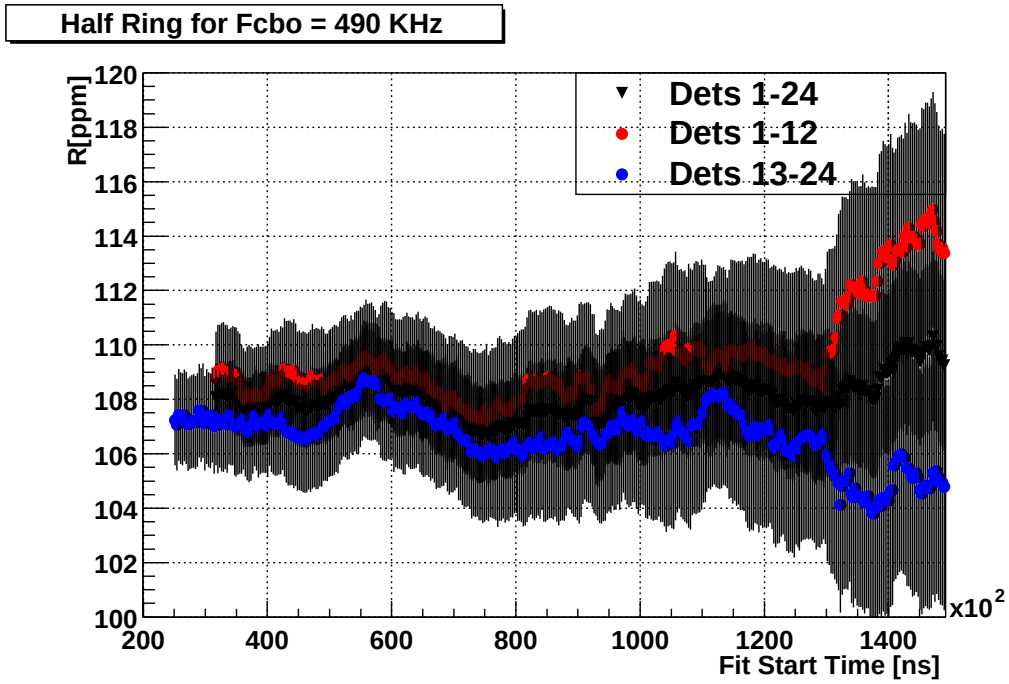

Figure 115: R values for the main CBO frequency 7-parameter fit function. Black points - value for the sum of 23 detectors. Red points - first half of the ring, blue - second half. High n data set.

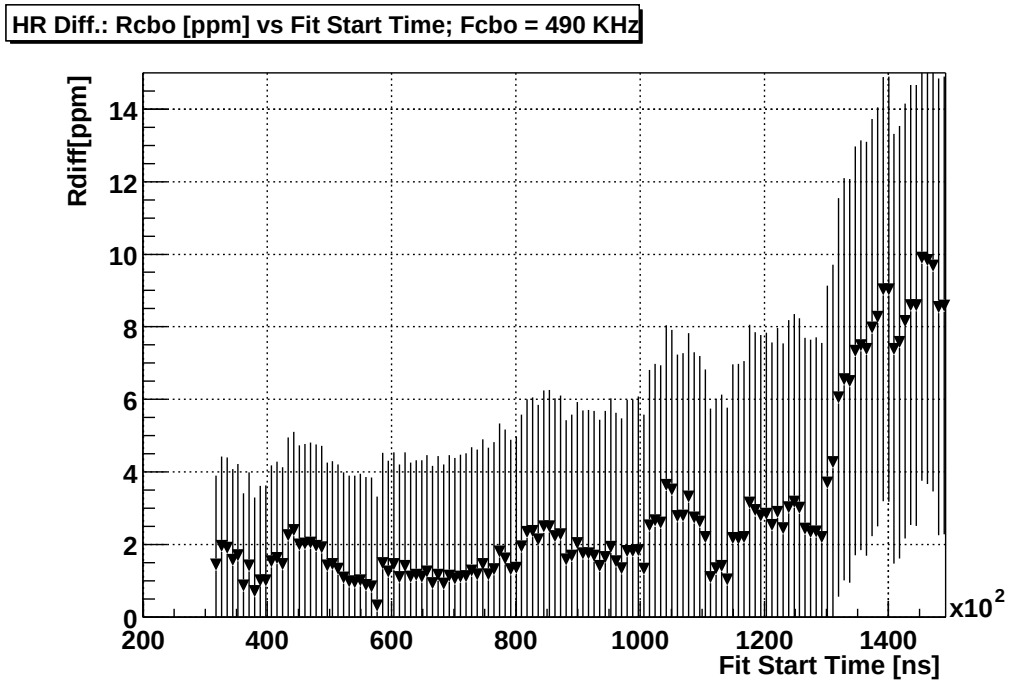

Figure 116: Difference of R values (main CBO 7-parameter fit function) for the first and second halves of the ring. High n data set.

The difference of fit results using 3 parameter and modified 7-parameters function versus fit start time are plotted in Figs. 117-118.

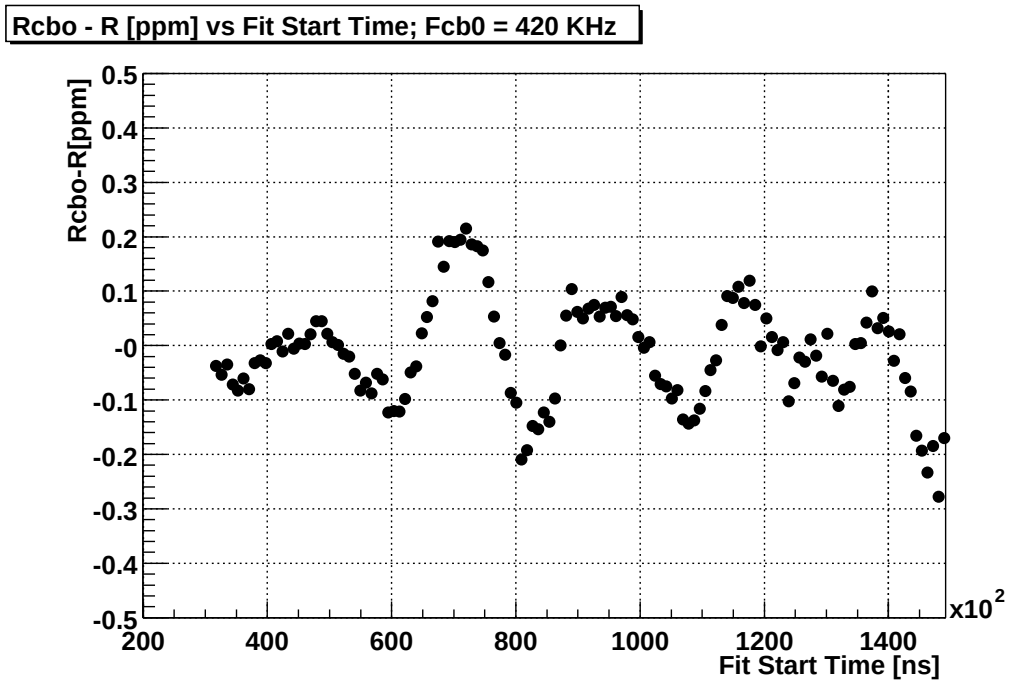

Figure 117: Difference of R values (main CBO 7-parameter - 3 parameter ratio fit function). Low n data set. Experimental data.

When CBO parameters are included in fitting function the difference between 7(main CBO) and 3 parameters fit results oscillate with the beating frequency close to $\omega_{beat} = \omega_{cbo} - 2\omega_a$. The amplitude of the oscillation is 0.1 ppm for low n data and 0.2 ppm for high n data. Zero crossing points are close to 32(49) μs for high n data and to 29(41) μs for low n data. Oscillation amplitude for the high n data is almost twice (may be even three times, see data earlier than 60 μs) higher then for the low n data.

The CBO related uncertainty is 0.117(0.155) ppm for the combined data set. The 0.155 ppm value include effect of detectors 4 and 5 shifts in time by 1 g-2 period (shifting the earliest fit start time to 27.5 μs) and possible Rob/Jim term envelope variation. A quick study was performed. The envelope for Rob/Jim terms of CBO was modified to be two different exponential forms (see g-2 Note 427) with phase difference between two exponents to be 90 degrees (from Jon's tracking study) . The relative weights of long and short exponents were selected 0.8 and 0.2 respectively. The result of R (fit - input) difference is plotted in Fig. 119 versus fit start time for $10 - 60$ μs interval. One exponential Rob/Jim envelope is also shown. Rfit - Rinput (two exponents, $\pi/2$ out of phase) is plotted in Fig. 120 versus fit start time for $0 - 150$ μs time range.

The distribution of the differences in R for case of two exponential envelope is plotted in Fig. 121. The distribution of the differences in R for case of two exponential envelope is plotted in Fig. 122. RMS of this distribution 0.168 ppm is used as CBO systematic uncertainty for the case of

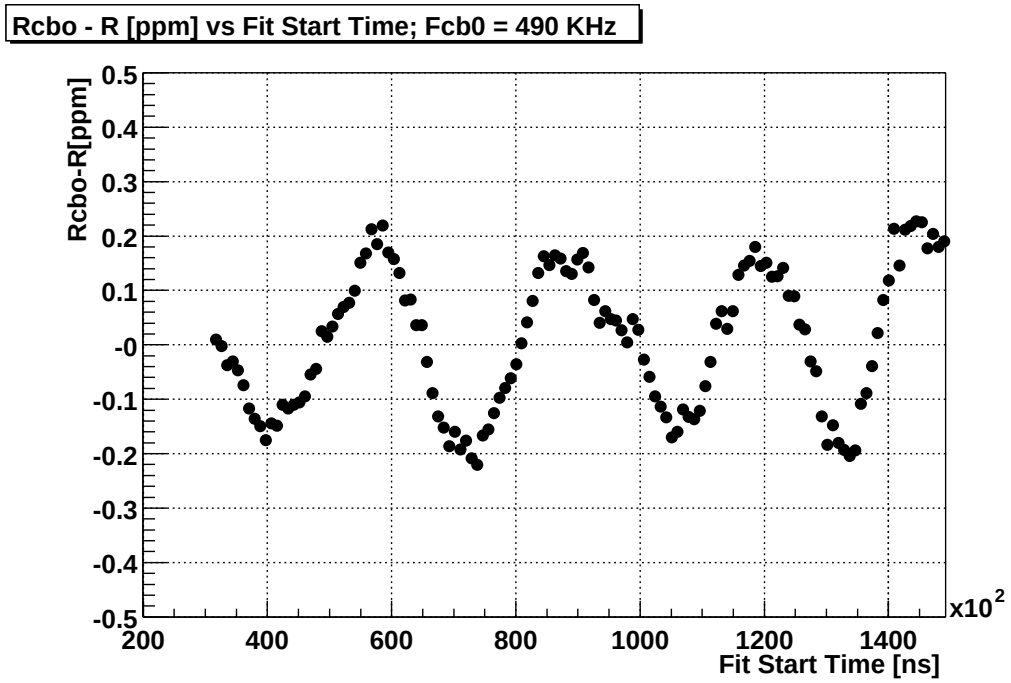

Figure 118: Difference of R values (main CBO 7-parameter - 3 parameter ratio fit function). High n data set. Experimental data.

two exponential out of phase envelope (Rob/Jim). The difference 0.05 ppm between one and two exponential envelopes can be considered as the systematic uncertainty due to Rob/Jim envelope.

4.9 Summary of systematic uncertainties

Table 8 gives a summary of my systematic uncertainties for 3-parameter fit function. All errors correspond to the sum of 23 detectors.

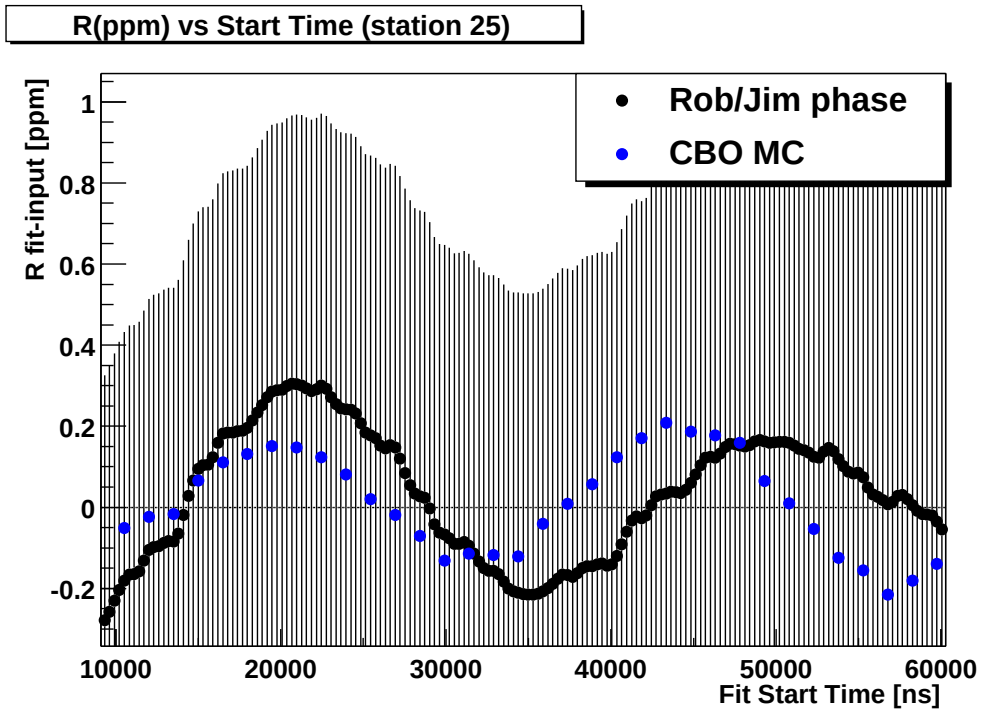

Figure 119: Difference of R values (fit - input) versus fit start time for modified Rob/Jim envelope (two exponent) and for one exponent in CBO lifetime. Low and high n data sets combined. MC data.

Table 8: Table of systematic uncertainties for Ratio Method (in ppm). Gain and Pile-up are summed according to the correlation coefficient, then squared and added to the other values.

source of uncertainty	3-parameter fit [ppm]	Comment
fitting uncertainty	0.01	
Minuit calls	0.0025	
Free constant	0.005	
fill rand.	0.04	
bin width + Ta shift	0.05	
pile-up subtraction	0.07	
gain correction	0.087	
CBO one exp. Rob/Jim	0.117	
CBO two exp. Rob/Jim	0.168	
Rob/Jim env.	0.05	
flashlets	0.02	Chris report
muon losses	0.08	Jon's report
unseen pile-up	0.016	Gerco's note
Total uncertainty	0.23	

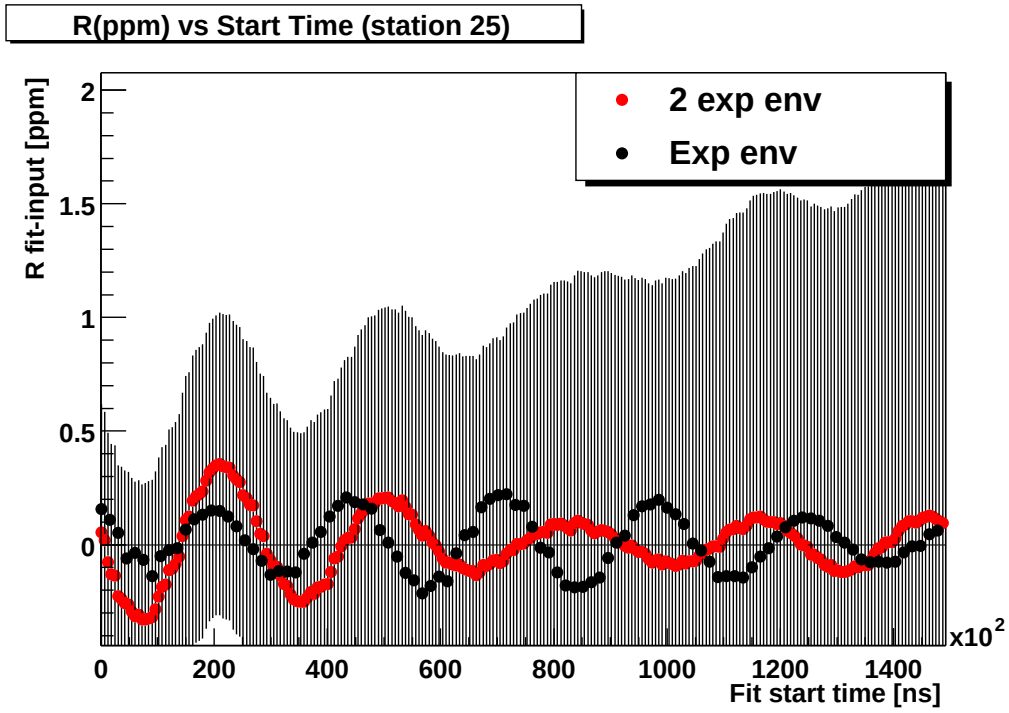

Figure 120: Difference of R values (fit - input) versus fit start time for modified Rob/Jim envelope (two exponent $\pi/2$ out of phase) and for one exponent in CBO lifetime. Low and high n data sets combined. MC data.

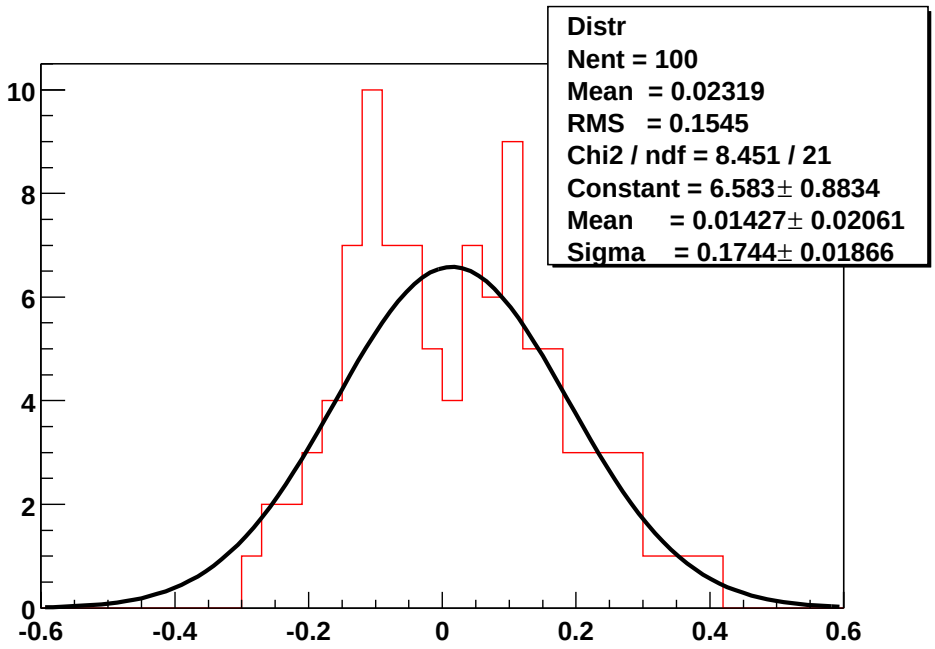

Figure 121: Difference of R values (fit - input) for the modified Rob/Jim envelope (two exponent). Low and high n data sets combined. MC data.

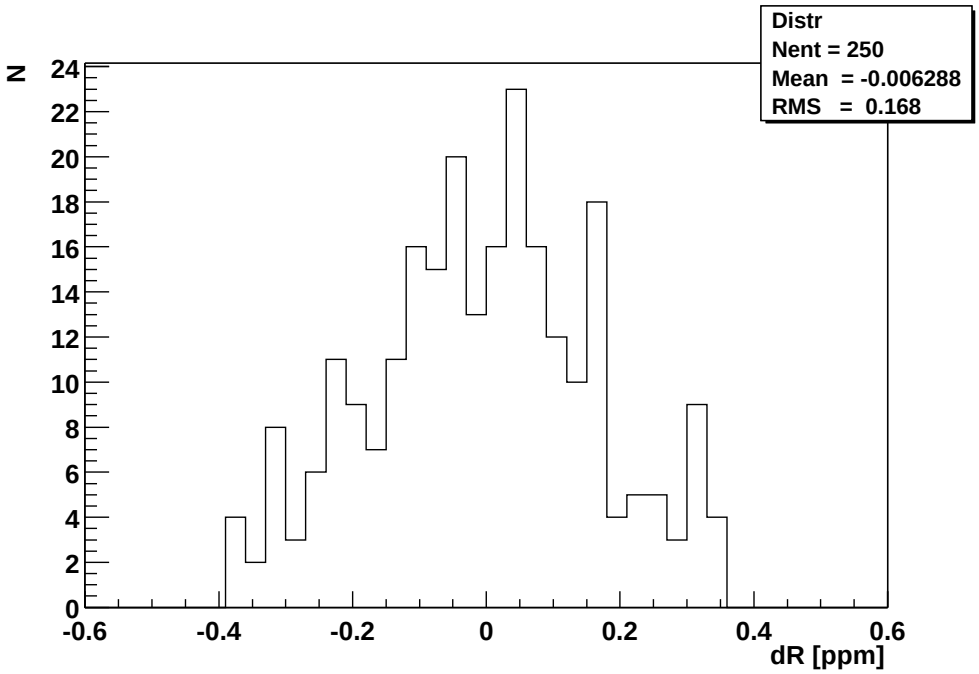

Figure 122: Difference of R values (fit - input) for the modified Rob/Jim envelope (two exponent out of phase $\pi/2$). Low and high n data sets combined. MC data.

5 Conclusions

In conclusion, I have selected preliminary R value of 107.95 ppm $\pm$ 0.686 (stat.) $\pm$0.23 (syst.) for the moment (may be changed later). This choice was explained in Secs. 3.6 and 4.9.

As stated earlier, I will continue to modify text of this report in the coming days in order to include updated plots.

References

[1] Long Duong, Ph.D. dissertation, University of Minnesota, 2001.

[2] B. Bousquet and L. Duong, $g-2$ Technical Note 402, 2001.

[3] B. Bousquet and L. Duong, A Comment on the CBO, 2001.

[4] Long Duong, private communication.

[5] Cenap Ozben, private communication.

[6] Chris Polly, G2Too production and Run selection for 2001 data set.

[7] Cenap Ozben, 2000 ω_a Analysis Report.

[8] B. Bousquet, L. Duong and P. Shagin, $g-2$ Technical Note 424, 2002.

[9] Fred Gray, 2000 ω_a Analysis Report.

[10] Tao Qian, Parameterized calorimeter end points for 2001 data (G2Too).

[11] C.S. Osben and Y.K.Semertzidis, $g-2$ Technical Note 365, July 2000.

[12] C.S. Ozben and Y.K. Semertzidis, $g-2$ Technical Note 397.